Charm production and fragmentation fractions at midrapidity in pp collisions at s = 13 TeV

11 July 2024

C.; Grigoriev, V.; Grigoryan, S.; Grosa, F.; Grosse-Oetringhaus, J. F.; Grosso, R.; Grund, D.; Grunwald, N. A.; Guardiano, G. G.; Guernane, R.; Guilbaud, M.; Gulbrandsen, K.; Gündem, T.; Gunji, T.; Guo, W.; Gupta, A.; Gupta, R.; Gupta, R.; Guzman, S. P.; Gwizdziel, K.; Gyulai, L.; Hadjidakis, C.; Haider, F. U.; Haidlova, S.; Hamagaki, H.; Hamdi, A.; Han, Y.; Hanley, B. G.; Hannigan, R.; Hansen, J.; Haque, M. R.; Harris, J. W.; Harton, A.; Hassan, H.; Hatzifotiadou, D.; Hauer, P.; Havener, L. B.; Heckel, S. T.; Hellbär, E.; Helstrup, H.; Hemmer, M.; Herman, T.; Herrera Corral, G.; Herrmann, F.; Herrmann, S.; Het, K. F.; Heybeck, B.; Hillemanns, H.; Hippolyte, B.; Hoffmann, F. W.; Hofman, B.; Hong, G. H.; Horst, M.; Horzyk, A.; Hou, Y.; Hristov, P.; Hughes, C.; Huhn, P.; Huhta, L. M.; Humanic, T. J.; Hutson, A.; Hutter, D.; Ilkaev, R.; Ilyas, H.; Inaba, M.; Innocenti, G. M.; Ippolitov, M.; Isakov, A.; Isidori, T.; Islam, M. S.; Ivanov, M.; Ivanov, M.; Ivanov, V.; Iversen, K. E.; Jablonski, M.; Jacak, B.; Jacazio, N.; Jacobs, P. M.; Jadlovska, S.; Jadlovsky, J.; Jaelani, S.; Jahnke, C.; Jakubowska, M. J.; Janik, M. A.; Janson, T.; Ji, S.; Jia, S.; Jimenez, A. A. P.; Jonas, F.; Jones, D. M.; Jowett, J. M.; Jung, J.; Jung, M.; Junique, A.; Jusko, A.; Kabus, M. J.; Kaewjai, J.; Kalinak, P.; Kalteyer, A. S.; Kalweit, A.; Kaplin, V.; Karasu Uysal, A.; Karatovic, D.; Karavichev, O.; Karavicheva, T.; Karczmarczyk, P.; Karpechev, E.; Kebschull, U.; Keidel, R.; Keijdener, D. L. D.; Keil, M.; Ketzer, B.; Khade, S. S.; Khan, A. M.; Khan, S.; Khanzadeev, A.; Kharlov, Y.; Khatun, A.; Khuntia, A.; Kileng, B.; Kim, B.; Kim, C.; Kim, D. J.; Kim, E. J.; Kim, J.; Kim, J. S.; Kim, J.; Kim, J.; Kim, M.; Kim, S.; Kim, T.; Kimura, K.; Kirsch, S.; Kisel, I.; Kiselev, S.; Kisiel, A.; Kitowski, J. P.; Klay, J. L.; Klein, J.; Klein, S.; Klein-Bösing, C.; Kleiner, M.; Klemenz, T.; Kluge, A.; Knospe, A. G.; Kobdaj, C.; Kollegger, T.; Kondratyev, A.; Kondratyeva, N.; Kondratyuk, E.; Konig, J.; Konigstorfer, S. A.; Konopka, P. J.; Kornakov, G.; Koryciak, S. D.; Kotliarov, A.; Kovalenko, V.; Kowalski, M.; Kozhuharov, V.; Králik, I.; Kraváková, A.; Krcal, L.; Krivda, M.; Krizek, F.; Krizkova Gajdosova, K.; Kroesen, M.; Krüger, M.; Krupova, D. M.; Kryshen, E.; Kuera, V.; Kuhn, C.; Kuijer, P. G.; Kumaoka, T.; Kumar, D.; Kumar, L.; Kumar, N.; Kumar, S.; Kundu, S.; Kurashvili, P.; Kurepin, A.; Kurepin, A. B.; Kuryakin, A.; Kushpil, S.; Kweon, M. J.; Kwon, Y.; La Pointe, S. L.; La Rocca, P.; Lakrathok, A.; Lamanna, M.; Langoy, R.; Larionov, P.; Laudi, E.; Lautner, L.; Lavicka, R.; Lea, R.; Lee, H.; Leg, I.; Legras, G.; Lehrbach, J.; Lelek, T. M.; Lemmon, R. C.; León Monzón, I.; Lesch, M. M.; Lesser, E. D.; Lévai, P.; Li, X.; Lien, J.; Lietava, R.; Likmeta, I.; Lim, B.; Lim, S. H.; Lindenstruth, V.; Lindner, A.; Lippmann, C.; Liu, D. H.; Liu, J.; Liveraro, G. S. S.; Lofnes, I. M.; Loizides, C.; Lokos, S.; Lomker, J.; Loncar, P.; Lopez, X.; López Torres, E.; Lu, P.; Lugo, F. V.; Luhder, J. R.; Lunardon, M.; Luparello, G.; Ma, Y. G.; Mager, M.; Maire, A.; Makariev, M. V.; Malaev, M.; Malfattore, G.; Malik, N. M.; Malik, Q. W.; Malik, S. K.; Malinina, L.; Mallick, D.; Mallick, N.; Mandaglio, G.; Mandal, S. K.; Manko, V.; Manso, F.; Manzari, V.; Mao, Y.; Marcjan, R. W.; Margagliotti, G. V.; Margotti, A.; Marín, A.; Markert, C.; Martinengo, P.; Martínez, M. I.; Martínez García, G.; Martins, M. P. P.; Masciocchi, S.; Masera, M.; Masoni, A.; Massacrier, L.; Massen, O.; Mastroserio, A.; Matonoha, O.; Mattiazzo, S.; Matyja, A.; Mayer, C.; Mazuecos, A. L.; Mazzaschi, F.; Mazzilli, M.; Mdhluli, J. E.; Melikyan, Y.; Menchaca-Rocha, A.; Mendez, J. E. M.; Meninno, E.; Menon, A. S.; Meres, M.; Mhlanga, S.; Miake, Y.; Micheletti, L.; Mihaylov, D. L.; Mikhaylov, K.; Mishra, A. N.; Mikowiec, D.; Modak, A.; Mohanty, B.; Mohisin Khan, M.; Molander, M. A.; Monira, S.; Mordasini, C.; Moreira De Godoy, D. A.; Morozov, I.; Morsch, A.; Mrnjavac, T.; Muccifora, V.; Muhuri, S.; Mulligan, J. D.; Mulliri, A.; Munhoz, M. G.; Munzer, R. H.; Murakami, H.; Murray, S.; Musa, L.; Musinsky, J.; Myrcha, J. W.; Naik, B.; Nambrath, A. I.; Nandi, B. K.; Nania, R.; Nappi, E.; Nassirpour, A. F.; Nath, A.; Nattrass, C.; Naydenov, M. N.; Neagu, A.; Negru, A.; Nellen, L.; Nepeivoda, R.; Nese, S.; Neskovic, G.; Nicassio, N.; Nielsen, B. S.; Nielsen, E. G.; Nikolaev, S.; Nikulin, S.; Nikulin, V.; Noferini, F.; Noh, S.; Nomokonov, P.; Norman, J.; Novitzky, N.; Nowakowski, P.; Nyanin, A.; Nyst, J.; Ogino, M.; Oh, S.; Ohlson, A.; Okorokov, V. A.; Oleniacz, J.; Oliveira Da Silva, A. C.; Onnerstad, A.; Oppedisano, C.; Ortiz Velasquez, A.; Otwinowski, J.; Oya, M.; Oyama, K.; Pachmayer, Y.; Padhan, S.; Pagano, D.; Pai, G.; Palasciano, A.; Panebianco, S.; Park, H.; Park, H.; Park, J.; Parkkila, J. E.; Patley, Y.; Patra, R. N.; Paul, B.; Pei, H.; Peitzmann, T.; Peng, X.; Pennisi, M.; Perciballi, S.; Peresunko, D.; Perez, G. M.; Pestov, Y.; Petrov, V.; Petrovici, M.; Pezzi, R. P.; Piano, S.; Pikna, M.; Pillot, P.; Pinazza, O.; Pinsky, L.; Pinto, C.; Pisano, S.; Posko, M.; Planinic, M.; Pliquett, F.; Poghosyan, M. G.; Polichtchouk, B.; Politano', S.; Poljak, N.; Pop, A.; Porteboeuf-Houssais, S.; Pozdniakov, V.; Pozos, I. Y.; Pradhan, K. K.; Prasad, S. K.; Prasad, S.; Preghenella, R.; Prino, F.; Pruneau, C. A.; Pshenichnov, I.; Puccio, M.; Pucillo, S.; Pugelova, Z.; Qiu, S.; Quaglia, L.; Ragoni, S.; Rai, A.; Rakotozafindrabe, A.; Ramello, L.; Rami, F.; Ramirez, S. A. R.; Rancien, T. A.; Rasa, M.; Räsänen, S. S.; Rath, R.; Rauch, M. P.; Ravasenga, I.; Read, K. F.; Reckziegel, C.; Redelbach, A. R.; Redlich, K.; Reetz, C. A.; Rehman, A.; Reidt, F.; Reme-Ness, H. A.; Rescakova, Z.; Reygers, K.; Riabov, A.; Riabov, V.; Ricci, R.; Richter, M.; Riedel, A. A.; Riegler, W.; Riffero, A. G.; Ristea, C.; Rodriguez, M. V.; Rodríguez Cahuantzi, M.; Røed, K.; Rogalev, R.; Rogochaya, E.; Rogoschinski, T. S.; Rohr, D.; Röhrich, D.; Rojas, P. F.; Rojas Torres, S.; Rokita, P. S.; Romanenko, G.; Ronchetti, F.; Rosano, A.; Rosas, E. D.; Roslon, K.; Rossi, A.; Roy, A.; Roy, S.; Rubini, N.; Ruggiano, D.; Rui, R.; Russek, P. G.; Russo, R.; Rustamov, A.; Ryabinkin, E.; Ryabov, Y.; Rybicki, A.; Rytkonen, H.; Ryu, J.; Rzesa, W.; Saarimaki, O. A. M.; Sadhu, S.; Sadovsky, S.; Saetre, J.; Šafařík, K.; Saha, P.; Saha, S. K.; Saha, S.; Sahoo, B.; Sahoo, B.; Sahoo, R.; Sahoo, S.; Sahu, D.; Sahu, P. K.; Saini, J.; Sajdakova, K.; Sakai, S.; Salvan, M. P.; Sambyal, S.; Samitz, D.; Sanna, I.; Saramela, T. B.; Sarma, P.; Sarritzu, V.; Sarti, V. M.; Sas, M. H. P.; Sawan, S.; Schambach, J.; Scheid, H. S.; Schiaua, C.; Schicker, R.; Schmah, A.; Schmidt, C.; Schmidt, H. R.; Schmidt, M. O.; Schmidt, M.; Schmidt, N. V.; Schmier, A. R.; Schotter, R.; Schröter, A.; Schukraft, J.; Schweda, K.; Scioli, G.; Scomparin, E.; Seger, J. E.; Sekiguchi, Y.; Sekihata, D.; Selina, M.; Selyuzhenkov, I.; Senyukov, S.; Seo, J. J.; Serebryakov, D.; Šerkšnyt, L.; Sevcenco, A.; Shaba, T. J.; Shabetai, A.; Shahoyan, R.; Shangaraev, A.; Sharma, A.; Sharma, B.; Sharma, D.; Sharma, H.; Sharma, M.; Sharma, S.; Sharma, S.; Sharma, U.; Shatat, A.; Sheibani, O.; Shigaki, K.; Shimomura, M.; Shin, J.; Shirinkin, S.; Shou, Q.; Sibiriak, Y.; Siddhanta, S.; Siemiarczuk, T.; Silva, T. F.; Silvermyr, D.; Simantathammakul, T.; Simeonov, R.; Singh, B.; Singh, B.; Singh, K.; Singh, R.; Singh, R.; Singh, R.; Singh, S.; Singh, V. K.; Singhal, V.; Sinha, T.; Sitar, B.; Sitta, M.; Skaali, T. B.;

Skorodumovs, G.; Slupecki, M.; Smirnov, N.; Snellings, R. J. M.; Solheim, E. H.; Song, J.; Sonnabend, C.; Soramel, F.; Soto-hernandez, A. B.; Spijkers, R.; Sputowska, I.; Staa, J.; Stachel, J.; Stan, I.; Steffanic, P. J.; Stiefelmaier, S. F.; Stocco, D.; Storehaug, I.; Stratmann, P.; Strazzi, S.; Sturniolo, A.; Stylianidis, C. P.; Suaide, A. A. P.; Suire, C.; Sukhanov, M.; Suljic, M.; Sultanov, R.; Sumberia, V.; Sumowidagdo, S.; Swain, S.; Szarka, I.; Szymkowski, M.; Taghavi, S. F.; Taillepied, G.; Takahashi, J.; Tambave, G. J.; Tang, S.; Tang, Z.; Tapia Takaki, J. D.; Tapus, N.; Tarasovicova, L. A.; Tarzila, M. G.; Tassielli, G. F.; Tauro, A.; Tejeda Muñoz, G.; Telesca, A.; Terlizzi, L.; Terrevoli, C.; Thakur, S.; Thomas, D.; Tikhonov, A.; Timmins, A. R.; Tkacik, M.; Tkacik, T.; Toia, A.; Tokumoto, R.; Tomohiro, K.; Topilskaya, N.; Toppi, M.; Tork, T.; Torres, V. V.; Torres Ramos, A. G.; Trifiró, A.; Triolo, A. S.; Tripathy, S.; Tripathy, T.; Trogolo, S.; Trubnikov, V.; Trzaska, W. H.; Trzcinski, T. P.; Tumkin, A.; Turrisi, R.; Tveter, T. S.; Ulla, K.; Ulukutlu, B.; Uras, A.; Usai, G. L.; Vala, M.; Valle, N.; van Doremalen, L. V. R.; van Leeuwen, M.; van Veen, C. A.; van Weelden, R. J. G.; Vande Vyvre, P.; Varga, D.; Varga, Z.; Vasileiou, M.; Vasiliev, A.; Vázquez Doce, O.; Vazquez Rueda, O.; Vechernin, V.; Vercellin, E.; Vergara Limón, S.; Verma, R.; Vermunt, L.; Vértesi, R.; Verweij, M.; Vickovic, L.; Vilakazi, Z.; Villalobos Baillie, O.; Villani, A.; Vinogradov, A.; Virgili, T.; Virta, M. M. O.; Vislavicius, V.; Vodopyanov, A.; Volkel, B.; Völkl, M. A.; Voloshin, K.; Voloshin, S. A.; Volpe, G.; von Haller, B.; Vorobyev, I.; Vozniuk, N.; Vrláková, J.; Wan, J.; Wang, C.; Wang, D.; Wang, Y.; Wang, Y.; Wegrzynek, A.; Weiglhofer, F. T.; Wenzel, S. C.; Wessels, J. P.; Weyhmiller, S. L.; Wiechula, J.; Wikne, J.; Wilk, G.; Wilkinson, J.; Willems, G. A.; Windel, B.; Winn, M.; Wright, J. R.; Wu, W.; Wu, Y.; Xu, R.; Yadav, A.; Yadav, A. K.; Yalcin, S.; Yamaguchi, Y.; Yang, S.; Yano, S.; Yin, Z.; Yoo, I. -K.; Yoon, J. H.; Yu, H.; Yuan, S.; Yuncu, A.; Zaccolo, V.; Zampolli, C.; Zanone, F.; Zardoshti, N.; Zarochentsev, A.; Závada, P.; Zaviyalov, N.; Zhalov, M.; Zhang, B.; Zhang, C.; Zhang, L.; Zhang, S.; Zhang, X.; Zhang, Y.; Zhang, Z.; Zhao, M.; Zherebchevskii, V.; Zhi, Y.; Zhou, D.; Zhou, Y.; Zhu, J.; Zhu, Y.; Zugravel, S. C..

Charm production and fragmentation fractions at midrapidity in pp collisions at $\sqrt{s} = 13\,\text{TeV}$

The ALICE collaboration

E-mail: ALICE-publications@cern.ch

ABSTRACT: Measurements of the production cross sections of prompt D^0, D^+, D^{*+}, D_s^+, Λ_c^+, and Ξ_c^+ charm hadrons at midrapidity in proton-proton collisions at $\sqrt{s} = 13\,\text{TeV}$ with the ALICE detector are presented. The D-meson cross sections as a function of transverse momentum (p_T) are provided with improved precision and granularity. The ratios of p_T-differential meson production cross sections based on this publication and on measurements at different rapidity and collision energy provide a constraint on gluon parton distribution functions at low values of Bjorken-x (10^{-5}–10^{-4}). The measurements of Λ_c^+ (Ξ_c^+) baryon production extend the measured p_T intervals down to $p_T = 0(3)\,\text{GeV}/c$. These measurements are used to determine the charm-quark fragmentation fractions and the $c\bar{c}$ production cross section at midrapidity ($|y| < 0.5$) based on the sum of the cross sections of the weakly-decaying ground-state charm hadrons D^0, D^+, D_s^+, Λ_c^+, Ξ_c^0 and, for the first time, Ξ_c^+, and of the strongly-decaying J/ψ mesons. The first measurements of Ξ_c^+ and $\Sigma_c^{0,++}$ fragmentation fractions at midrapidity are also reported. A significantly larger fraction of charm quarks hadronising to baryons is found compared to e^+e^- and ep collisions. The $c\bar{c}$ production cross section at midrapidity is found to be at the upper bound of state-of-the-art perturbative QCD calculations.

Contents

1 Introduction

Measurements of heavy-flavour (i.e. charm and beauty) hadron production in ultra-relativistic proton-proton (pp) collisions provide fundamental tests of perturbative quantum chromodynamics (pQCD) calculations. The transverse momentum (p_T) differential production cross section of heavy-flavour hadrons is usually calculated in pQCD by the convolution of three ingredients employing a factorisation approach [1]. The first ingredient

corresponds to the parton distribution functions (PDFs), which describe the probability distributions of the parton momentum fractions in the proton. The second term is the partonic cross section, which defines the scattering probability calculated as a perturbative series expansion in the strong coupling constant (α_s). The third ingredient corresponds to the fragmentation function (FF) which parametrises the non-perturbative transition of a heavy quark into a hadron.

Factorisation can be implemented in pQCD-based calculations in different ways, for example in terms of the transferred momentum squared Q^2 (collinear factorisation) [1] or of the parton transverse momentum k_T [2–6]. Calculations for LHC energies implementing the former approach, like the general-mass variable-flavour-number scheme (GM-VFNS) [7–12] and the fixed order plus next-to-leading logarithms (FONLL) approach [13, 14] provide a next-to-leading order (NLO) accuracy with all-order resummation of next-to-leading logarithms. Calculations of heavy-flavour hadron production in the k_T framework are also able to go beyond leading-order expansions in α_s [5, 6]. The most recent implementation of k_T-factorisation has also employed the variable-flavour-number scheme approach [15]. D-meson production down to low p_T is calculable at p_T scales far below the charm mass with transverse-momentum dependent factorisation approach (TMD [16, 17]), and in the low-x regime with the colour-glass condensate model (CGC [18]).

All of these models describe the production of heavy-flavour mesons within uncertainties, in different kinematic regions and at different energies in pp and p$\bar{\text{p}}$ collisions [19–29]. In this article, the measured p_T-differential production cross sections of prompt D^0, D^+, D_s^+, and D^{*+} mesons at midrapidity in pp collisions at $\sqrt{s} = 13\,\text{TeV}$ are compared with the predictions from these models, which are significantly less precise than the available experimental measurements. The main source of theoretical uncertainty is related to the choice of the energy scales for the validity of the perturbative regime (factorisation and renormalisation scales). However, as explained in ref. [30], these uncertainties may become subdominant in the calculation of cross section ratios at different rapidities and energies. For this reason, precise measurements of charm meson-to-meson production ratios originating from charm-quark hadronisation (i.e. prompt) down to low p_T (i.e. $p_T \lesssim 5\,\text{GeV}/c$) are sensitive to gluon PDFs at low Bjorken-x.

Calculations based on a collinear factorisation approach, and using fragmentation functions tuned on e^+e^- collision data, do not describe the production of charm baryons at midrapidity in pp collisions at the LHC [31]. The Λ_c^+-baryon production cross section at low p_T and midrapidity ($|y| < 0.5$) in pp collisions at $\sqrt{s} = 5.02\,\text{TeV}$ [32–35] is underestimated by a factor 3–4 by GM-VFNS calculations adopting Λ_c^+-baryon fragmentation functions derived from the fit of OPAL data [36], and by a factor 15 by the POWHEG predictions [37] matched with PYTHIA 6 [38] to generate the parton shower. The prediction from the PYTHIA 8 Monte Carlo (MC) generator [39] with the standard Monash tune [40], where the charm-quark fragmentation is constrained with e^+e^- and ep measurements, underestimates the measurement by a factor 2–10 depending on p_T in the region $p_T < 12\,\text{GeV}/c$. The baryon production observed in pp collisions at the LHC challenges the concept of "jet universality", according to which the parton fragmentation is universal between collision systems and can be constrained from e^+e^- results. This implies

the breakdown of multi-parton interaction (MPI)-based event generators implementing jet universality [39, 41, 42].

The measured baryon production in pp collision can only be described by model calculations that account for novel hadronisation mechanisms. The data description in PYTHIA improves when colour reconnection mechanisms beyond the leading-colour approximation (CR-BLC) are adopted in PYTHIA simulations [43]. In these cases, the predicted Λ_c^+-baryon production is enhanced by the presence of new topologies, called "junctions", which preferentially fragment into baryons. Several other model calculations foresee a relative increase of charm-baryon production with respect to that of mesons in pp collisions at the LHC. In the statistical hadronisation model with relativistic quark model (SHM+RQM) [44] the presence of a large set of mostly unobserved excited charm baryons, which decay strongly and enrich the abundance of ground-state charm baryons, is foreseen. These excited charm baryons are predicted by the RQM model [45]. Their abundances are assumed to follow the thermal densities derived from the SHM [46] depending only on their mass and spin degeneracy. Different assumptions are made in the Catania model [47], where the charm quark can hadronise either via fragmentation, or by recombining with surrounding light quarks already produced from the event underlying the hard scattering. In this model, the recombination mechanisms enhances the production of baryons at intermediate p_T. In the quark (re)combination model (QCM) [48] the charm quarks produced in the hard scatterings hadronise by recombining with surrounding equal-velocity light quarks. In this model, thermal weights regulate the relative abundances of different charm baryons.

Further information can be derived from the measurement of the relative production rates of different charm hadrons as a function of p_T. The measured Λ_c^+/D^0 ratios at midrapidity in pp collisions at $\sqrt{s} = 5.02\,\text{TeV}$ and $13\,\text{TeV}$ are described by the predictions provided by these model calculations. The measurements at the two collision energies are compatible within uncertainty, and they show an enhancement of about a factor 5 at low p_T with respect to e^+e^- and ep collisions. The $\Sigma_c^{0,+,++}/D^0$ ratio at midrapidity in pp collisions at $\sqrt{s} = 13\,\text{TeV}$ [49] is described by the predictions of PYTHIA CR-BLC, SHM+RQM, and QCM models. This ratio is severely underestimated by the PYTHIA Monash tune simulations and is larger by around a factor 10 at $p_T < 6\,\text{GeV}/c$ compared to that observed in e^+e^- collisions [50]. Given the available precision, the current experimental results are not sufficient to fully distinguish between the pictures described above. Finally, further measurements of $\Xi_c^{0,+}$ and Ω_c^0 at midrapidity demonstrate that even the hadronisation mechanisms discussed above do not provide a complete picture, since significant tensions are observed when describing the relative abundance of charm baryons containing a strange valence quark [51–53]. In this article, the production of Λ_c^+ and Ξ_c^+ baryons is measured down to lower transverse momenta, extending the comparison with the theoretical predictions in a kinematic region where the models calculations differ from each other.

The enhancement of the relative abundance of baryons compared to that of mesons at midrapidity in pp collisions at the LHC has a strong impact on the charm-quark fragmentation fractions $f(c \rightarrow h_c)$. These describe the probability of a charm quark to produce a hadron of species h_c. The measurement of $f(c \rightarrow h_c)$ for a given charm hadron implies

integrating the p_T-differential production cross section and dividing it by the sum of the p_T-integrated production cross sections of all charm hadrons. It is crucial to extend the measurements of the p_T-differential production cross section down to $p_T = 0 \, \mathrm{GeV}/c$, in order to minimise the uncertainties arising from extrapolations. The most recent measurement from the ALICE collaboration in pp collisions at $\sqrt{s} = 5.02 \, \mathrm{TeV}$ [54] shows a drop by about a factor 1.2–1.4 of the D^0-meson fragmentation fraction with respect to that observed in e^+e^- collisions at the B-factories and at LEP, as well as in deep-inelastic scattering measurements in ep collisions at HERA [55]. An increase by about a factor 3.3 is observed for the Λ_c^+-baryon fragmentation fraction, while the relative fraction of the Ξ_c^0 baryon in pp collisions was measured to be similar to that of the D_s^+ meson. In this article, the analogous result in pp collisions at $\sqrt{s} = 13 \, \mathrm{TeV}$ is proposed.

The fragmentation fractions also impact the determination of the $c\bar{c}$ production cross section. The first measurements of the $c\bar{c}$ cross sections at $\sqrt{s} = 2.76 \, \mathrm{TeV}$ [20] and 7 TeV [22] at midrapidity ($|y| < 0.5$) were derived only from D-meson cross section measurements using the fragmentation fractions from e^+e^- collisions. They were thus affected by an underestimation of the charm-baryon contribution, and they increased by about 40% when applying updated D-meson fragmentation fractions taking the measured charm-baryon yields into account [54]. Such precise measurements of the $c\bar{c}$ cross section are not only important tests of pQCD calculations, but they also provide a reference to study the charm dynamics in the quark-gluon plasma (QGP) produced in ultra-relativistic heavy-ion collisions. For example, the knowledge of the $c\bar{c}$ production cross section per nucleon-nucleon collision is a key ingredient to determine the production of charmonia and the influence of recombination effects in the QGP [56–58]. Finally, precise results of p_T-differential production cross sections of different charm-hadron species are crucial as a reference for measurements of the nuclear modification factor (R_{AA}) [59].

In this article, the p_T-differential production cross sections of prompt D^0, D^+, D_s^+, and D^{*+} mesons at midrapidity in pp collisions at $\sqrt{s} = 13 \, \mathrm{TeV}$ are reported. The production cross sections of prompt D^0 and D_s^+ mesons in this article supersede those published in refs. [49, 60], and provide an extended p_T coverage and a finer granularity in p_T than the previous results. In addition, the first results of the Λ_c^+-baryon reconstruction in both $pK^-\pi^+$ and pK_S^0 decay channels down to $p_T = 0$ at midrapidity at the LHC, as well as that of the Ξ_c^+ baryon down to $p_T = 3 \, \mathrm{GeV}/c$, are presented. These results extend the already published ones in refs. [49] and [52], respectively. This article then presents the first measurements of the $c\bar{c}$ production cross section per unit of rapidity at midrapidity and the charm-quark fragmentation fractions at midrapidity in pp collisions at $\sqrt{s} = 13 \, \mathrm{TeV}$. Using similar methods as in ref. [54], these measurements consider the sum of ground-state charm hadrons D^0, D^+, D_s^+, Λ_c^+, Ξ_c^0 and, for the first time, Ξ_c^+, and of the strongly-decaying J/ψ mesons. Furthermore, the first measurement of the $\Sigma_c^{0,+,++}$-baryon fragmentation fraction is presented. The paper is organised as follows. The ALICE detector and the properties of the data samples used in these analyses are described in section 2. The details of the data analysis are provided in section 3 and the estimation of the systematic uncertainties is described in section 4. The results of the analyses and their comparison with model calculations are discussed in section 5. Finally, a brief summary is given in section 6.

2 Experimental apparatus and data sample

The ALICE apparatus and its performance are comprehensively described in refs. [61, 62]. The charm-hadron decays were reconstructed with the central barrel detectors, which cover the pseudorapidity interval $|\eta| < 0.9$ and are embedded in a cylindrical solenoid providing a magnetic field $B = 0.5$ T along the beam direction. The trajectories of charged particles are reconstructed with the Inner Tracking System (ITS) and the Time Projection Chamber (TPC). The ITS detector is the innermost ALICE subsystem. It is composed of six cylindrical layers of silicon detectors for precise measurements of track parameters in the vicinity of the interaction point (primary vertex). The ITS detector provides a precise determination of the track impact parameter (i.e. the distance of closest approach of the track to the interaction point). For tracks with $p_T > 1\,\mathrm{GeV}/c$, a resolution better than $75\,\mu\mathrm{m}$ is achieved in the plane orthogonal to the beam direction (transverse plane) [63]. Therefore, this detector is crucial to reconstruct the decay vertex of heavy-flavour hadrons (secondary vertex) and to distinguish it from the beam interaction point. The TPC provides track reconstruction with up to 159 three-dimensional space points per track and charged-particle identification (PID) via the measurement of the specific ionisation energy loss ($\mathrm{d}E/\mathrm{d}x$). The charm-hadron decay products are also identified with the Time-Of-Flight (TOF) detector, which measures the flight time of the charged particles. For triggering and event selection, the V0 detector is used. It is composed of two scintillator arrays located on both sides of the nominal collision point covering the pseudorapidity intervals $-3.7 < \eta < -1.7$ and $2.8 < \eta < 5.1$.

The pp collisions considered in the analyses presented in this article were collected at a centre-of-mass energy $\sqrt{s} = 13\,\mathrm{TeV}$ in 2016, 2017, and 2018 at the LHC using a minimum bias (MB) trigger, requiring coincident signals in the V0 scintillators on both sides. Background events coming from possible interactions between protons in the beam and residual gas inside the beam pipe were rejected offline exploiting the timing information of the V0 arrays and the correlation between the number of hits and tracks reconstructed in the two innermost layers of the ITS consisting of silicon pixel detectors (SPD). Furthermore, all events with more than one reconstructed primary vertex were rejected in the analyses in order to exclude pile-up events within the same bunch crossing [62]. Finally, only events with a position along the beam direction within $\pm 10\,\mathrm{cm}$ from the centre of the apparatus were considered in this analysis to grant a uniform pseudorapidity acceptance. The number of analysed MB-triggered events corresponds to an integrated luminosity of $\mathcal{L}_{\mathrm{int}} = 31.9 \pm 0.5\,\mathrm{nb}^{-1}$ [64].

Monte Carlo samples of pp collisions at the same centre-of-mass energy were used for efficiency and acceptance corrections as well as to train the machine learning algorithm to classify the signal and background candidates. This will be discussed in more detail in section 3. These MC samples were generated by simulating pp collisions with the Monash tune of the PYTHIA 8.243 event generator [43] requiring for each of them the production of at least a $c\bar{c}$ or $b\bar{b}$ pair. The produced charm hadrons were forced to decay in the channels of interest for the analyses discussed in this paper. The produced particles were propagated through the detector using the GEANT3 transport code [65]. In the simulations, the conditions during the data taking were reproduced.

Decay channel	Charm-hadron BR (%)	Daughter decay	BR$_{\text{daughter}}$ (%)
$D^0 \to K^-\pi^+$	3.95 ± 0.03	—	—
$D^+ \to K^-\pi^+\pi^+$	9.38 ± 0.16	—	—
$D_s^+ \to \phi\pi^+ \to K^+K^-\pi^+$	2.22 ± 0.06	—	—
$D^{*+} \to D^0\pi^+$	67.7 ± 0.5	$D^0 \to K^-\pi^+$	3.95 ± 0.03
$\Lambda_c^+ \to pK^-\pi^+$	6.28 ± 0.32	—	—
$\Lambda_c^+ \to pK_S^0$	1.59 ± 0.08	$K_S^0 \to \pi^+\pi^-$	69.20 ± 0.05
$\Xi_c^+ \to \Xi^-\pi^+\pi^+$	2.86 ± 1.21 (stat.) ± 0.38 (syst.) [67]	$\Xi^- \to \Lambda\pi^-$	99.887 ± 0.035
		$\Lambda \to p\pi^-$	63.9 ± 0.5

Table 1. Reconstructed decay channels for the measurement of D^0-, D^+-, D_s^+-, D^{*+}-, Λ_c^+-, and Ξ_c^+-hadron signals. The branching ratios (BR) are taken from ref. [66], with the exception of BR($\Xi_c^+ \to \Xi^-\pi^+\pi^+$) which is taken from ref. [67].

3 Data analysis

The charm hadrons and their charge conjugates were reconstructed via the decay channels reported in table 1. The D^0, D^+, D_s^+, and $\Lambda_c^+ \to pK^-\pi^+$ signals were measured by combining pairs or triplets of tracks with $|\eta| < 0.8$ and $p_T > 0.3\,\text{GeV}/c$. Only tracks crossing at least 70 pad rows in the TPC and reconstructed with at least one hit in the SPD detector and further selected with the track-quality criteria described in ref. [19] were considered. The D^{*+}-meson candidates were formed by combining pion tracks selected with the criteria described in ref. [19] with D^0-meson candidates within about 3 standard deviations from the PDG mass [66]. Pions and kaons were identified by requiring the dE/dx and time-of-flight signals measured respectively by the TPC and TOF detectors to be compatible with the expected values within 3 times the detector resolution.

For the measurement of the $\Lambda_c^+ \to pK_S^0$ signal, the reconstruction of the $K_S^0 \to \pi^+\pi^-$ candidates was performed by pairing opposite-sign tracks, selected as discussed in ref. [33], into a neutral decay vertex displaced from the primary vertex. An additional primary proton [68] was considered to reconstruct the Λ_c^+-baryon decay.

The tracks used to reconstruct the Λ- and Ξ^--baryon signals from the Ξ_c^+-baryon cascades were selected as described in ref. [52] and references therein. For this analysis, pion and proton tracks were identified requiring that the measured signals were compatible with the expected values within 3 and 5 times the detector resolution in the TPC and TOF, respectively. The Λ-baryon candidates, reconstructed as pairs of pion and proton tracks, were combined with pion tracks with a transverse momentum larger than $0.15\,\text{GeV}/c$ to form the Ξ^--baryon decay vertex. The masses of the reconstructed Λ and Ξ^- particles were constrained to not deviate more than 1% from their respective PDG masses [66]. Positively charged pion tracks with at least 3 hits in the ITS detector and a transverse momentum larger than $0.4\,\text{GeV}/c$ were selected and combined with the reconstructed Ξ^- baryon to form the Ξ_c^+-baryon candidates.

As in ref. [19], the applied track selections affect the D-meson and Λ_c^+-baryon acceptance in rapidity, which decreases rapidly for $|y| > 0.5$ at low p_T and $|y| > 0.8$ for

$p_T > 5\,\mathrm{GeV}/c$. Therefore, a fiducial acceptance selection was applied on the D-meson and Λ_c^+-baryon rapidity, $|y| < y_{\mathrm{fid}}(p_T)$. The $y_{\mathrm{fid}}(p_T)$ factor increases with a polynomial form from 0.5 to 0.8 in the range $0 < p_T < 5\,\mathrm{GeV}/c$ and $y_{\mathrm{fid}} = 0.8$ above $5\,\mathrm{GeV}/c$. For the reconstruction of the Ξ_c^+-baryon the acceptance criterion $|y| < 0.8$ was applied.

3.1 Analyses with charm-hadron secondary vertex reconstruction

The reconstruction of charm-hadron signals in exclusive hadronic channels is characterised by a substantial combinatorial background arising from the erroneous association of charged tracks to the charm-hadron decays. Given the typical proper lifetime of a few hundred micrometres ($c\tau \approx 120$–$300\,\mu\mathrm{m}$ [66]) the measurement of D^0-, D^+-, D_s^+-meson, and Ξ_c^+-baryon signals was based on the reconstruction of the decay-vertex topologies displaced from the primary vertex. The spatial separation between the production and the decay vertices, allowed the signal-to-background separation to be improved exploiting variables related to the displaced vertex decay topology.

The topological variables considered in the analyses reported in this article are similar to those already used in previous works [19, 20, 23, 49, 52]. Some of them are the track impact parameter in the transverse plane, the distance between the primary and decay vertices (decay length, L), and the pointing angle of the reconstructed charm-hadron momentum to the primary vertex ($\theta_{\mathrm{pointing}}$). As the D^{*+} meson decays strongly, its decay vertex cannot be resolved from the primary one, and so topological selections are only used on the reconstructed D^0 daughter.

The $\Xi_c^+ \to \Xi^- \pi^+ \pi^+$ secondary vertex was reconstructed from the decay channels $\Xi^- \to \Lambda \pi^-$ and $\Lambda \to p\pi^-$ together with their charge conjugates using a Kalman Filter (KF) vertexing algorithm [69]. The algorithm provides a full description of the decay particle both at its production and decay vertex. As discussed in ref. [52], the KF software gives the possibility to set constraints to the mass and the production point of the reconstructed particles using information about the uncertainties of the daughter particle trajectories. Setting the mass constraint to the reconstructed decay products of a decay chain helps to improve the mass and momentum resolution of the reconstructed mother particle, while the production point constraint can be used to determine whether the particle emerges either from the primary or from a displaced vertex. A χ^2 is calculated for the reconstructed particle, which quantifies the probability of the hypothesis that the particle truly emerges from the assigned vertex. In this analysis the mass constraint was applied to the Λ- and Ξ^--baryon candidates. Furthermore, the topological constraint was applied to the reconstructed trajectory of the Ξ_c^+ baryon by fitting it to the primary vertex of the collision.

3.2 Background rejection of D^+, D_s^+, and Ξ_c^+ hadrons with Boosted Decision Trees

To further reduce the background contribution for the reconstruction of the D_s^+-, D^+-, and Ξ_c^+-hadron signals, machine-learning approaches based on Boosted Decision Trees (BDT) with the gradient boosting algorithm XGBoost [70, 71] were adopted. The algorithm was provided with signal examples of D^+, D_s^+, and Ξ_c^+ hadrons from simulations based on the PYTHIA 8 event generator as described in section 2, while the background samples were

obtained from data using candidates in regions of the invariant mass distribution far from the signal peak. For the D^+ mesons, these regions were defined by requiring at least 4σ difference from the expected D^+-meson mass in data, where σ indicates the width of the signal in MC simulations. For the D_s^+ mesons the intervals $1.72 < M(KK\pi) < 1.83\,\mathrm{GeV}/c^2$ and $2.01 < M(KK\pi) < 2.12\,\mathrm{GeV}/c^2$ were considered. These intervals were specifically chosen for the D_s^+ mesons to exclude contributions from D^+ mesons decaying through the same decay channel. For the training sample of Ξ_c^+-baryon background the invariant mass intervals $2.168 < M(\Xi\pi\pi) < 2.411\,\mathrm{GeV}/c^2$ and $2.525 < M(\Xi\pi\pi) < 2.768\,\mathrm{GeV}/c^2$ were considered. The regions correspond to a separation of at least 8σ from the signal in data.

Signals decaying either directly to the expected final state or via resonances were weighted in the training according to their natural abundances [66]. Loose selection criteria were applied to the D-meson and Ξ_c^+-baryon candidates before the training, following the same procedures as described in refs. [19, 23, 52]. For D_s^+-meson candidates, the reconstructed invariant mass of the K^+K^- pair was further required to match the world-average ϕ-meson mass within $\pm 15\,\mathrm{MeV}/c^2$. The main information provided to the BDT to classify signal candidates from background ones relates to the decay-vertex topology and PID. In addition, the χ^2 of the Ξ_c^+ baryons to the primary vertex, and the distance of closest approach between the daughters of the Ξ^- baryon as well as between the daughters of the Ξ_c^+ baryons were considered to discriminate the Ξ_c^+-baryon signal. Independent BDTs were trained in the different p_T intervals of all the analyses, and samples with signal and background similar to those used for the training were employed to test and validate the trained models. Subsequently, they were applied to the real data sample presented in section 2, in which the type of candidate is unknown. The output of the BDT is related to the candidate probability to be a charm hadron or combinatorial background. Selections on the BDT outputs were optimised to obtain a large statistical significance for the signal along with a high fraction of prompt charm hadrons.

3.3 D^0-meson and Λ_c^+-baryon reconstruction down to $p_T = 0$

For tracks with $p_T \lesssim 500\,\mathrm{MeV}/c$, the spatial resolution of the impact parameter measurement is poor ($\gtrsim 100\,\mu m$), weakening the effectiveness of selections based on displaced decay-vertex topology. Furthermore, such selections at low p_T would favour the reconstruction of hadrons originating from beauty-hadron decays (non-prompt), which are by construction more displaced than the prompt ones given the larger proper lifetime of beauty hadrons. For these reasons, the reconstruction of prompt D^0 mesons and Λ_c^+ baryons down to $p_T = 0$ did not apply any topological selections, and instead was performed by simply building pairs and triplets of identified decay tracks.

The measurement of the D^0-meson signals exploited the reconstruction of its secondary vertex, as discussed above, only for candidates with $p_T > 1.5\,\mathrm{GeV}/c$. In the interval $p_T < 1.5\,\mathrm{GeV}/c$, D^0-meson candidates were reconstructed by pairing opposite-charged tracks compatible with the kaon and pion hypotheses without selection criteria on the displaced decay topology. A similar procedure was also used for the prompt D^0-meson measurement in pp collisions at $\sqrt{s} = 5.02\,\mathrm{TeV}$ [19], where the p_T cut-off value between the two techniques was $1\,\mathrm{GeV}/c$. In the present work, the D^0-meson signal was measured

without reconstructing the secondary vertex up to $p_T = 1.5\,\mathrm{GeV}/c$ to reduce the total uncertainty. In fact, this reconstruction technique grants a higher efficiency. In addition, the statistical uncertainties of the measured signal at low p_T were reduced compared to the same measurement in pp collisions at $\sqrt{s} = 5.02\,\mathrm{TeV}$, given that the analysed data sample is larger by about a factor 1.8.

The reconstruction of the Λ_c^+ baryons was performed as reported in ref. [49] and references therein. Given that $c\tau(\Lambda_c^+) \approx 61\,\mu\mathrm{m}$, which is below the spatial pointing resolution at the primary vertex for $p_T < 1\,\mathrm{GeV}/c$, the candidate reconstruction for $p_T < 1\,\mathrm{GeV}/c$ does not exploit the reconstruction of the Λ_c^+-baryon secondary vertex. In this analysis, the $\Lambda_c^+ \to pK^-\pi^+$ signal was reconstructed for the first time in the interval $0 < p_T < 1\,\mathrm{GeV}/c$ by combining triplets of tracks identified as a charged pion, kaon, or proton using the Bayesian PID approach based on the "maximum probability criterion" [72]. The $\Lambda_c^+ \to pK_S^0$ signal measurement in the same p_T interval was performed as in ref. [49]. To select $\Lambda_c^+ \to pK_S^0$ signals, a machine-learning approach based on BDTs with AdaBoost was adopted [73]. The BDTs were trained to disentangle signal from background candidates according to the kinematics of the K_S^0 decay. Some variables utilised in the training were the reconstructed $c\tau$ and the $\pi^+\pi^-$ invariant mass, the impact parameter to the primary vertex of the K_S^0 candidate and its decay daughters, and the PID information of the bachelor track. More details can be found in ref. [33].

3.4 Raw-yield measurement from an invariant mass analysis

The p_T-differential charm-hadron raw yield was measured in the range $0 < p_T < 50\,\mathrm{GeV}/c$ for D^0 and D^+ mesons, $1 < p_T < 50\,\mathrm{GeV}/c$ for D^{*+} mesons, $1 < p_T < 36\,\mathrm{GeV}/c$ for D_s^+ mesons, $0 < p_T < 1\,\mathrm{GeV}/c$ for Λ_c^+ baryons, and $3 < p_T < 4\,\mathrm{GeV}/c$ for Ξ_c^+ baryons. A binned maximum-likelihood fit of the invariant mass distributions of candidates surviving the selection criteria mentioned above was performed. The signal peak was parameterised with a Gaussian function, whose variance was left free for the D mesons and fixed to the value observed in the simulations for the baryons. For the D^0-meson signal extraction, the background was described with a polynomial of second order for $p_T < 2\,\mathrm{GeV}/c$ and an exponential function in all other p_T intervals. The combinatorial background contribution to the invariant mass of $K\pi$ pairs reconstructed in $p_T < 1.5\,\mathrm{GeV}/c$ was described with the track-rotation technique discussed in ref. [19]. Following this method, for each candidate $K\pi$ pair, 19 background candidates were built by rotating the kaon-track momentum in the transverse plane from $\pi/10$ to $19\pi/10$ radians. The resulting combinatorial background was finally subtracted before fitting the invariant mass distribution of the reconstructed $K\pi$ pairs. In all the considered p_T intervals, the contribution of D^0 candidates in the invariant mass distribution reconstructed with the wrong decay particle mass assignment (reflections) was included in the fit. This contribution corresponds to the invariant mass distributions of the reflected signal in MC simulation, as discussed in ref. [19].

For the D^+- and D_s^+-meson signal measurement, the background was described with an exponential function. To grant a better stability in the measurement of the D_s^+-meson signal, an independent Gaussian function was used to fit the peak related to the $D^+ \to K^+K^-\pi^-$ reconstructed signal. The D^{*+}-meson raw yield was measured consider-

ing a threshold function multiplied by an exponential for the background ($a\sqrt{\Delta M - m_\pi} \times e^{b(\Delta M - m_\pi)}$), where ΔM is the mass-difference $M(\mathrm{K}\pi\pi) - M(\mathrm{K}\pi)$, m_π is the pion mass, and a, b are free parameters.

For the Λ_c^+ measurement in $0 < p_T < 1\,\mathrm{GeV}/c$, the combinatorial background in the invariant mass distributions of $\mathrm{pK}^-\pi^+$ triplets and pK_S^0 pairs was described with a polynomial of third and second order, respectively. The combinatorial background for the $\Xi_c^+ \to \Xi^-\pi^+\pi^+$ raw yield measurement was fitted with an exponential.

Figure 1 shows examples of fits to the invariant mass distributions for D-meson candidates in different p_T intervals. This is also shown for Λ_c^+ and Ξ_c^+ baryons in figure 2, where the invariant mass distributions after the subtraction of the parametrised background are shown in the sub-panels together with the Gaussian function describing the signal.

3.5   Cross sections

The p_T-differential cross section of prompt charm hadrons was measured as follows:

$$\left.\frac{\mathrm{d}\sigma^{\mathrm{H}}}{\mathrm{d}p_T}\right|_{|y|<0.5} = \frac{1}{2}\frac{1}{\Delta p_T} \times \frac{f_{\mathrm{prompt}} \times N^{\mathrm{H}+\overline{\mathrm{H}}}_{|y|<y_{\mathrm{fid.}}}}{c_{\Delta y}(\mathrm{Acc} \times \varepsilon)_{\mathrm{prompt}}} \times \frac{1}{\mathrm{BR}} \times \frac{1}{\mathcal{L}_{\mathrm{int}}}. \tag{3.1}$$

The term $N^{\mathrm{H}+\overline{\mathrm{H}}}_{|y|<y_{\mathrm{fid.}}}$ refers to the raw yield, the sum of reconstructed particles and antiparticles obtained from the invariant mass fits shown in figures 1 and 2. This quantity was divided by 2 to obtain the averaged yields between particles and antiparticles, and it was scaled by the prompt fraction f_{prompt} to correct for the charm-hadron signal originating from beauty-hadron decays. The raw yield was corrected by the $c_{\Delta y}(\mathrm{Acc} \times \varepsilon)_{\mathrm{prompt}}$ term, which accounts for the rapidity coverage, the detector acceptance, and the reconstruction and selection efficiency of the prompt charm hadron signal [19]. The production cross section in each p_T interval was obtained by further scaling the raw yield by the p_T-interval width (Δp_T), the branching ratio of the decay channel chosen to reconstruct the signal (BR), and the integrated luminosity ($\mathcal{L}_{\mathrm{int}}$).

Figure 3 shows $c_{\Delta y}(\mathrm{Acc} \times \varepsilon)$ as a function of p_T for prompt and non-prompt D^0, D^+, D^{*+}, and D_s^+ mesons, where the non-prompt D mesons are those produced in beauty-hadron decays. Given the average larger displacement from the primary vertex of beauty-hadron decay vertices due to their long lifetime, the selection criteria applied on the decay length in general enhance the $c_{\Delta y}(\mathrm{Acc} \times \varepsilon)$ factor of non-prompt D mesons with respect to that of prompt ones, especially at low p_T. The $c_{\Delta y}(\mathrm{Acc} \times \varepsilon)$ values of non-prompt D^0 mesons for $p_T > 1.5\,\mathrm{GeV}/c$ are higher than those of prompt ones. On the other hand, the values for prompt and non-prompt D^0 mesons are compatible for $p_T < 1.5\,\mathrm{GeV}/c$, because in this interval no selection criteria based on the intrinsic displacement of the decay are applied. This explains the significant drop of the efficiency at $p_T = 1.5\,\mathrm{GeV}/c$, as shown in the top-left panel of figure 3. The $c_{\Delta y}(\mathrm{Acc} \times \varepsilon)$ factor of prompt and non-prompt D^{*+} mesons are compatible above $p_T = 5\,\mathrm{GeV}/c$, while the $c_{\Delta y}(\mathrm{Acc} \times \varepsilon)$ factor for prompt D^+ and D_s^+ mesons is larger than that of non-prompt mesons for p_T higher than $5\,\mathrm{GeV}/c$. Conversely, in the low-p_T region, the trend is reversed.
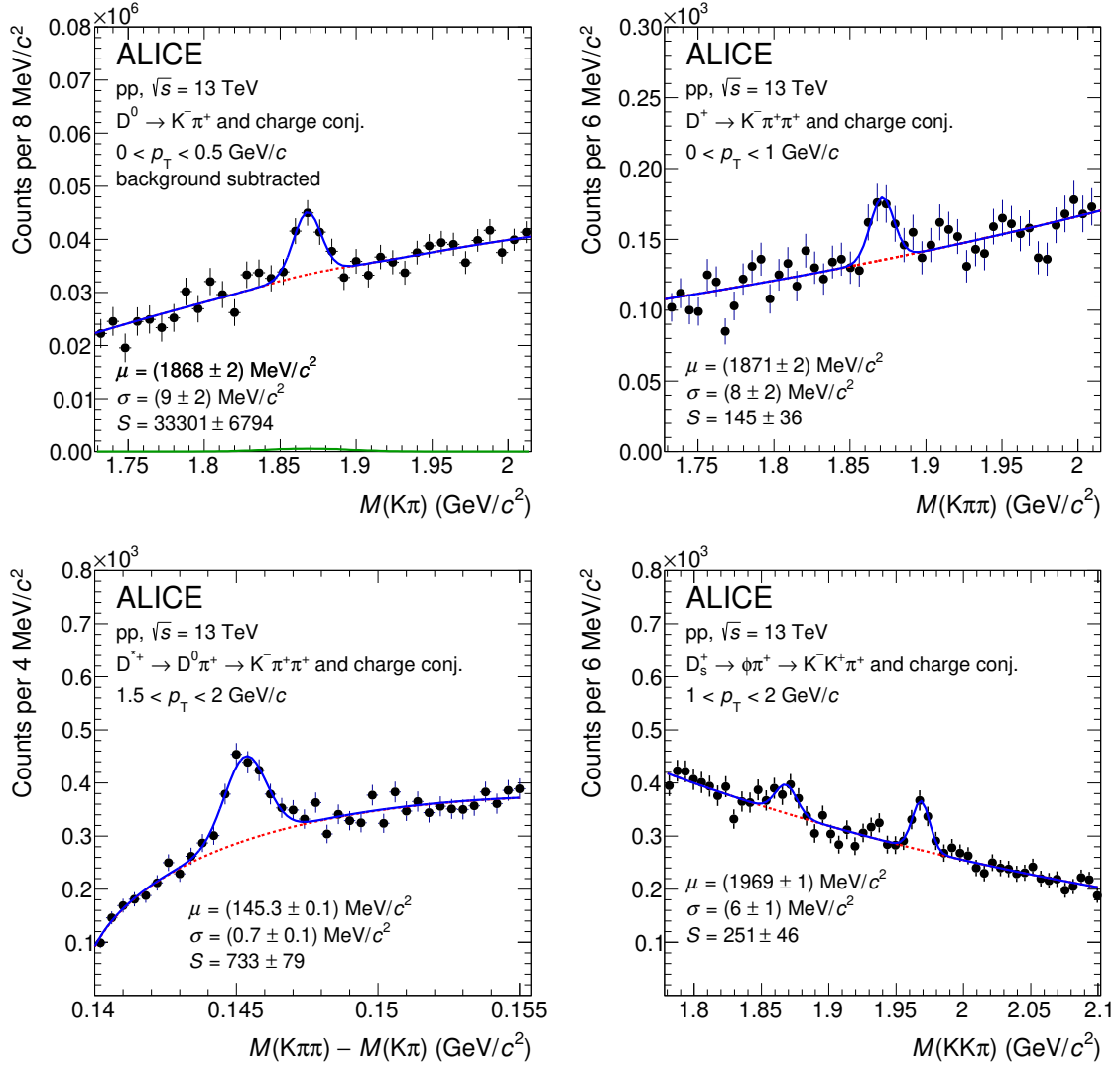
Figure 1. Invariant mass or mass-difference distributions of D^0-meson candidates (top-left), D^+-meson candidates (top-right), D^{*+}-meson candidates (bottom-left), D_s^+-meson candidates (bottom-right), and charge conjugates in $0 < p_T < 0.5\,\mathrm{GeV}/c$, $0 < p_T < 1\,\mathrm{GeV}/c$, $1.5 < p_T < 2.0\,\mathrm{GeV}/c$, and $1 < p_T < 2\,\mathrm{GeV}/c$, respectively. The blue solid lines show the total fit functions as described in the text and the red dashed lines represent the background. In the case of D^0, the combinatorial background estimated with the track-rotation technique was subtracted, the red-dashed line is the residual background, and the green line represents the contribution of the reflections. In the case of D_s^+, the peak at lower invariant mass represents the reconstructed $D^+ \to K^+K^-\pi^+$ signal. The values of the mean (μ) and the peak width (σ) of the signal peak are reported together with the signal counts (S). The reported uncertainties are only the statistical uncertainties from the fit.
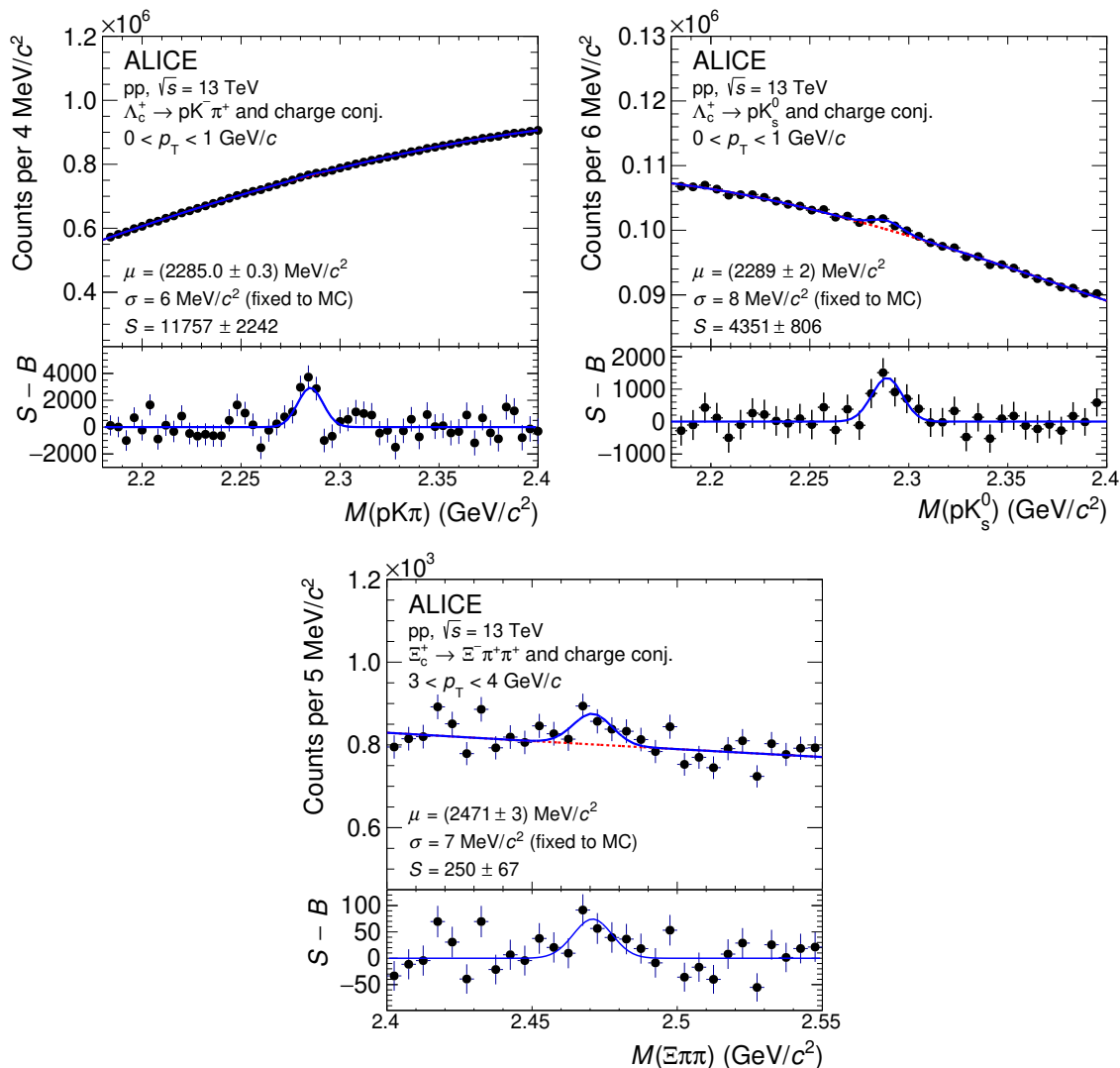
Figure 2. Invariant mass distributions of Λ_c^+- and Ξ_c^+-baryon candidates and charge conjugates at low transverse momentum in pp collisions at $\sqrt{s} = 13\,\mathrm{TeV}$. The blue solid lines show the total fit functions as described in the text and the red dashed lines represent the background. The values of the mean (μ) and the peak width (σ) of the signal peak are reported together with the signal counts (S). The bottom panels report the charm-baryon invariant mass distribution after the subtraction of the background candidates parametrised as detailed in the main text ($S - B$). The Gaussian σ are fixed to values from MC simulations. The reported uncertainties are only the statistical uncertainties from the fit.
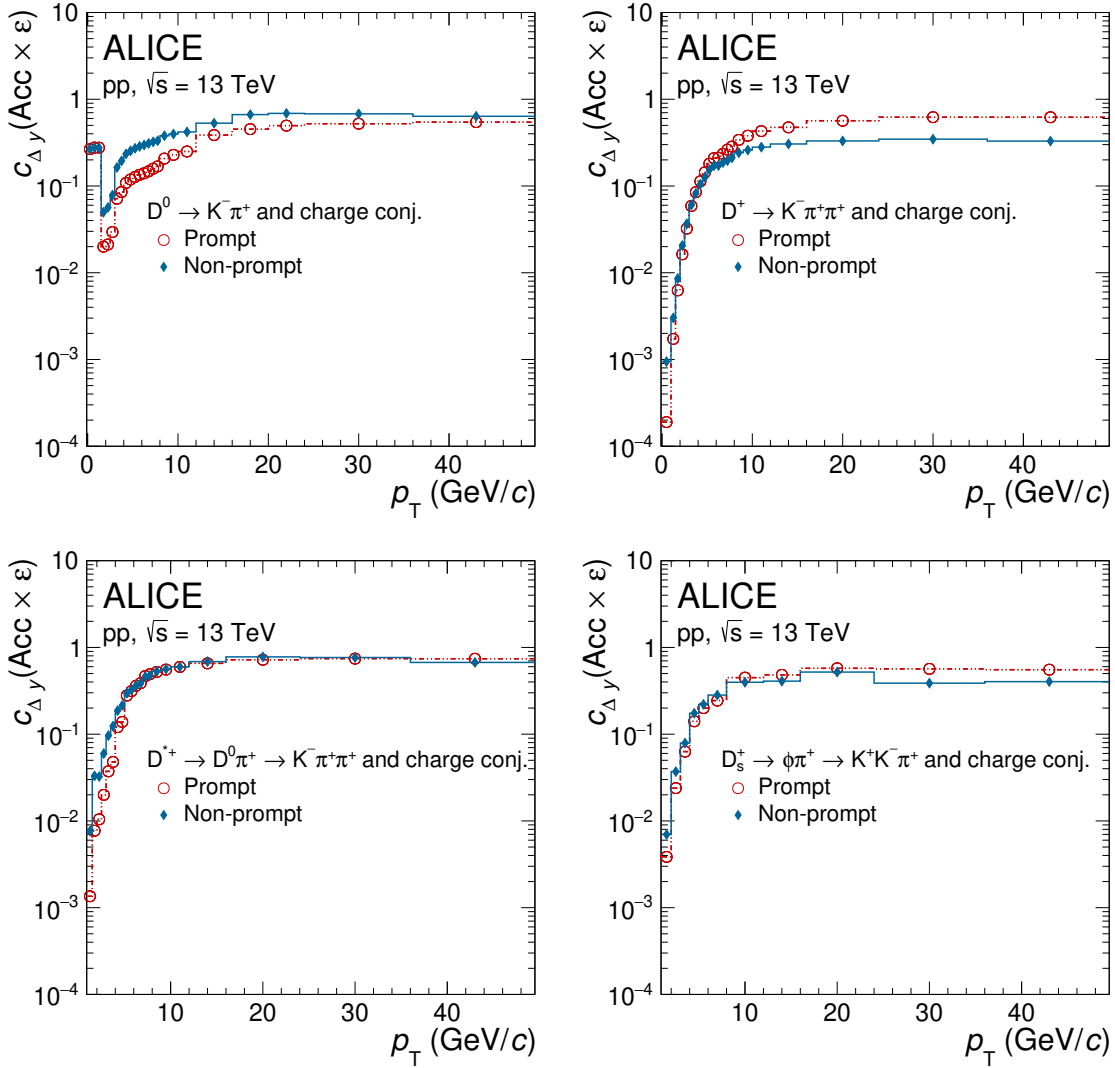
Figure 3. Correction factors $c_{\Delta y}(\text{Acc} \times \varepsilon)$ for the prompt and non-prompt D^0-meson (top-left), the D^+-meson (top-right), the D^{*+}-meson (bottom-left), and the D_s^+-meson (bottom-right) as a function of p_T.

The $c_{\Delta y}(\text{Acc} \times \varepsilon)$ term for the prompt and non-prompt $\Lambda_c^+ \to pK^-\pi^+$ signal reconstruction without selections on topological variables is about 3% in the interval $0 < p_T < 1\,\text{GeV}/c$, while that for the $\Lambda_c^+ \to pK_S^0$ in the same p_T interval with selections based on the BDT classification is about 11% for the prompt signal and about 10% for the non-prompt one. The same term for the prompt and non-prompt Ξ_c^+-baryon reconstruction in the interval $3 < p_T < 4\,\text{GeV}/c$ is around 0.7%. In the case of the Ξ_c^+ baryon, the efficiency was calculated after weighting the simulated p_T distributions to match the Ξ_c^0-baryon p_T-differential cross section measured in pp collisions at $\sqrt{s} = 13\,\text{TeV}$ following the procedure described in ref. [52]. The $c_{\Delta y}(\text{Acc} \times \varepsilon)$ correction factors of all mesons and baryons were computed taking into account all the possible resonant channels which produce the final states chosen for the reconstruction, as described in refs. [33, 52, 74].

The measured raw yield was further corrected by the fraction of prompt reconstructed hadrons (f_{prompt}). This fraction was calculated similarly to previous measurements (see e.g. refs. [19, 22]) adopting the beauty-hadron production cross sections from FONLL calculations, the beauty-hadron decay kinematics modelled with PYTHIA 8 [39], and the efficiencies reported in figure 3 for the non-prompt D mesons. In the beauty-hadron production cross section calculations from FONLL, the beauty-quark fragmentation fractions were taken from LHCb measurements [75] for $b \to \Lambda_b^0$ and the averaged results from LEP for B mesons [76]. A prediction for the non-prompt Ξ_c^+-baryon cross section was made by scaling the prediction for the non-prompt Λ_c^+-baryon cross section with the ratio of the sums of the beauty hadron fragmentation fractions times branching ratios, $\sum_{h_b} b \to h_b \to \Xi_c^+$ and $\sum_{h_b} b \to h_b \to \Lambda_c^+$. Using the fragmentation fractions from LHCb measurements [75] and the BR from PYTHIA 8 [39] simulations the ratio of the beauty-hadron sums can be approximated as $(b \to \Xi_b^{0,-} \to \Xi_c^+)/(b \to \Lambda_b^0 \to \Lambda_c^+)$. Furthermore, the $b \to \Xi_b$ fragmentation fraction was assumed to be equal to $c \to \Xi_c$ and the non-prompt Ξ_c^+/Λ_c^+ ratio was taken to be equal to the prompt ratio. Under these assumptions the scaling factor for the non-prompt Λ_c^+-baryon cross section can be approximated as the prompt cross section ratio of Λ_c^+- and Ξ_c-baryons, which was taken from ref. [52].

For D^0, D^+, D^{*+}, and D_s^+ mesons, the values of f_{prompt} range between 81% and 96% depending on the D-meson species and p_T interval. The f_{prompt} fractions for Λ_c^+ baryons reconstructed in $0 < p_T < 1\,\mathrm{GeV}/c$ in the $pK^-\pi^+$ and pK_S^0 decay channels are about 98% and 97%, respectively. The same quantity for Ξ_c^+ baryons was found to be 97% in the p_T interval $3 < p_T < 4\,\mathrm{GeV}/c$.

4 Systematic uncertainties

The systematic uncertainties of the prompt charm-hadron production cross sections were estimated taking into account the following sources: (i) the stability of the signal extraction from the fits to the invariant mass distribution described in section 3; (ii) the track reconstruction efficiency; (iii) the selection efficiency of charm hadrons; (iv) the PID selection efficiency; (v) the shape of the generated p_T distribution for charm hadrons in MC simulations; (vi) the detector material budget description in MC simulations; (vii) the estimation of the fraction of prompt hadrons; (viii) the branching ratios of the decay channels used in the analyses; (ix) the collected luminosity. The values of the estimated uncertainties in some representative p_T intervals are reported in tables 2 and 3 for the prompt D mesons and charm baryons, respectively. The total uncertainties in the analyses of each cross section measurement were calculated as the quadratic sum of these contributions. The uncertainty sources were assumed to be uncorrelated among the charm-hadron species, with the exception of (ii), (vi), (vii) and (ix). In the following, the strategies used to estimate the values of each source of uncertainty are briefly described. More details on the methodologies used to estimate the systematic uncertainties can be found in previous publications (see refs. [19–23, 49, 51–53]).

The systematic uncertainty of the charm-hadron raw yield extraction was estimated in each p_T interval by repeating the fits several hundred times by varying the fit configurations.

	D^0		D$^+$		D^{*+}		D$_s^+$	
p_T (GeV/c)	0–0.5	36–50	0–1	36–50	1–1.5	36–50	1–2	24–36
Signal extraction	9%	5%	10%	5%	10%	2%	8%	5%
Tracking efficiency	4%	6%	5.5%	8%	4.5%	6.5%	4%	8%
Selection efficiency	negl.	3%	7%	2%	10%	2%	10%	3%
PID efficiency	negl.	negl.	negl.	negl.	negl.	negl.	negl.	negl.
p_T shape in MC	1%	negl.	5%	negl.	3%	negl.	1%	negl.
Material budget in MC	negl.	negl.	negl.	negl.	negl.	negl.	negl.	negl.
Prompt fraction	+2.4% −2.3%	+1.8% −0.8%	+6.1% −6.0	+0.9% −0.8%	+8.6% −8.6%	+1.2% −0.8%	+6% −6%	+2% −2%
Branching ratio	0.8%		1.7%		1.1%		2.7%	
Luminosity	1.6%							
Total uncertainty	10%	9%	16%	9%	18%	7%	15%	11%

Table 2. Relative systematic uncertainties of the measured cross section of prompt D^0, D$^+$, D^{*+}, and D$_s^+$ mesons in pp collisions at $\sqrt{s} = 13$ TeV. The values reported in this table are those from the lowest and highest p_T intervals considered in the analyses. Uncertainties found to be negligible are indicated as such (negl.).

	$\Lambda_c^+ \rightarrow pK^-\pi^+$	$\Lambda_c^+ \rightarrow pK_S^0$	Ξ_c^+
p_T (GeV/c)	0–1	0–1	3–4
Signal extraction	12%	11%	9%
Tracking efficiency	5%	5%	6%
Selection efficiency	10%	5%	3%
PID efficiency	5%	1%	negl.
p_T shape in MC	1%	negl.	3%
Material budget in MC	negl.	4%	4%
Prompt fraction	+0.9% −1.3%	+1.6% −2.1%	+2.9% −3.3%
Branching ratio	5.1%	5.0%	44.4%
Luminosity	1.6%		
Total uncertainty	18%	15%	46%

Table 3. Relative systematic uncertainties of the measured cross section of prompt Λ_c^+ and Ξ_c^+ baryons in pp collisions at $\sqrt{s} = 13$ TeV. The systematic uncertainties evaluated for the two Λ_c^+-baryon decay channels are reported separately. Uncertainties found to be negligible are indicated as such (negl.).

Such variations included, for example, the change of the lower and the upper limits of the fit range and of the background fit function. The same approach was considered using a method based on bin counting after subtracting the background estimated from a fit of the sidebands to test the description of the line shape of the signal. The uncertainty was assigned by calculating the RMS of the distribution of the signal yields obtained from all these variations. The uncertainty for the D-meson measurements ranges from about 2% to 10% depending on the p_T interval and the particle species. The uncertainty for the Ξ_c^+ baryon is about 9% in $3 < p_T < 4\,\mathrm{GeV}/c$. For the Λ_c^+-baryon signal in the interval $0 < p_T < 1\,\mathrm{GeV}/c$, additional trials to further test the stability of the background parametrisation were included, similarly to what was done for the $\Sigma_c^{0,++}$-baryon signal measurement in ref. [49]. The combinatorial background was described with a template distribution multiplied by a parabola. The template was obtained by recalculating the invariant mass after rotating a daughter track similarly to what was done for the D^0-meson signal extraction at low p_T (see section 3). The uncertainty for the Λ_c^+-baryon raw yield measurement in $0 < p_T < 1\,\mathrm{GeV}/c$ was estimated to be about 12% and 11% in the analyses of the $pK^-\pi^+$ and pK_S^0 channels, respectively.

The systematic uncertainty of the track reconstruction efficiency accounts for possible discrepancies between data and MC in the TPC-ITS track prolongation efficiency and in the selection efficiency due to track-quality criteria. The per-track systematic uncertainty was evaluated by varying the track-quality selection criteria in the TPC detector and by comparing the prolongation probability of the TPC tracks to the ITS hits in data and MC simulations. They are subsequently propagated to the charm-hadron candidates via their decay kinematics evaluated with MC simulations. For the D mesons, this source introduces an uncertainty that grows with increasing p_T from about 4% at low transverse momenta up to about 7% in the highest p_T intervals. For the Λ_c^+- and Ξ_c^+-baryon reconstruction, the value of this uncertainty is about 5% and 6%, respectively.

The systematic uncertainty related to the selection efficiency was studied by repeating the full analyses with varied selection criteria compared to the reference ones, resulting in a noticeable modification of the efficiencies, raw yield, and background values. The magnitude for this source of uncertainty was then assigned considering the dispersion and the shift of the production cross sections with respect to the reference one. The value of this uncertainty generally decreases with increasing p_T. For the D mesons, it ranges from roughly 10% at low p_T to about 2% at high p_T. In the case of the D^0-meson analysis at $p_T < 1.5\,\mathrm{GeV}/c$, where no selections on the displaced decay vertex topologies are applied, the stability was tested against variations of the single-track p_T selection, and no systematic effect was observed. With a similar procedure, a 10% uncertainty was assigned in the $\Lambda_c^+ \to pK^-\pi^+$ analysis. The uncertainties for the $\Lambda_c^+ \to pK_S^0$ and the Ξ_c^+-baryon selection amount to 5% and 3%, respectively.

The systematic uncertainty of the PID selection efficiency for the D-meson species was estimated by comparing the PID selection efficiencies in the data and in the simulation for pions and kaons. A pure sample of pions was isolated considering decays of strange hadrons. To evaluate the systematic uncertainty of the kaon identification using the TPC information, a pure sample of kaons was isolated applying a strict selection on the TOF

information, and vice versa. The resulting per-track uncertainty was then propagated to the D mesons using their decay kinematics. As an additional test, the analyses were repeated without any PID requirement on the candidate D-meson daughter tracks. The systematic uncertainty of the PID selection efficiency was found to be negligible in the analysed p_T intervals. A similar strategy was adopted to estimate an uncertainty related to the PID selections adopted for the $\Lambda_c^+ \to pK_S^0$ candidate reconstruction before the BDT application, and a 1% uncertainty was assigned in this case. For the $\Lambda_c^+ \to pK^-\pi^+$ reconstruction, this uncertainty was estimated as done in refs. [33, 49, 60], namely repeating the cross section measurement using the threshold probability criterion for the application of the Bayesian PID approach. The assigned uncertainty in this case is around 5%.

Possible differences between the generated hadron p_T distributions from simulation and the spectra observed in data influence the calculation of the $c_{\Delta y}(\mathrm{Acc} \times \varepsilon)$ factor and introduce an additional source of systematic uncertainty. To estimate this effect, the simulated p_T distributions were weighted to match the charm-hadron p_T spectra from different model calculations. The $c_{\Delta y}(\mathrm{Acc} \times \varepsilon)$ correction factor was recomputed using the weighted spectra and an uncertainty was assigned based on the difference between the charm-hadron production cross sections obtained with the default and the weighted $c_{\Delta y}(\mathrm{Acc} \times \varepsilon)$. For D mesons, this uncertainty was estimated using FONLL as an alternative with respect to PYTHIA 8 to simulate the D-meson p_T distributions. It was found to range between 1% and 5% for $p_T < 2\,\mathrm{GeV}/c$ depending on the D-meson species, and to be negligible at higher p_T. For the Λ_c^+-baryon analyses, the reconstruction efficiency was recalculated by considering the shape from the PYTHIA 8 Monash tune, which is the default adopted in the MC simulations, and that of PYTHIA 8 CR-BLC Mode 2. The assigned uncertainty is about 1%, corresponding to the maximum variation observed in the efficiency-times-acceptance quantity. In a similar way, spectra from Catania, SHM+RQM, QCM, and PYTHIA 8 CR-BLC Mode 0, 2, 3 were considered for recalculating the reconstruction efficiency for the Ξ_c^+-baryon signal and an uncertainty of 3% was assigned.

To provide an unbiased efficiency correction, the real detector geometry must be accurately implemented in the MC simulations. Recent investigations based on the reconstruction of photons in the material of the ALICE apparatus highlighted a difference of 24% and 7% in the current MC simulations for the material budget description of the silicon pixels in the ITS and the thermal shield in the TPC inner containment vessel [77]. Such discrepancies may introduce biases in the description of multiple scattering and absorption probability in the material. This may affect in particular the heaviest particles (i.e. protons), for which such effects are expected to be more significant. The $c_{\Delta y}(\mathrm{Acc} \times \varepsilon)$ term was recomputed in dedicated MC productions covering the material budget variations mentioned above. A systematic uncertainty was assigned according to the difference to the $c_{\Delta y}(\mathrm{Acc} \times \varepsilon)$ correction factor calculated with the default MC simulations used to correct the data. A value of 4% corresponding to the maximum observed variation was assigned to the measurement of the $\Lambda_c^+ \to pK_S^0$ and Ξ_c^+ signals. No significant effects were observed for the prompt $\Lambda_c^+ \to pK^-\pi^+$ and D^0-meson signal reconstruction, given the looser selections employed in the reconstruction, as well as in the other D-meson analyses. Therefore, no systematic uncertainty was assigned in these cases.

The systematic uncertainty related to the correction for the fraction of charm hadrons originating from beauty-hadron decays accounts for the uncertainties accompanying the several ingredients adopted in the calculation of f_{prompt}, as described in section 3. The uncertainties for the D mesons were estimated by varying the FONLL parameters, namely the b-quark mass, the renormalisation (μ_R), and factorisation scales (μ_F), as discussed in ref. [19]. The assigned values range from 1% to 9% depending on the p_T interval and the D-meson species. Similarly, those assigned to the Λ_c^+-baryon analyses range from 1% to 2%. For the estimation of the fraction of prompt Ξ_c^+ baryons, the uncertainties of the non-prompt Λ_c^+-baryon cross section were taken into account. In addition, in order to account for possible differences between the Ξ_c^0/Λ_c^+ and Ξ_b^-/Λ_b^0 ratios, the latter cross section ratio was scaled up by a conservative factor of 2. The lower uncertainty of the ratio was obtained by scaling it down by a factor of 0.05 to capture the Ξ_b^-/Λ_b^0 value measured at forward rapidity by the LHCb collaboration [78]. The upper and lower limits of the uncertainty band of f_{prompt} were taken as the quadratic sum of the two described contributions. The systematic uncertainty assigned to the Ξ_c^+-baryon measurement is around 2%.

5 Results

5.1 Prompt D-meson p_T-differential cross sections

The p_T-differential production cross sections of prompt D^0, D^+, D^{*+}, and D_s^+ mesons at midrapidity ($|y| < 0.5$) in pp collisions at $\sqrt{s} = 13\,\text{TeV}$ are shown in figure 4. Statistical and systematic uncertainties are depicted as vertical lines and empty boxes, respectively. The p_T-differential production cross sections of prompt D^0 and D_s^+ mesons are compatible with previously published results [49, 60], providing an extended p_T coverage and a finer p_T binning.

The measured prompt D-meson p_T-differential cross sections are compared in figure 5 with results from pQCD calculations performed with different schemes: FONLL [13, 14] (not available for the D_s^+ mesons), GM-VFNS framework [7, 8], and a calculation based on the k_T-factorisation approach [15]. The theoretical uncertainties of the predictions based on these calculations are depicted as boxes.

In the case of FONLL, the theoretical uncertainty includes the variation of the factorisation and renormalisation scales, the variation of the charm-quark mass value, and the uncertainties on the PDFs employed on the calculations from the reference case (CTEQ6.6 [79]), as discussed in refs. [14, 30]. The D-meson fragmentation fractions, $f(c \to D)$ adopted in the FONLL calculations were taken from ref. [76].

The configuration of the GM-VFNS calculations was the same as the one employed in ref. [23]. The CTEQ6.6 PDFs [79] are used as default. The factorisation and renormalisation scales μ_F and μ_R used for the central values correspond to those adopted in ref. [19]. The calculations based on GM-VFNS were performed in the same p_T intervals as the measurements, except for the first interval of the D^0- and D^+-meson results that start from $0.5\,\text{GeV}/c$. According to the authors, calculations down to $p_T = 0$ at such values of $\sqrt{s}$ were compromised by numerical instabilities.
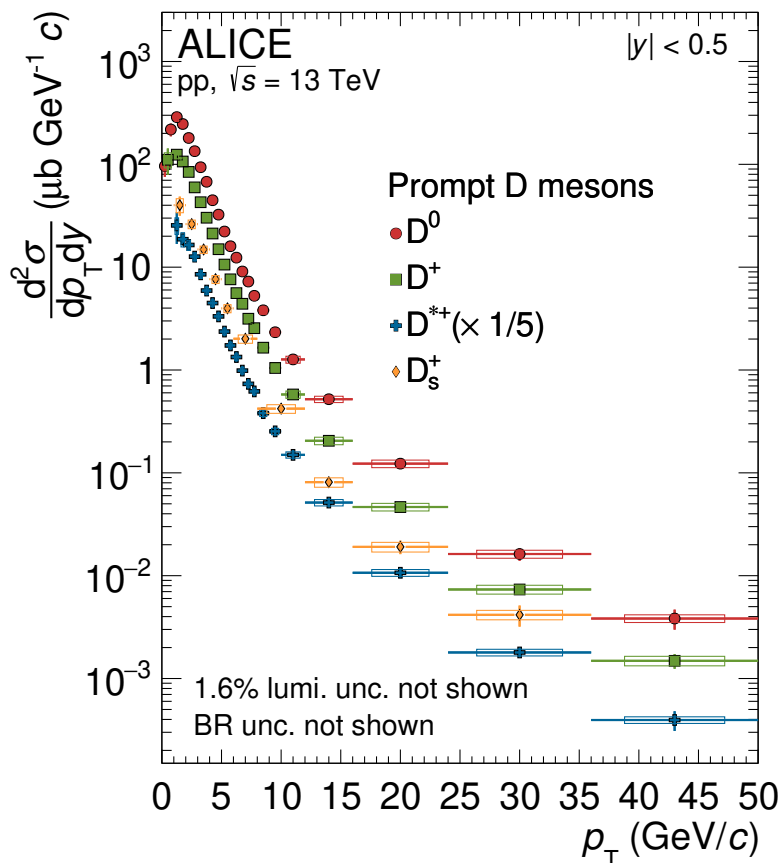
Figure 4. p_{T}-differential production cross sections of prompt D^0, D^+, D^{*+}, and $\mathrm{D}_{\mathrm{s}}^+$ mesons at midrapidity ($|y| < 0.5$) in pp collisions at $\sqrt{s} = 13\,\mathrm{TeV}$. The vertical bars and boxes report the statistical and systematic uncertainties, respectively. The total systematic uncertainties reported in the plots do not include the contributions of the luminosity and the branching ratio, which are reported separately. The measured prompt D^{*+}-meson production cross section was scaled by a factor of 1/5 for better visibility reasons.

A variable-flavour-number scheme was adopted in the case of QCD calculations within the k_{T}-factorisation framework. The k_{T}-factorisation calculations overcame the factorisation scheme employed in the predictions reported in refs. [22, 23] for the estimation of the unintegrated PDFs and the final production cross section. As discussed in ref. [15], the variable-flavour-number scheme was demonstrated to be more efficient, resumming to all orders some large logarithms $\ln(p_{\mathrm{T}}^2/m_{\mathrm{Q}}^2)$ thanks to the heavy-quark distribution function. The authors also demonstrated the importance of excitation quantum processes to correctly describe the production of charm quarks. The theoretical uncertainties were estimated by varying the μ_{F} scale.

In analogy to what was observed at $\sqrt{s} = 5.02\,\mathrm{TeV}$ [19, 23] and $\sqrt{s} = 7\,\mathrm{TeV}$ [22], the pQCD calculations implementing the factorisation approach describe within uncertainties the measured D-meson production cross sections in pp collisions at LHC energies. In the case of FONLL calculations, the data systematically lie on the upper edge of the theoretical uncertainty up to $p_{\mathrm{T}} = 36\,\mathrm{GeV}/c$. In the interval $36 < p_{\mathrm{T}} < 50\,\mathrm{GeV}/c$, the data are in
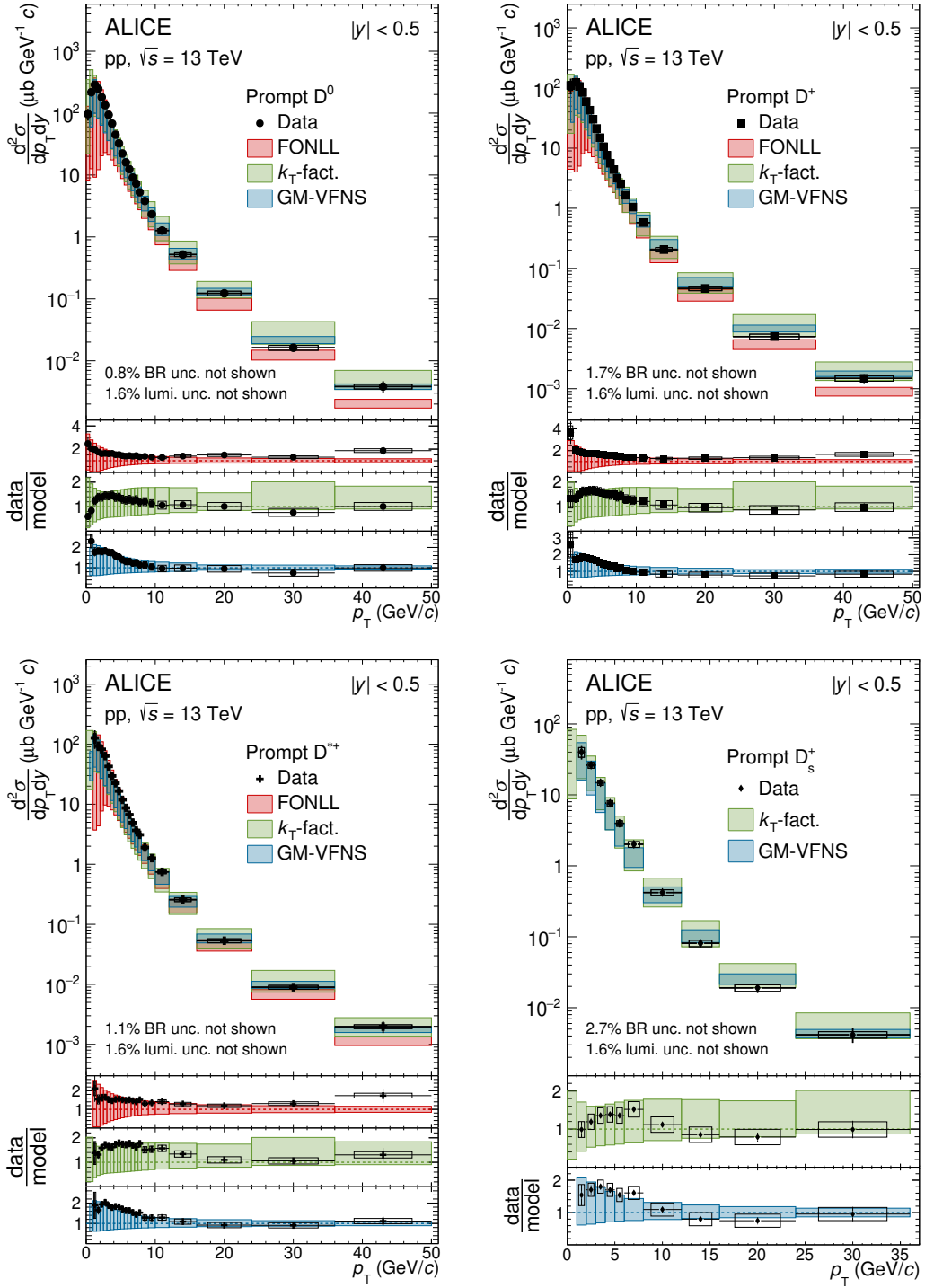
Figure 5. p_{T}-differential production cross sections for prompt D mesons in comparison with pQCD calculations: FONLL [13, 14], GM-VFNS [7, 8], and k_{T}-factorisation [15]. The uncertainty on the predictions is depicted as coloured boxes. The ratios of the data to the theoretical predictions are shown in the lower part of each panel. The statistical (systematic) uncertainties are depicted as vertical bars (boxes).
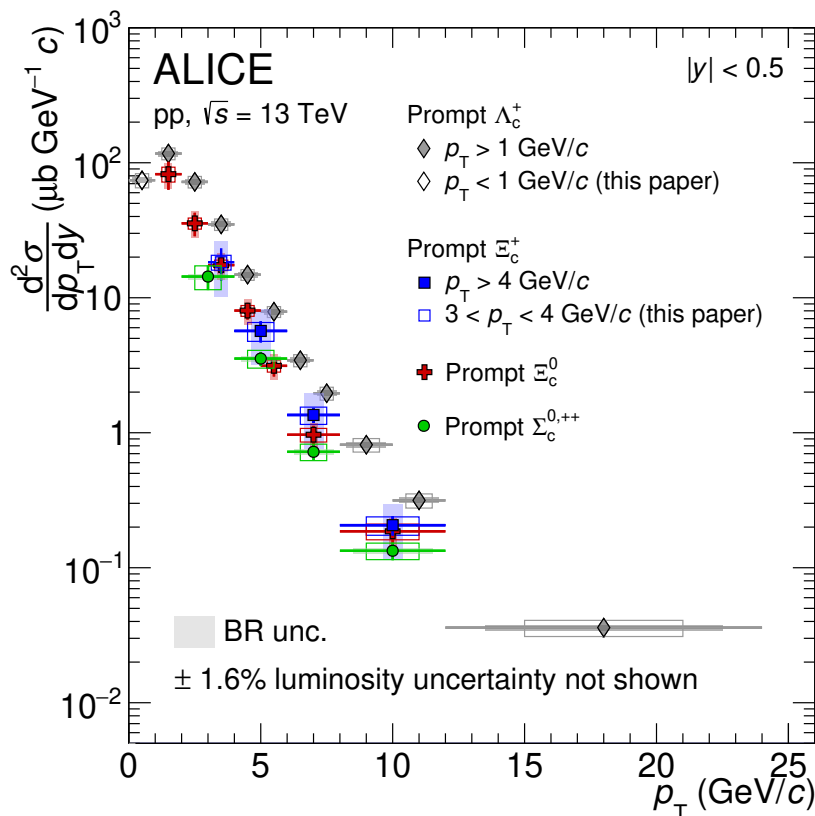
Figure 6. p_T-differential production cross sections of prompt Λ_c^+, Ξ_c^0, Ξ_c^+, and $\Sigma_c^{0,++}$ baryons at midrapidity ($|y| < 0.5$) in pp collisions at $\sqrt{s} = 13$ TeV [49, 52]. The statistical (systematic) uncertainties are shown as vertical bars (boxes). The shaded boxes report the BR uncertainty.

agreement with the upper edge of the calculations within about 2σ. The central values of the calculation in the GM-VFNS framework slightly underestimate (overestimate) the data in the low-(high-)p_T region. The k_T-factorisation calculation is in good agreement with the data in the low-p_T and intermediate-p_T region. However, the ratio between the measurement and the calculation is not flat as a function of p_T, and the model prediction tends to overestimate the data at high p_T.

5.2 Prompt charm-baryon measurements down to low p_T

A compilation of the p_T-differential production cross sections of prompt charm baryons measured at midrapidity ($|y| < 0.5$) in pp collisions at $\sqrt{s} = 13$ TeV is shown in figure 6. The p_T-differential cross section of prompt Λ_c^+ baryons for $p_T > 1$ GeV/c and that of $\Sigma_c^{0,++}$ baryons are those published in ref. [49].

The new measurement of the prompt Λ_c^+-baryon production cross section in the interval $0 < p_T < 1$ GeV/c was obtained by averaging the Λ_c^+-baryon cross sections measured via both the $\Lambda_c^+ \to pK^-\pi^+$ and $\Lambda_c^+ \to pK_S^0$ decay channels, which are compatible within about 2σ. The weights adopted in the average were calculated using the relative uncertainties of the sources assumed as uncorrelated between the two decay channels, and accounting for

the partial correlation between their branching ratios. The strategy was the same as the one followed in ref. [49].

The production cross section of the prompt Ξ_c^+ baryons in the interval $3 < p_T < 4\,\mathrm{GeV}/c$ is the first measurement of the prompt Ξ_c^+-baryon cross section down to $p_T = 3\,\mathrm{GeV}/c$, and it extends the Ξ_c^+-baryon results already published in ref. [52]. Within the current uncertainties, especially those related to the branching ratio of the Ξ_c^+ baryons, the p_T-differential cross sections of the Ξ_c^+ and Ξ_c^0 baryons do not show any significant charge dependence in the common range of the measurements.

5.3   Charm-hadron cross section ratios

5.3.1   Meson-to-meson ratios

The ratios of the p_T-differential cross sections of prompt D^+, D^{*+}, and D_s^+ mesons to prompt D^0 mesons as well as prompt D_s^+ to prompt D^+ meson in pp collisions at $\sqrt{s} = 13\,\mathrm{TeV}$ are reported in figure 7. In the evaluation of the systematic uncertainties, the contributions of the yield extraction and selection efficiency were considered as uncorrelated, while those of the prompt-fraction correction, the tracking efficiency and the luminosity were treated as fully correlated among the different D-meson species.

The results in pp collisions at $\sqrt{s} = 13\,\mathrm{TeV}$ are compared with the ones obtained at $\sqrt{s} = 5.02\,\mathrm{TeV}$ [19, 23] and $\sqrt{s} = 7\,\mathrm{TeV}$ [22]. A hint of increase with p_T is visible for the D_s^+/D^0, D_s^+/D^+, and $D_s^+/(D^0 + D^+)$ ratios in the interval $p_T < 8\,\mathrm{GeV}/c$. In the other cases, the p_T-differential cross section ratios do not show any significant dependence on the p_T of the D mesons considering the uncertainties. No appreciable dependence on the collision energy is observed within the current experimental uncertainties. This suggests common fragmentation functions of charm quarks to pseudoscalar and vector mesons and to mesons with and without strange quark content at different LHC energies.

5.3.2   Baryon-to-meson ratios

The ratio of the p_T-differential cross sections of the prompt Λ_c^+ baryons to D^0 mesons at midrapidity ($|y| < 0.5$) in pp collisions at $\sqrt{s} = 13\,\mathrm{TeV}$ is shown in the left panels of figure 8. The measurement at $p_T > 1\,\mathrm{GeV}/c$ was performed with the prompt Λ_c^+-baryon cross section published in ref. [49], which was extended down to $p_T = 0$ with the measurement in $0 < p_T < 1\,\mathrm{GeV}/c$ from this paper. The ratio was then obtained by using the prompt D^0-meson cross section reported in section 5.1 as denominator. In the ratio, the systematic uncertainties related to the tracking efficiency, the prompt fraction correction, and the luminosity were propagated as correlated, while those from other sources were treated as fully uncorrelated.

The results were compared with several model calculations, namely different tunes of PYTHIA 8, the Catania and QCM models implementing quark recombination, and the SHM+RQM model based on statistical hadronisation with additional excited charm-baryon states. The uncertainty band assigned to the predictions from Catania model is related to the variations on the width of the Wigner function used to calculate the probability of baryon formation. The uncertainty band assigned to the predictions from
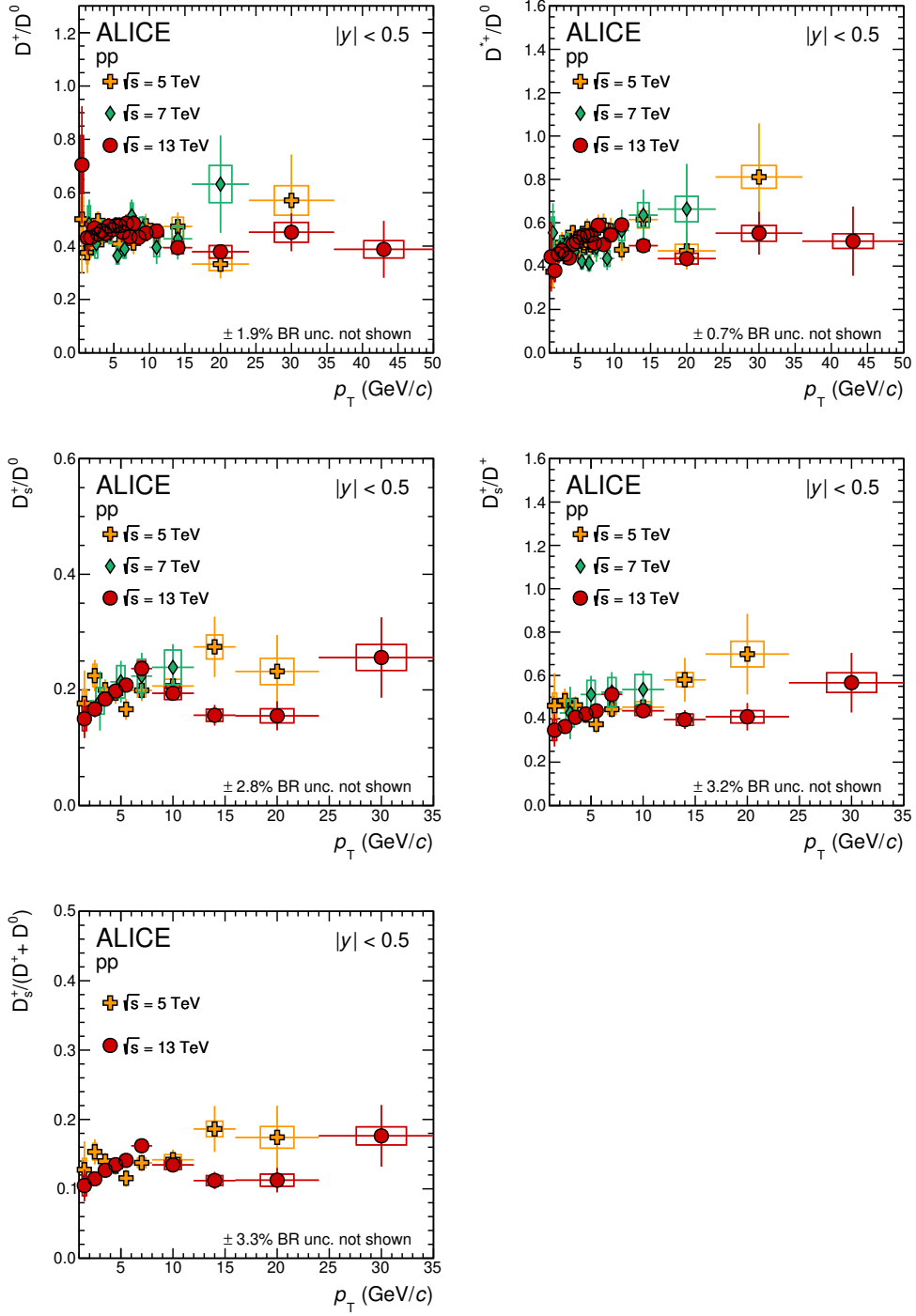
Figure 7. Ratios of production cross sections as a function of p_T of prompt D^+/D^0, D^{*+}/D^0, D_s^+/D^0, D_s^+/D^+, and $D_s^+/(D^0 + D^+)$ mesons in pp collisions at $\sqrt{s} = 5.02$ TeV [19, 23], $\sqrt{s} = 7$ TeV [22], and $\sqrt{s} = 13$ TeV. Vertical bars (boxes) report the statistical (systematic) uncertainties.
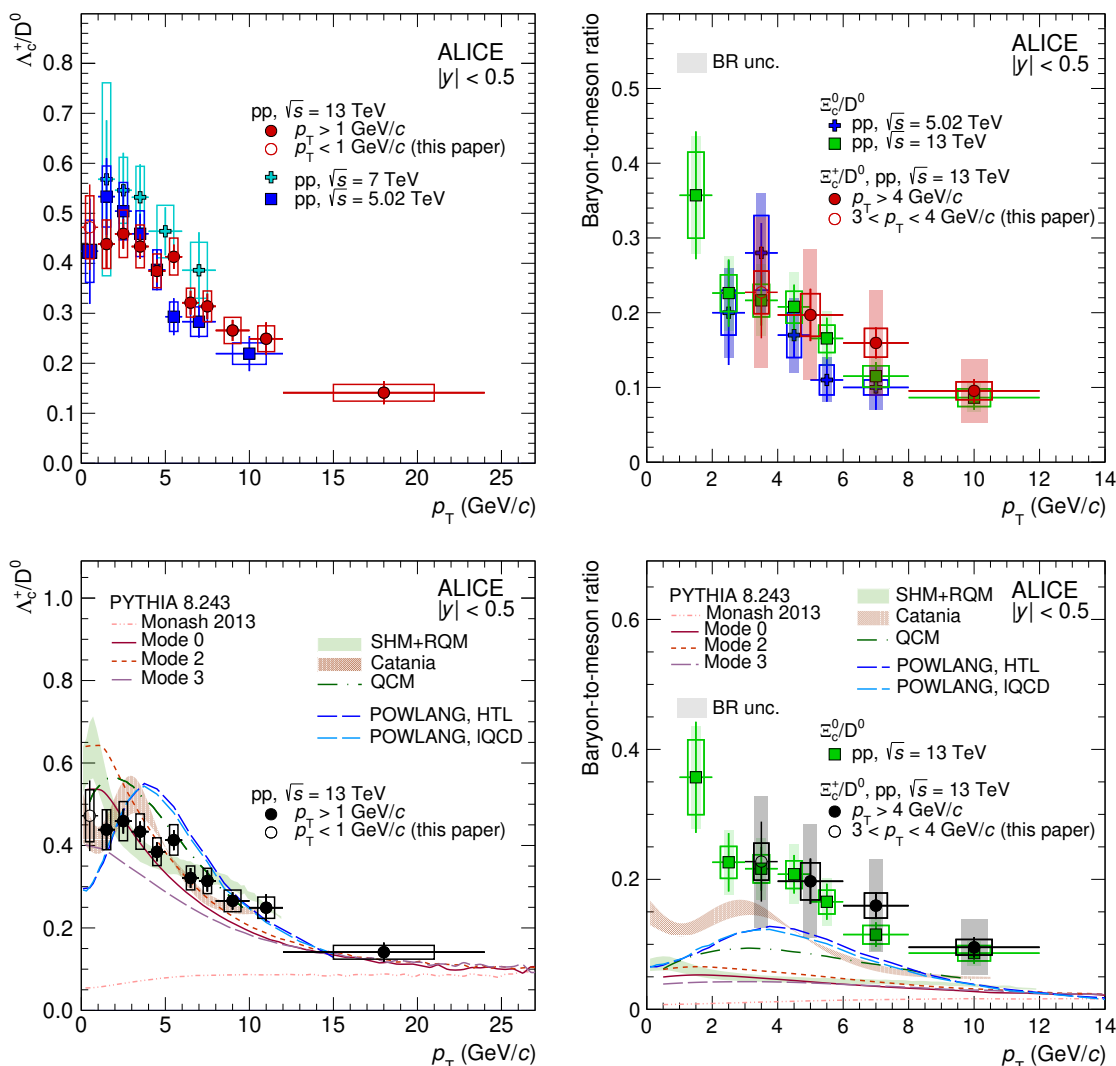
Figure 8. Top left: ratio between the p_T-differential cross sections at midrapidity ($|y| < 0.5$) of prompt Λ_c^+ baryons and D^0 mesons in pp collisions at $\sqrt{s} = 5.02$ TeV [32, 33, 35], 7 TeV [74] and 13 TeV [49]. The measurement of Λ_c^+/D^0 ratio in pp collisions at $\sqrt{s} = 13$ TeV for $p_T > 1$ GeV/c uses the Λ_c^+-baryon cross section published in ref. [49]. Bottom left: ratio between the p_T-differential cross sections at midrapidity ($|y| < 0.5$) of prompt Λ_c^+ baryons and D^0 mesons in pp collisions at $\sqrt{s} = 13$ TeV compared with the predictions from PYTHIA Monash tune [40], PYTHIA CR-BLC Mode 0, 2 and 3 [43], SHM+RQM [44], Catania [47], QCM [48], and POWLANG [80] models in pp collisions at $\sqrt{s} = 13$ TeV. Top right: p_T-differential Ξ_c^+/D^0 ratio in pp collisions at $\sqrt{s} = 13$ TeV and Ξ_c^0/D^0 ratio in pp collisions at $\sqrt{s} = 5.02$ TeV [51] and $\sqrt{s} = 13$ TeV [52]. The Ξ_c^+/D^0 ratio in pp collisions at $\sqrt{s} = 13$ TeV for $p_T > 4$ GeV/c uses the Ξ_c^+ published in ref. [52]. Statistical (systematic) uncertainties are reported as vertical bars (open boxes). The shaded boxes show the BR uncertainty. Bottom right: p_T-differential Ξ_c^0/D^0 and Ξ_c^+/D^0 ratio in pp collisions at $\sqrt{s} = 13$ TeV compared with the predictions from the models reported above.

the SHM+RQM model accounts for the uncertainty on the branching ratios of resonance decays to ground-state charm hadrons. As discussed in ref. [49], the measured baryon-to-meson ratio is underestimated in the interval $p_T < 5\,\mathrm{GeV}/c$ by a factor 4–5 by the prediction from PYTHIA 8 with the Monash tune, which is not able to describe the p_T dependence of the measurement. On the other hand, the predictions from the PYTHIA 8 CR-BLC Mode 0, 2, 3, SHM+RQM, and Catania models describe the measurement within uncertainties in the full range ($p_T > 0$), but the current precision and granularity of the measurement does not allow one model to be favoured over the others. The prediction from the QCM model is compatible with the measured Λ_c^+/D^0 ratio within 2σ, tending to overestimate it in the interval $3 < p_T < 8\,\mathrm{GeV}/c$.

In the bottom-left panel of figure 8, the prompt Λ_c^+/D^0 baryon-to-meson ratios in pp collisions at $\sqrt{s} = 13\,\mathrm{TeV}$ are compared also with the predictions from the POWLANG model [80]. In these calculations, the formation of a small, deconfined, and expanding fireball even in pp collisions is assumed, where the same in-medium hadronization mechanism developed for heavy-ion collisions is employed. In this model, the formation of charm baryons is promoted by the recombination of charm quarks with light diquark excitations in the hot medium. The first predictions from this model were provided in pp collisions at $\sqrt{s} = 5.02\,\mathrm{TeV}$ for the prompt Λ_c^+/D^0 ratio at midrapidity in ref. [80], employing transport coefficients calculated by weak-coupling (Hard-Thermal-Loop, HTL) and the most recent lattice-QCD calculations [81]. The model predictions were found to qualitatively describe the measurement, tending to overestimate the magnitude of the ratio in the interval $3 < p_T < 8\,\mathrm{GeV}/c$. In the bottom-left panel of figure 8, the same comparison for the prompt Λ_c^+/D^0 ratio in pp collisions at $\sqrt{s} = 13\,\mathrm{TeV}$, extended down to $p_T = 0$, is shown. In particular, in the interval $0 < p_T < 1\,\mathrm{GeV}/c$ the prediction tends to underestimate the measurement. Overall, the model does not describe the p_T dependence of the prompt Λ_c^+/D^0 ratio in pp collisions at $\sqrt{s} = 13\,\mathrm{TeV}$.

The Λ_c^+/D^0 ratio in pp collisions at $\sqrt{s} = 13\,\mathrm{TeV}$ is also compared to the same results obtained in pp collisions at $\sqrt{s} = 5.02\,\mathrm{TeV}$ [32, 33, 35] and $\sqrt{s} = 7\,\mathrm{TeV}$ [74]. Within the current uncertainties, no significant energy dependence is observed in pp collisions at midrapidity at the LHC.

In the top-right panel of figure 8, the p_T-differential ratio of prompt Ξ_c^+/D^0 at midrapidity in pp collisions at $\sqrt{s} = 13\,\mathrm{TeV}$ is reported. This result was obtained from the Ξ_c^+-baryon measurement in $p_T > 4\,\mathrm{GeV}/c$ published in ref. [52] and it was extended with the Ξ_c^+-baryon measurement in $3 < p_T < 4\,\mathrm{GeV}/c$ reported in this paper. The same strategy as for the Λ_c^+/D^0 measurement was used for the error propagation. The results are also compared with the Ξ_c^0/D^0 ratio at midrapidity in pp collisions at $\sqrt{s} = 5.02\,\mathrm{TeV}$ [51] and $\sqrt{s} = 13\,\mathrm{TeV}$. The Ξ_c^+/D^0 and Ξ_c^0/D^0 ratios in pp collisions at $\sqrt{s} = 13\,\mathrm{TeV}$ are found to be compatible within uncertainties (top-right panel of figure 8). Also in this case no significant energy dependence is observed for the p_T-differential baryon-to-meson ratio.

As visible in the bottom-right panel of figure 8, only the Catania and POWLANG models are compatible with the measured Ξ_c^+/D^0 ratio within about 1σ. The other model predictions are compatible with the measurement within about 2σ, even if they systematically underestimate the Ξ_c^+/D^0 ratio for all p_T. None of these models is significantly

disfavoured by the measurement. Given the better precision of the measured Ξ_c^0/D^0 ratio, only the predictions from Catania, POWLANG and QCM coalescence models are in agreement within at most 3σ with the measured Ξ_c^0/D^0 ratio. On the other hand, a larger tension with SHM+RQM prediction and PYTHIA predictions is observed in all the p_T intervals. As discussed in ref. [53], only coalescence models including contributions from strong decays of additional excited charm baryons can describe the measured productions of strange-charm baryons. This comparison suggests that the coalescence models provide the best description of the data. Meanwhile, the tension between the measured Ξ_c^0/D^0 ratio and the SHM+RQM suggests that additional excited charm baryons predicted by the RQM are not enough to account for the Ξ_c^0- and Ξ_c^+-baryon abundance, despite the good description of Λ_c^+/D^0 ratio.

5.3.3 Ratios of charm-hadron cross sections at different collision energies

To further investigate the dependence of the D-meson production on the pp collision centre-of-mass energy, the ratio of the p_T-differential D-meson cross sections at $\sqrt{s} = 13\,\mathrm{TeV}$ to the ones at $\sqrt{s} = 5.02\,\mathrm{TeV}$ [19, 23] was computed for the different D-meson species. The results are shown in the left panel of figure 9. The systematic uncertainties were propagated as fully uncorrelated between the results at the two energies, with the exception of those related to the prompt-fraction correction, and the branching ratio which were propagated as correlated. The latter uncertainties cancel out in the ratios. The ratios for the different D-meson species are compatible within the uncertainties and show a common increase with increasing p_T. This effect is similar to that seen for the D-meson production cross sections ratios between $\sqrt{s} = 7\,\mathrm{TeV}$ and $\sqrt{s} = 5.02\,\mathrm{TeV}$ [19]. Furthermore, as discussed in ref. [19], these results are in agreement with pQCD calculations, which benefit from the cancellation of a portion of the uncertainties in the ratio. This cancellation enables a precise description of the observed trend in the data.

An analogous study was performed in the baryon sector by measuring the ratios of the Λ_c^+-, Ξ_c^0-, and Ξ_c^+-baryon p_T-differential cross sections at $\sqrt{s} = 13\,\mathrm{TeV}$ to the ones at $\sqrt{s} = 5.02\,\mathrm{TeV}$ [32, 33, 35, 51]. For the Ξ_c^+ baryon, the ratio was computed with respect to the measurement of the Ξ_c^0 baryon, since due to isospin symmetry the two baryons are expected to be produced with equal yields. This was supported by the fact that their p_T-differential cross sections were found to be fully compatible in the measured p_T range at $\sqrt{s} = 13\,\mathrm{TeV}$ [52]. The ratios for the baryon sector are reported in the right panel of figure 9, and they share a similar increasing trend as a function of p_T. This result suggests a compatible p_T-spectrum hardening between mesons and baryons from $\sqrt{s} = 5.02\,\mathrm{TeV}$ to $\sqrt{s} = 13\,\mathrm{TeV}$.

5.3.4 Ratios of D^0-meson cross section at different rapidities and collision energies

The rapidity dependence of the D-meson production in pp collisions at $\sqrt{s} = 13\,\mathrm{TeV}$ was studied by computing the ratio between the presented measurements at midrapidity and the results from the LHCb collaboration at forward rapidity at the same collision energy [27]. Figure 10 shows the ratios between the D-meson production cross sections
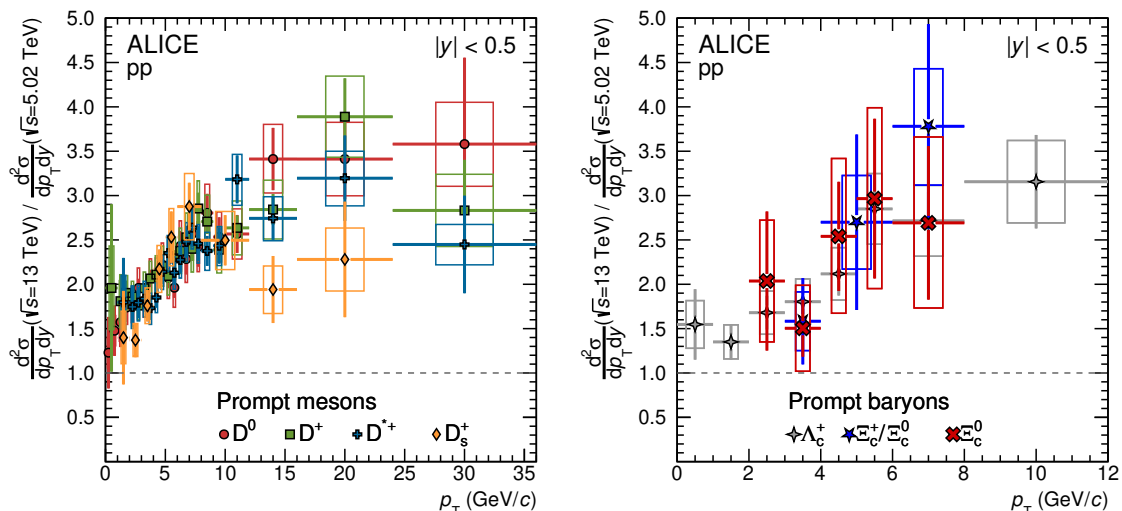
Figure 9. Left: ratios between prompt D^0, D^+, D^{*+}, and D_s^+ mesons production cross sections in pp collisions at $\sqrt{s} = 13$ TeV and those in pp collisions at $\sqrt{s} = 5.02$ TeV [19, 23] as a function of p_T. Right: ratios between the prompt Λ_c^+-, Ξ_c^0-, and Ξ_c^+-baryon production cross sections in pp collisions at $\sqrt{s} = 13$ TeV and those in pp collisions at $\sqrt{s} = 5.02$ TeV [32, 33, 35, 51] as a function of p_T. Vertical bars (boxes) report the statistical (systematic) uncertainties.

measured by ALICE at midrapidity and by LHCb in three intervals at forward rapidity (top-left: $2 < y < 2.5$, top-right: $3 < y < 3.5$, bottom-left: $4 < y < 4.5$) in pp collisions at $\sqrt{s} = 13$ TeV. The uncertainties of the measurement involved in the ratios were propagated as fully uncorrelated. Within current uncertainties, a common trend and magnitude are observed among the different D-meson species in all three rapidity intervals. The significant increase at high p_T of such ratios when going to more forward regions suggests softer p_T-spectra at forward rapidity. Such behaviour is reproduced by FONLL calculations, as discussed in refs. [19, 22].

As discussed in ref. [30], the uncertainty on the PDFs in FONLL calculation can be severely constrained at small values of Bjorken-x (10^{-4}–10^{-5}) [30] by performing precise measurements of ratios at different centre-of-mass energies of D-meson production cross sections in different rapidity intervals. The computation of such ratios between measurements at different energies and rapidity intervals was performed considering the p_T-differential cross section of the prompt D^0 mesons measured at midrapidity ($|y| < 0.5$) and those measured at forward rapidity by the LHCb collaboration [27, 28]. The choice of using the prompt D^0 mesons for this study is motivated by the observation that the p_T dependence of the cross sections of the different D-meson species are compatible among each other (as can be seen in figure 10) and that the measurements of prompt D^0 mesons are the most precise down to $p_T = 0$. The ratios are shown in figure 11 and compared with FONLL predictions. In the top row, the p_T-differential ratios between the prompt D^0-meson production cross section at midrapidity and that at forward rapidity (left: $2 < y < 2.5$, middle: $3 < y < 3.5$, right: $4 < y < 4.5$) measured by the LHCb collaboration are shown in pp collisions at $\sqrt{s} = 5.02$ TeV and 13 TeV. The results at the two energies are fully compatible within uncertainties when the forward rapidity interval $2 < y < 2.5$ is considered. However, when
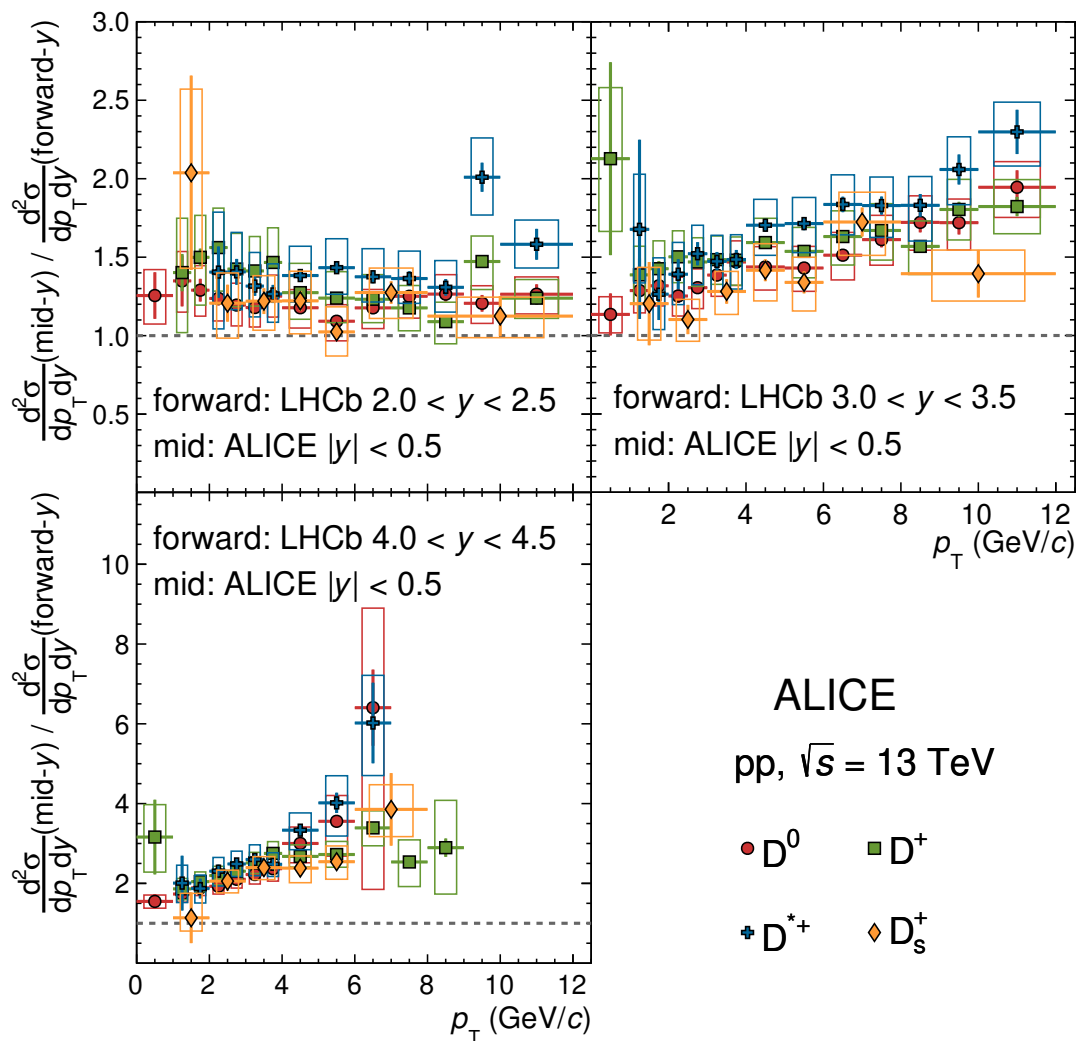
Figure 10. Ratios of D-meson production cross sections per unit of rapidity at midrapidity ($|y| <$ 0.5) to those measured by LHCb [27] in three rapidity intervals: $2 < y < 2.5$ (top-left panel), $3 < y < 3.5$ (top-right panel), and $4 < y < 4.5$ (bottom-left panel), as a function of p_{T}. Statistical (systematic) uncertainties are reported as vertical bars (boxes).

moving to more forward rapidities the ratio in pp collisions at $\sqrt{s} = 5.02\,\mathrm{TeV}$ gets systematically higher than the one at $\sqrt{s} = 13\,\mathrm{TeV}$, with a hint of a harder p_{T} shape for the ratio at lower energy. This behaviour reflects the different Bjorken-x values, which depend on $\sqrt{s}$ for the same hadron rapidity and p_{T}, that are probed by measuring a charm hadron in several rapidity intervals at different centre-of-mass energies. Such values at low p_{T} go from $x \sim 10^{-4}$ at midrapidity to $x \sim 10^{-6}$ at $y = 4.5$.

The results obtained at $\sqrt{s} = 13\,\mathrm{TeV}$ can be further divided by those at $\sqrt{s} = 5.02\,\mathrm{TeV}$ for each rapidity interval, providing the "double ratios" that are useful to constrain the PDF uncertainties, as discussed in ref. [30]. The resulting double ratios

$$\rho = \left(\sigma_{\mathrm{mid}\text{-}y}^{13\,\mathrm{TeV}} \Big/ \sigma_{\mathrm{forward}\text{-}y}^{13\,\mathrm{TeV}} \right) \Big/ \left(\sigma_{\mathrm{mid}\text{-}y}^{5.02\,\mathrm{TeV}} \Big/ \sigma_{\mathrm{forward}\text{-}y}^{5.02\,\mathrm{TeV}} \right) , \tag{5.1}$$
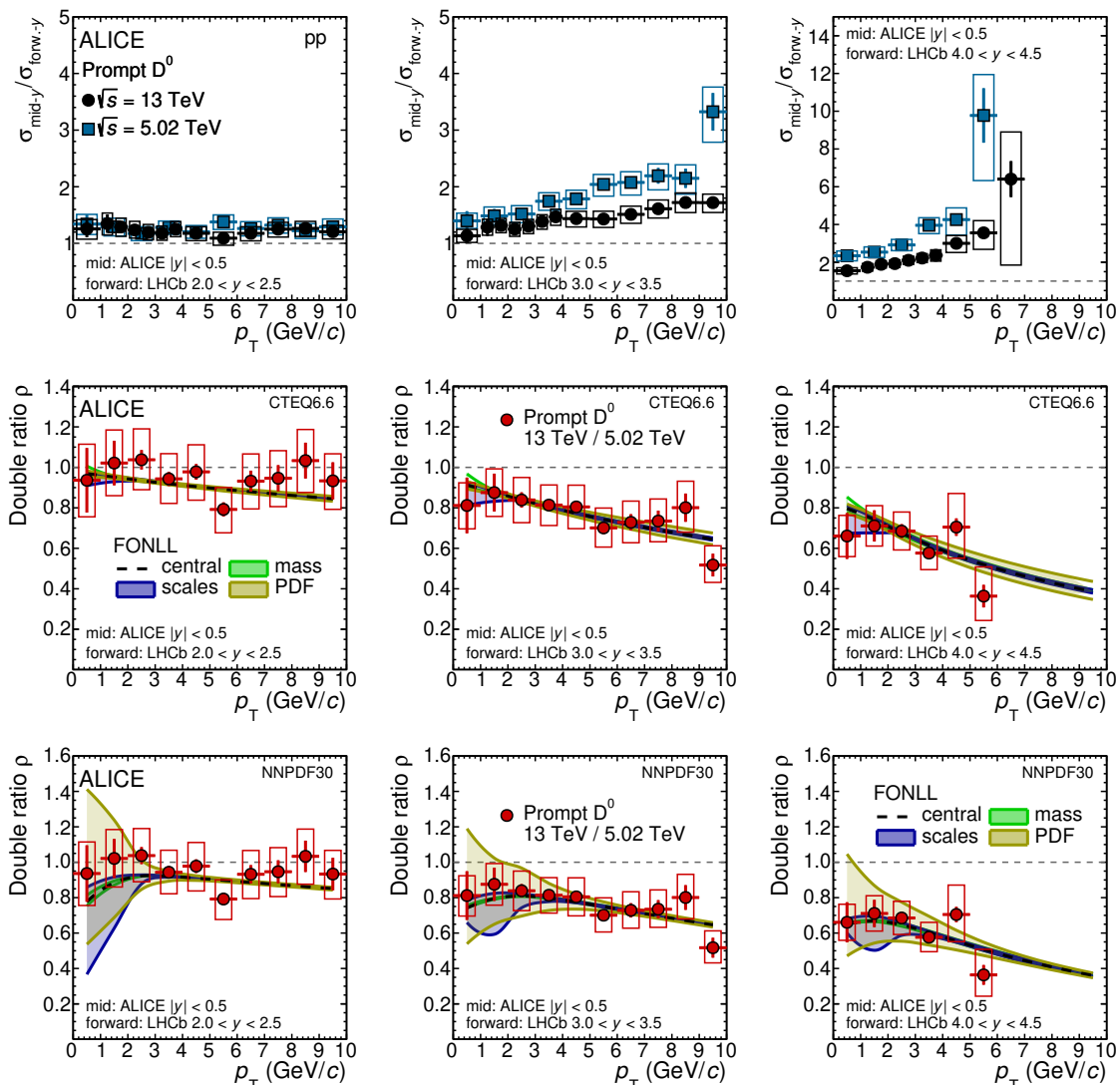
Figure 11. Ratio between p_T-differential cross sections of prompt D^0 mesons at midrapidity ($|y| < 0.5$) in pp collisions at $\sqrt{s} = 5.02$ TeV [19] and 13 TeV and those at forward rapidity in three rapidity intervals (left: $2 < y < 2.5$, middle: $3 < y < 3.5$, right: $4 < y < 4.5$) measured by the LHCb collaboration [27]. The double ratios ρ, defined in eq. (5.1), are shown in the middle and bottom rows together with FONLL calculations employing the CTEQ6.6 [79] (middle row) and NNPDF30 [82] (bottom row) PDF sets. The statistical (systematic) uncertainties are shown as vertical bars (boxes).

where the symbol σ indicates the p_T-differential production cross section of prompt D^0 mesons, are shown in the middle and bottom rows of figure 11. Both the statistical and systematic uncertainties associated to the measurements were propagated as uncorrelated. The double ratios are compared with FONLL calculations performed employing the CTEQ6.6 [79] and NNPDF30 [82] PDF sets respectively. The CTEQ6.6 PDF set is the same used for the FONLL calculations shown in figure 5, as well as in comparison with the measured ratio of the prompt D^0-meson production cross section at midrapidity with that at forward rapidity in pp collisions at $\sqrt{s} = 5.02$ TeV and $\sqrt{s} = 7$ TeV [19, 83]. The

NNPDF30 PDF set is the one considered in ref. [30]. It was obtained with a more robust and efficient fitting code to include also LHC measurements, as discussed in ref. [82].

The different sources of uncertainty in the FONLL calculations are shown separately as coloured bands. They correspond to: (i) the value assumed for the charm-quark mass, by default $m_c = 1.5\,\mathrm{GeV}/c^2$ and varied to 1.3 and $1.7\,\mathrm{GeV}/c^2$; (ii) the values assumed for the factorisation and renormalisation scales, as discussed in ref. [84]; (iii) the uncertainty on the PDFs. The calculation of the theoretical uncertainties related to the charm-quark mass and scale variations was performed by computing the double-ratio considering the same variation for all the four cross sections involved, and the uncertainty band of each source corresponds to the envelope of the calculated double ratios. The bands associated to the PDF uncertainty were provided by the authors of ref. [30], employing the recipes prescribed for the CTEQ6.6 and NNPDF30 PDF sets in ref. [79] and ref. [82] respectively. The theoretical predictions reproduce both the magnitude and the p_T-dependence of the measured double ratios computed in all the three forward rapidity ranges. The uncertainties of the FONLL calculations employing the CTEQ6.6 PDF sets (middle row in figure 11) are significantly lower than the experimental uncertainties for $p_T > 2\,\mathrm{GeV}/c$, while at lower p_T their magnitude is of the same order. In this case, the uncertainties are dominated by the variations of the charm-quark mass and the $\mu_{\mathrm{F,R}}$ scale values. The uncertainties of the PDFs become dominant for $p_T < 2\,\mathrm{GeV}/c$ when employing the NNPDF30 PDF sets in the FONLL calculations (bottom row in figure 11), as discussed in ref. [30]. In this p_T range, the measured double ratios are within the PDF uncertainty band of the calculations and the measured uncertainties are about a factor 2–3 smaller than the PDF ones.

The comparisons of ρ between data and FONLL indicate that the measured double ratios of prompt D^0 mesons shown in figure 11 are precise enough in the range $p_T < 2\,\mathrm{GeV}/c$ to put quantitative constraints on the gluon PDFs employed in the NNPDF30 set. For this PDF set, the PDF uncertainties become equivalent to the scale ones at high p_T. This happens at about $p_T = 2\,\mathrm{GeV}/c$ for the double ratios considering the forward-y range $2 < y < 2.5$. This threshold increases up to $p_T = 6\,\mathrm{GeV}/c$ going to more forward rapidities, where the PDF uncertainty remains dominant in a wider p_T interval. At high p_T, the overall uncertainties become negligible compared to the experimental ones and the calculations reproduce the decreasing trend of the measurement, which becomes steeper going to $4 < y < 4.5$. As discussed in ref. [30], (double-)ratios at such forward rapidity and at high p_T ($p_T \gtrsim 20\,\mathrm{GeV}/c$) would probe gluon densities in the range of Bjorken-$x \sim 0.2$, which has not been well constrained by the experiments so far. However, given the lack of measurements at forward rapidity for $p_T \gtrsim 15\,\mathrm{GeV}/c$, this regime cannot be tested experimentally with the current measurements.

5.4 Charm-quark production in pp collisions at $\sqrt{s} = 13\,\mathrm{TeV}$

5.4.1 Charm-hadron p_T-integrated cross sections and extrapolation down to $p_T = 0$

For the measurement of the charm-quark fragmentation fractions and the c$\bar{\mathrm{c}}$ production cross section per unit of rapidity at midrapidity in pp collisions at $\sqrt{s} = 13\,\mathrm{TeV}$ (sections 5.4.3 and 5.4.4), the total production cross section of each hadron species must be

considered. In the case of D^0 and D^+ mesons and Λ_c^+ baryons, for which the p_T-differential cross sections were measured down to $p_T = 0$, the total cross section was calculated by integrating the p_T-differential results over the p_T interval of the measurement, considering that the contribution to the cross section in the unmeasured interval ($p_T > 24\,\mathrm{GeV}/c$ for the Λ_c^+ baryon, $p_T > 36\,\mathrm{GeV}/c$ for the D_s^+ meson, and $p_T > 50\,\mathrm{GeV}/c$ for the D^0 meson) is negligible. All the systematic uncertainties were propagated assuming them as correlated among the p_T intervals, with the exception of those related to the signal extraction, which were assumed to be uncorrelated. For the other charm-hadron species, for which the analysis down to $p_T = 0$ was not possible, the measured p_T-differential cross sections were extrapolated as described below.

The measurement of the D^{*+}-meson cross section at midrapidity ($|y| < 0.5$) was integrated over the measured momentum interval ($p_T > 1\,\mathrm{GeV}/c$) to obtain $\sigma_{\mathrm{visible}}$ and was then extrapolated down to $p_T = 0\,\mathrm{GeV}/c$ with the strategy described in ref. [19]. The p_T-integrated cross section in the full p_T range, σ_{full}, was measured by scaling $\sigma_{\mathrm{visible}}$ by the extrapolation factor $C^{\mathrm{FONLL}} \equiv \sigma_{\mathrm{full}}^{\mathrm{FONLL}}/\sigma_{\mathrm{visible}}^{\mathrm{FONLL}}$ calculated from the FONLL predictions for the D^{*+} meson at midrapidity. The systematic uncertainties of the extrapolation factor accounted for the uncertainties of the PDF, the variation of the charm-quark mass, and the values of the renormalisation and factorisation scales for the FONLL calculations.

The extrapolation of the D_s^+-meson cross section was performed as described in refs. [19, 23]. Due to the lack of FONLL predictions for the D_s^+-meson production, the extrapolation factor was calculated using the p_T-differential cross section of charm quarks provided by FONLL calculations, the fragmentation fractions $f(\mathrm{c} \to D_s^+)$ and $f(\mathrm{c} \to D_s^{*+})$ from ALEPH measurements [85], and the charm-quark fragmentation functions from ref. [86].

The extrapolation of the $\Sigma_c^{0,+,++}$-baryon cross section was performed by computing a scaling factor based on the prediction from PYTHIA CR-BLC Mode 0, which among the CR-BLC modes was observed to better describe both the magnitude and the p_T dependence of the measured cross section. The other modes were used to estimate the extrapolation systematic uncertainty, together with the SHM-RQM, QCM, and the Catania models, which provided predictions only for the $\Sigma_c^{0,+,++}/D^0$ ratio. In this case, the model predictions were used to fit the measured ratio from ref. [49], leaving only the normalisation as a free parameter. The fit function was scaled by the measured D^0-meson cross section in the range $0 < p_T < 2\,\mathrm{GeV}/c$, where no $\Sigma_c^{0,+,++}$ measurement is currently available. The extrapolation systematic uncertainty was calculated as the envelope of the values of the p_T-integrated cross sections obtained with all the considered variations. To a minimum and maximum $\Sigma_c^{0,+,++}$-baryon cross section extrapolated from these ratios, the measured D^0-meson cross section in $0 < p_T < 2\,\mathrm{GeV}/c$ was shifted up and down by one standard deviation, defined by the quadrature sum of the statistical and systematic uncertainties.

The extrapolation of the Ξ_c^+-baryon cross section was performed following the same strategy as for the $\Sigma_c^{0,+,++}$ baryon. The Catania model was used as the central value prediction as it was observed to best describe the p_T-dependence and magnitude of the measured cross section. A Tsallis fit to the measurement and predictions from the PYTHIA CR-BLC Modes 0, 2 and 3, the SHM+RQM model, and the QCM model were used for the estimation of the systematic uncertainty.

	$\mathrm{d}\sigma/\mathrm{d}y|_{|y|<0.5}$ (μb), $p_\mathrm{T} > 0$
D^0	749 ± 27 (stat.) $^{+48}_{-50}$ (syst.) ± 12 (lumi.) ± 6 (BR)
D^+	375 ± 32 (stat.) $^{+35}_{-35}$ (syst.) ± 6 (lumi.) ± 6 (BR)
D_s^+	120 ± 11 (stat.) $^{+12}_{-13}$ (syst.) $^{+25}_{-10}$ (extrap.) ± 2 (lumi.) ± 3 (BR)
Λ_c^+	329 ± 15 (stat.) $^{+28}_{-29}$ (syst.) ± 5 (lumi.) ± 15 (BR)
Ξ_c^0 [52]	194 ± 27 (stat.) $^{+46}_{-46}$ (syst.) $^{+18}_{-12}$ (extrap.) ± 3 (lumi.)
Ξ_c^+	187 ± 25 (stat.) $^{+19}_{-19}$ (syst.) $^{+13}_{-59}$ (extrap.) ± 3 (lumi.) ± 82 (BR)
J/ψ [87]	7.29 ± 0.27 (stat.) $^{+0.52}_{-0.52}$ (syst.) $^{+0.04}_{-0.01}$ (extrap.)
D^{*+}	306 ± 26 (stat.) $^{+33}_{-34}$ (syst.) $^{+48}_{-17}$ (extrap.) ± 5 (lumi.) ± 3 (BR)
$\Sigma_\mathrm{c}^{0,+,++}$	142 ± 22 (stat.) $^{+24}_{-24}$ (syst.) $^{+24}_{-32}$ (extrap.) ± 2 (lumi.) ± 6 (BR)

Table 4. $\mathrm{d}\sigma/\mathrm{d}y|_{|y|<0.5}$ of all measured charm-hadron species in pp collisions at $\sqrt{s} = 13$ TeV. These results are obtained by integrating the measured p_T-differential cross section at midrapidity and extrapolating down to $p_\mathrm{T} = 0$ if necessary.

The p_T-integrated cross sections of all the charm hadrons at midrapidity ($|y| < 0.5$) in pp collisions at $\sqrt{s} = 13$ TeV are listed in table 4.

5.4.2 Strange to-non strange charm-meson production ratio $f_\mathrm{s}/(f_\mathrm{u} + f_\mathrm{d})$

The relative production of strange to non-strange D-meson production can be studied using the ratio of fragmentation fractions $f_\mathrm{s}/(f_\mathrm{u} + f_\mathrm{d})$, where f_x represents the probability for a charm quark to hadronise with another quark of flavour x. In the charm-meson sector, this ratio corresponds experimentally to the prompt cross section ratio $\mathrm{D}_\mathrm{s}^+/(\mathrm{D}^0 + \mathrm{D}^+)$, as all D^{*+} and D^{*0} mesons decay to D^0 and D^+ mesons, and all $\mathrm{D}_\mathrm{s}^{*+}$ mesons decay to D_s^+ mesons. The contribution of the decays of excited states that change the strange/non-strange D-meson content (e.g. $\mathrm{D}_{\mathrm{s}1}^+ \to \mathrm{D}^{*+}\mathrm{K}_\mathrm{S}^0$ or $\mathrm{D}_{\mathrm{s}2}^{*+} \to \mathrm{D}^+\mathrm{K}_\mathrm{S}^0$) was neglected in the computation of the ratio $f_\mathrm{s}/(f_\mathrm{u} + f_\mathrm{d})$.

The p_T-integrated cross sections reported in table 4 were used to compute the ratios of production yields among the different D-meson species in pp collisions at $\sqrt{s} = 13$ TeV. The ratios of prompt D mesons $\mathrm{D}^+/\mathrm{D}^0$, $\mathrm{D}_\mathrm{s}^+/\mathrm{D}^0$, $\mathrm{D}_\mathrm{s}^+/\mathrm{D}^+$, and $\mathrm{D}_\mathrm{s}^+/(\mathrm{D}^0 + \mathrm{D}^+)$ for $p_\mathrm{T} > 0$ are reported in table 5. The systematic uncertainties related to the tracking efficiency, luminosity, extrapolation, and to the subtraction of the component from beauty-hadron decays were propagated as correlated among the D-meson species. All the other sources of systematic uncertainties were propagated as uncorrelated. The same ratios measured in pp collisions at $\sqrt{s} = 5.02$ TeV [23] are also reported in table 5. The results do not show any significant dependence on the collision energy.

The uncertainty on the $\mathrm{D}_\mathrm{s}^+/(\mathrm{D}^0 + \mathrm{D}^+)$ ratios reported in table 5 are dominated by the limited precision of the measurements in the low-p_T intervals, and by the uncertainty related to the extrapolation of the cross section of prompt D_s^+ mesons down to $p_\mathrm{T} = 0$. For

pp, $\sqrt{s} = 5.02\,\text{TeV}$ [23]	
D^+/D^0	$0.442 \pm 0.055\,(\text{stat.}) \pm 0.033\,(\text{syst.}) \pm 0.008\,(\text{BR})$
$\text{D}_\text{s}^+/\text{D}^0$	$0.186 \pm 0.028\,(\text{stat.}) \pm 0.015\,(\text{syst.})^{+0.051}_{-0.018}\,(\text{extrap.}) \pm 0.007\,(\text{BR})$
$\text{D}_\text{s}^+/\text{D}^+$	$0.419 \pm 0.078\,(\text{stat.}) \pm 0.041\,(\text{syst.})^{+0.116}_{-0.040}\,(\text{extrap.}) \pm 0.017\,(\text{BR})$
$\text{D}_\text{s}^+/(\text{D}^0 + \text{D}^+)$	$0.128 \pm 0.020\,(\text{stat.}) \pm 0.010\,(\text{syst.})^{+0.035}_{-0.012}(\text{extrap.}) \pm 0.005\,(\text{BR})$
pp, $\sqrt{s} = 13\,\text{TeV}$	
D^+/D^0	$0.500 \pm 0.047\,(\text{stat.}) \pm 0.033\,(\text{syst.}) \pm 0.009\,(\text{BR})$
$\text{D}_\text{s}^+/\text{D}^0$	$0.160 \pm 0.015\,(\text{stat.}) \pm 0.012\,(\text{syst.})^{+0.034}_{-0.013}\,(\text{extrap.}) \pm 0.004\,(\text{BR})$
$\text{D}_\text{s}^+/\text{D}^+$	$0.319 \pm 0.039\,(\text{stat.}) \pm 0.030\,(\text{syst.})^{+0.068}_{-0.024}\,(\text{extrap.}) \pm 0.010\,(\text{BR})$
$\text{D}_\text{s}^+/(\text{D}^0 + \text{D}^+)$	$0.106 \pm 0.010\,(\text{stat.}) \pm 0.008\,(\text{syst.})^{+0.023}_{-0.009}\,(\text{extrap.}) \pm 0.003\,(\text{BR})$

Table 5. Ratios of the measured production cross sections of prompt D mesons for $p_\text{T} > 0$ at midrapidity ($|y| < 0.5$) in pp collisions at $\sqrt{s} = 5.02\,\text{TeV}$ [23] and $\sqrt{s} = 13\,\text{TeV}$.

the measurement in pp collisions at $\sqrt{s} = 13\,\text{TeV}$, the total relative uncertainty amounts to about 22%. As discussed in ref. [23], the measurement of the ratio $f_\text{s}/(f_\text{u} + f_\text{d})$ in pp collisions at $\sqrt{s} = 5.02\,\text{TeV}$ was performed with a fit of the p_T-differential $\text{D}_\text{s}^+/(\text{D}^0 + \text{D}^+)$ ratios using a constant function, since the ratio was found to be constant within uncertainties. With this strategy, the total uncertainty of the measurement was reduced. Given the better precision, the $\text{D}_\text{s}^+/(\text{D}^0 + \text{D}^+)$ ratio in pp at $\sqrt{s} = 13\,\text{TeV}$ suggests a hint of increasing trend with p_T in the interval $p_\text{T} < 8\,\text{GeV}/c$, as visible in figure 7. Therefore, the approach based on a fit to a constant is no longer justified and the ratio $f_\text{s}/(f_\text{u} + f_\text{d})$ in pp collisions at $\sqrt{s} = 13\,\text{TeV}$ was measured considering the prompt D^0-, D^+-, and D_s^+-meson cross sections for $p_\text{T} > 1\,\text{GeV}/c$, corresponding to the interval of the D_s^+ measurement, reported in table 6. This led to:

$$\frac{\gamma_\text{s}}{2} \equiv \left(\frac{f_\text{s}}{f_\text{u} + f_\text{d}}\right)_{\text{charm}} = 0.116 \pm 0.011\,(\text{stat.}) \pm 0.009\,(\text{syst.}) \pm 0.003\,(\text{BR}), \qquad (5.2)$$

where γ_s denotes the strangeness suppression factor, as defined in ref. [90]. The systematic uncertainties were propagated as for the measurement for $p_\text{T} > 0$. The result shown in eq. (5.2) agrees with the $\text{D}_\text{s}^+/(\text{D}^0 + \text{D}^+)$ ratio reported in table 5, and it does not depend on the extrapolation down to $p_\text{T} = 0$ of the prompt D_s^+ mesons.

In figure 12, the ratio $f_\text{s}/(f_\text{u} + f_\text{d})$ (red) is compared with previous measurements of strangeness suppression factor γ_s or $f_\text{s}/(f_\text{u} + f_\text{d})$ from the ALICE [21, 23], H1 [88], ZEUS [89], and ATLAS [24] collaborations. In the cases where γ_s was used, the measurements were scaled by a factor of 0.5, accounting for the different normalisation between the two observables, as shown in eq. (5.2). The total experimental uncertainties are reported as bars, and the theoretical ones as shaded boxes. The theoretical uncertainties in the H1 measurement denote the branching ratio uncertainty and the model dependencies of the

$\mathrm{d}\sigma/\mathrm{d}y|_{|y|<0.5}$ (μb), $p_\mathrm{T} > 1$ GeV/c
$\mathrm{D^0}$ 592 ± 19 (stat.)$^{+40}_{-42}$ (syst.) ± 9 (lumi.) ± 4 (BR.)
$\mathrm{D^+}$ 264 ± 5 (stat.)$^{+20}_{-20}$ (syst.) ± 4 (lumi.) ± 5 (BR.)
$\mathrm{D_s^+}$ 99 ± 9 (stat.)$^{+10}_{-11}$ (syst.) ± 2 (lumi.) ± 3 (BR.)

Table 6. Production cross sections of prompt D mesons for $p_\mathrm{T} > 1$ GeV/c at midrapidity ($|y| < 0.5$) in pp collisions at $\sqrt{s} = 13$ TeV.
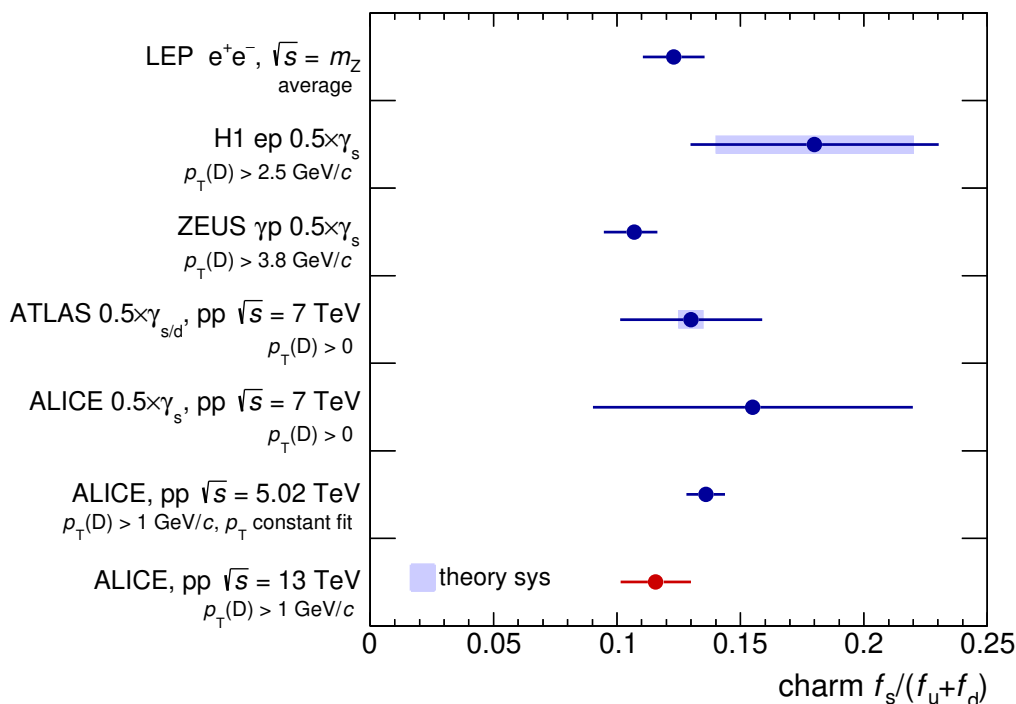
Figure 12. Charm-quark fragmentation-fraction ratio $f_\mathrm{s}/(f_\mathrm{u} + f_\mathrm{d})$ (red) compared with previous measurements performed by the ALICE [21, 23], H1 [88], ZEUS [89], and ATLAS [24] collaborations, and to the average of LEP measurements [76]. The total experimental uncertainties (bars) and the theoretical uncertainties (shaded boxes) are shown.

acceptance determination. In the case of the ATLAS measurement, they correspond to the extrapolation uncertainties to the full phase space. The values are compatible within uncertainties, and they are in agreement with the average of measurements at LEP [76]. This indicates that the production of prompt strange D mesons relative to that of prompt non-strange D mesons ($f_\mathrm{s}/(f_\mathrm{u} + f_\mathrm{d})$) in $\mathrm{e^+e^-}$, ep and pp collisions does not show any significant dependence on the collision system and energy. Furthermore, the $f_\mathrm{s}/(f_\mathrm{u} + f_\mathrm{d})$ is compatible with the ratio of the p_T-integrated cross sections at forward rapidity ($2 < y < 4.5$) of prompt $\mathrm{D_s^+}$, $\mathrm{D^+}$ and $\mathrm{D^0}$-meson in the interval $1 < p_\mathrm{T} < 8$ GeV/c measured by the LHCb collaboration [27], suggesting that the relative production of strange and non-strange D mesons does not depend on the meson rapidity.
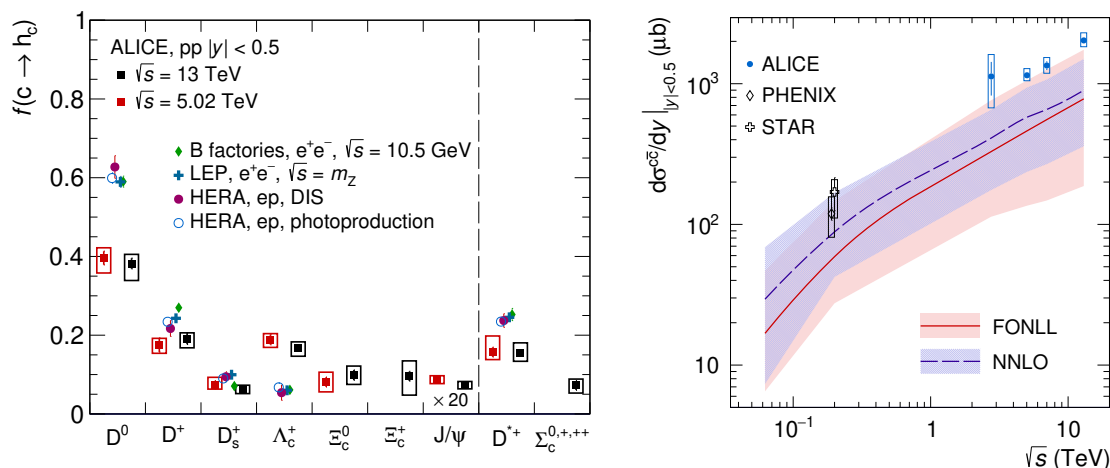
Figure 13. Left: charm-quark fragmentation fractions at midrapidity ($|y| < 0.5$) in pp collisions at $\sqrt{s} = 5.02$ TeV and $\sqrt{s} = 13$ TeV compared with results in e^+e^- and ep collisions [55]. The fragmentation fractions $f(c \to h_c)$ of J/ψ mesons are multiplied by a factor 20 for better visibility. Right: c$\bar{c}$ production cross section per unit of rapidity at midrapidity ($|y| < 0.5$) in pp collisions as a function of $\sqrt{s}$. The measurements are compared with predictions from FONLL [13, 14] and NNLO [91–93] calculations. The statistical and systematic uncertainties are reported as vertical bars and boxes, respectively.

5.4.3 Charm-quark fragmentation fractions in pp collisions

The charm-quark fragmentation fractions $f(c \to h_c)$ at midrapidity in pp collisions at $\sqrt{s} = 13$ TeV are shown in the left panel of figure 13. For each hadron species, the production cross section was normalised by the sum of the p_T-integrated production cross sections of the measured production cross sections of D^0, D^+, D_s^+, J/ψ, Λ_c^+, Ξ_c^0, and Ξ_c^+. The dashed vertical line separates the fragmentation fractions of the D^{*+} mesons and the $\Sigma_c^{0,+,++}$ baryons from those of the other charm-hadron species. These two hadrons were not considered in the denominator because they strongly decay into D^0 and D^+ mesons and to Λ_c^+ baryons, respectively, which are already included in the sum.

In this measurement, the systematic uncertainties related to the tracking efficiency and the prompt fraction correction were assumed to be fully correlated among all the particle species, while the uncertainties of the signal extraction and the statistical uncertainty were treated as fully uncorrelated. The extrapolation uncertainty was propagated as partially correlated depending on the adopted techniques for each species. In addition, the possible contribution from Ω_c^0-baryon production at midrapidity in pp collisions at $\sqrt{s} = 13$ TeV was taken into account in the systematic uncertainties. According to ref. [53], the $\sigma(\Omega_c^0) \times$ $\mathrm{BR}(\Omega_c^0 \to \Omega^-\pi^+)/\sigma(\Xi_c^0)$ ratio is around 0.005 in the interval $2 < p_T < 12$ GeV/c. Scaling the ratio by the theoretical value of the branching ratio $\mathrm{BR}(\Omega_c^0 \to \Omega^-\pi^+) = 0.51\%^{+2.19\%}_{-0.31\%}$ would imply that the Ω_c^0 baryons are produced as abundantly as the Ξ_c^0 baryon in this p_T range. However, the branching ratio $\mathrm{BR}(\Omega_c^0 \to \Omega^-\pi^+)$ has never been experimentally measured and the one quoted above corresponds to the envelope (uncertainties included) of the values calculated in refs. [94–98]. Given the large uncertainty of the branching ratio, the Ω_c^0-baryon measurement was used only to define an asymmetric systematic uncertainty for

$f(c \to h_c)$	pp, $\sqrt{s} = 5.02\,\mathrm{TeV}$ (%)	pp, $\sqrt{s} = 13\,\mathrm{TeV}$ (%)
D^0	39.6 ± 1.7 (stat.) $^{+2.6}_{-3.8}$ (syst.)	38.2 ± 1.3 (stat.) $^{+2.3}_{-4.3}$ (syst.)
D^+	17.5 ± 1.8 (stat.) $^{+1.7}_{-2.1}$ (syst.)	19.1 ± 1.4 (stat.) $^{+1.5}_{-2.3}$ (syst.)
D_s^+	7.4 ± 1.0 (stat.) $^{+1.9}_{-1.1}$ (syst.)	6.1 ± 0.5 (stat.) $^{+1.2}_{-0.9}$ (syst.)
Λ_c^+	18.9 ± 1.3 (stat.) $^{+1.5}_{-2.0}$ (syst.)	16.8 ± 0.8 (stat.) $^{+1.5}_{-2.1}$ (syst.)
Ξ_c^0	8.1 ± 1.2 (stat.) $^{+2.5}_{-2.5}$ (syst.)	9.9 ± 1.3 (stat.) $^{+2.3}_{-2.4}$ (syst.)
Ξ_c^+	Assumed to be the same as Ξ_c^0	9.6 ± 1.2 (stat.) $^{+3.9}_{-4.8}$ (syst.)
J/ψ	0.44 ± 0.03 (stat.) $^{+0.04}_{-0.06}$ (syst.)	0.37 ± 0.02 (stat.) $^{+0.04}_{-0.05}$ (syst.)
D^{*+}	15.7 ± 1.2 (stat.) $^{+4.1}_{-1.9}$ (syst.)	15.6 ± 0.7 (stat.) $^{+2.5}_{-2.2}$ (syst.)
$\Sigma_c^{0,+,++}$	—	7.2 ± 1.2 (stat.) $^{+1.6}_{-1.9}$ (syst.)

Table 7. Charm-quark fragmentation fractions in pp collisions at $\sqrt{s} = 5.02\,\mathrm{TeV}$ and $13\,\mathrm{TeV}$. The values for the Ξ_c^+ baryon at $\sqrt{s} = 5.02\,\mathrm{TeV}$ are assumed to be the same as the ones of the Ξ_c^0 baryon at the same centre-of-mass energy. The values published in ref. [54] were updated considering recent measurements of prompt Λ_c^+ baryon down to $p_\mathrm{T} = 0$ and of prompt J/ψ mesons, as mentioned in the text. The "syst." uncertainty also includes the contribution of the extrapolation uncertainty.

the sum of the charm-hadron cross sections used to normalise the fragmentation fraction, which accounts for $\sigma(\Omega_c^0) = \sigma(\Xi_c^0)$.

The results in pp collisions at $\sqrt{s} = 13\,\mathrm{TeV}$ are compared in the left panel of figure 13 and in table 7 with those in pp collisions at $\sqrt{s} = 5.02\,\mathrm{TeV}$. The previous measured values published in ref. [54] were updated for this paper considering more recent cross section measurements of prompt Λ_c^+ baryon down to $p_\mathrm{T} = 0$ [35] and of prompt J/ψ mesons [87]. As reported in ref. [35], the p_T-integrated Λ_c^+-baryon cross section in $|y| < 0.5$ decreases by about 10% compared to the previously published results [32, 33], where the measurement did not extend down to $p_\mathrm{T} = 0\,\mathrm{GeV}/c$ and instead relied on an extrapolation. This reduction of the Λ_c^+ production cross section leads to a reduction of the $f(c \to \Lambda_c^+)$ by about 7%.

To compute the $\Xi_c^{0,+}$ fragmentation fractions in pp collisions at $\sqrt{s} = 5.02\,\mathrm{TeV}$, the Ξ_c^0-baryon cross section was considered twice, as done in ref. [54]. This was due to the lack of Ξ_c^+-baryon measurements at this collision energy. The Ξ_c^+-baryon fragmentation fraction at midrapidity ($|y| < 0.5$) in pp collisions at $\sqrt{s} = 13\,\mathrm{TeV}$ is compatible with the Ξ_c^0-baryon fragmentation fractions in pp collisions at $\sqrt{s} = 5.02\,\mathrm{TeV}$ and $\sqrt{s} = 13\,\mathrm{TeV}$ within uncertainties. The uncertainties are dominated by the $\sim 44\%$ uncertainty of the branching ratio $\mathrm{BR}(\Xi_c^+ \to \Xi^- \pi^+ \pi^+)$. The measurements of the J/ψ fragmentation fraction at the two different centre-of-mass energies are also shown in the left panel of figure 13, where they are scaled by a factor 20 for visibility.

The measurements in pp collisions at the LHC are compared with those in $\mathrm{e}^+\mathrm{e}^-$ collisions at LEP and at B factories, as well as those in ep collisions at HERA [55]. The

prompt Λ_c^+-baryon fragmentation fraction in pp collisions at $\sqrt{s} = 13\,\mathrm{TeV}$ is about three times larger than in $\mathrm{e^+e^-}$ and ep collisions. Each of the $\Xi_c^{0,+}$ baryons accounts for about 10% of the total charm hadron production at midrapidity, while their production was considered to be negligible in $\mathrm{e^+e^-}$ and ep collisions. Since the fragmentation fractions sum to unity, this enhancement of baryon production implies an overall reduction of the relative D-meson abundance by about a factor 1.5 relative to $\mathrm{e^+e^-}$ and ep collisions.

In table 7 the first measurement of the $\Sigma_c^{0,+,++}$-baryon fragmentation fraction in pp collisions at the LHC is also provided. The charm-quark fragmentation fraction into $\Sigma_c^{0,+,++}$ baryons in $\mathrm{e^+e^-}$ collisions can be estimated to be about 1%, taking into account that $\Sigma_c^{0,+,++}/\mathrm{D^0} \approx 0.02$, as reported in ref. [49], calculated with the charm-hadron cross sections reported in ref. [50], and the fragmentation fraction $f(\mathrm{c} \to \mathrm{D^0}) \approx 0.59$ from ref. [55]. An enhancement of $f(\mathrm{c} \to \Sigma_c^{0,+,++})$ of about a factor seven is observed at the LHC compared to $\mathrm{e^+e^-}$ collisions. The $\Sigma_c^{0,+,++}$ production accounts for about 40% of the prompt Λ_c^+-baryon production at midrapidity in pp collisions at $\sqrt{s} = 13\,\mathrm{TeV}$ [49]. This is significantly larger than the $\Sigma_c^{0,+,++}/\Lambda_c^+ \approx 0.17$ measured in $\mathrm{e^+e^-}$ collisions by the Belle collaboration (table IV in ref. [50]) and the ≈ 0.13 from PYTHIA 8 Monash tune simulations. Therefore, a larger Λ_c^+ feed-down from $\Sigma_c^{0,+,++}$-baryon decays is observed in pp collisions at the LHC.

Within the current precision, the measured fragmentation fractions (left panel of figure 13) do not show any significant energy dependence of the relative charm-hadron production at midrapidity in pp collisions at the LHC. Therefore, these results confirm that the baryon enhancement at the LHC with respect to $\mathrm{e^+e^-}$ collisions is caused by different hadronisation mechanisms at play in the parton-rich environment produced in pp collisions, regardless of the centre-of-mass energy.

5.4.4 Production cross section of $c\bar{c}$ at midrapidity in pp collisions

The $c\bar{c}$ production cross section at midrapidity $(\mathrm{d}\sigma^{c\bar{c}}/\mathrm{d}y|_{|y|<0.5})$ in pp collisions at $\sqrt{s} = 13\,\mathrm{TeV}$ is shown in the right panel of figure 13. As for the measurement of the fragmentation fractions, the $c\bar{c}$ production cross section is calculated from the sum of the production cross sections at midrapidity $(\mathrm{d}\sigma^{\mathrm{H}}/\mathrm{d}y|_{|y|<0.5})$ of the $\mathrm{D^0}$, $\mathrm{D^+}$, $\mathrm{D_s^+}$, J/ψ, Λ_c^+, Ξ_c^0, and Ξ_c^+ hadrons. The possible contribution of Ω_c^0 baryons to the total cross section was taken into account as an asymmetric systematic uncertainty, as discussed in section 5.4.3 for the fragmentation fractions.

As done for the measurement in pp collisions at $\sqrt{s} = 5.02\,\mathrm{TeV}$ [54] and at $\sqrt{s} = 7\,\mathrm{TeV}$ [22], two correction factors were applied to account for the different shape of the rapidity distributions of charm hadrons, single charm quarks, and $c\bar{c}$ pairs. The first factor was evaluated with FONLL calculations in the relevant rapidity range and it accounted for the possible differences in the rapidity distributions of hadrons and single charm quarks. This factor was found to be at unity, excluding any relevant difference in the two rapidity distributions. A 2% uncertainty for this factor was estimated from the difference to PYTHIA 8 simulations. The second correction factor accounted for the possible differences between the rapidity distributions of single charm quarks and $c\bar{c}$ pairs. This was evaluated to be 1.036 according to NLO pQCD calculations using POWHEG [37]. An additional un-

certainty of 3% was estimated by varying independently by a factor of two the factorisation and normalisation scales in the calculations, and using different sets of PDFs [99–103].

The c$\bar{\text{c}}$ production cross section in pp collisions at $\sqrt{s} = 13$ TeV is

$$\left.\frac{\text{d}\sigma}{\text{d}y}\right|_{|y|<0.5}^{\text{pp},\sqrt{s}=13\,\text{TeV}} = 2031 \pm 61 \text{ (stat.)}_{-141}^{+135} \text{ (syst.)}_{-63}^{+196} \text{ (extrap.)} \pm 97 \text{ (BR)} \pm 33 \text{ (lumi.)} \pm 73 \text{ (y)}\,\mu\text{b}.$$

(5.3)

In the computation of the systematic uncertainties, those related to the tracking efficiency and the prompt fraction correction were propagated as fully correlated among the different hadron species. The systematic uncertainties related to the branching ratios of the channels chosen for the reconstruction (BR), the collected luminosity (lumi.), the rapidity correction factors (y), and the extrapolation factors (extrap.), which also includes the possible Ω_c^0-baryon contribution, are quoted separately.

As for the fragmentation fractions, the c$\bar{\text{c}}$ production cross section at midrapidity $\text{d}\sigma/\text{d}y|_{|y|<0.5}$ at $\sqrt{s} = 5.02$ TeV was updated taking into account the more recent cross section measurements of prompt Λ_c^+ baryon down to $p_\text{T} = 0$ [35] and of prompt J/ψ mesons [87]. The updated c$\bar{\text{c}}$ production cross section in pp collisions at $\sqrt{s} = 5.02$ TeV is

$$\left.\frac{\text{d}\sigma}{\text{d}y}\right|_{|y|<0.5}^{\text{pp},\sqrt{s}=5.02\,\text{TeV}} = 1148 \pm 43 \text{ (stat.)}_{-65}^{+62} \text{ (syst.)}_{-36}^{+98} \text{ (extrap.)} \pm 43 \text{ (BR)} \pm 24 \text{ (lumi.)} \pm 41 \text{ (y)}\,\mu\text{b}.$$

(5.4)

The extrapolated fraction of the c$\bar{\text{c}}$ cross section is around 11% for both the measurements at $\sqrt{s} = 5.02$ TeV and $\sqrt{s} = 13$ TeV. This is significantly reduced with respect to the previous measurement in pp collisions at $\sqrt{s} = 5.02$ TeV [54], where it reached about 20% of the c$\bar{\text{c}}$ cross section due to the smaller p_T reach of baryon measurements at low p_T. The right panel of figure 13 shows the c$\bar{\text{c}}$ production cross section at midrapidity ($|y| < 0.5$) in pp collisions as a function of centre-of-mass energy $\sqrt{s}$. The blue points represent the measurements from the ALICE collaboration. The result from this work corresponds to the first measurement of the c$\bar{\text{c}}$ production cross section at midrapidity in pp collisions at $\sqrt{s} = 13$ TeV based on the measured cross sections of several charm-hadron species, while previously only estimates based on dilepton measurements were available [104]. In figure 13 the results in pp collisions at $\sqrt{s} = 200$ GeV by the STAR [105] and PHENIX [106] collaborations are also shown. The c$\bar{\text{c}}$ cross section was obtained from the measurement of D^0- and D^{*+}-meson abundances and from the production cross section of electrons from heavy-flavour hadron decays, as discussed in ref. [54]. In these cases, the production cross sections were scaled by fragmentation fractions obtained from e$^+$e$^-$ collisions.

The measured c$\bar{\text{c}}$ production cross sections at midrapidity in pp collisions at different centre-of-mass energies are compared with the FONLL and NNLO predictions. The NNLO values were obtained by the authors of [91, 92] by applying a K scaling factor (NNLO/NLO) to the central value of $\text{d}\sigma^{\text{c}\bar{\text{c}}}/\text{d}y$ from FONLL, calculated as discussed in ref. [54]. The results from RHIC are compatible with the upper edge of the theoretical calculations. The results at the LHC are systematically higher as an effect of the measured baryon enhancement at midrapidity. However, within the current experimental precision the measured $\text{d}\sigma^{\text{c}\bar{\text{c}}}/\text{d}y|_{|y|<0.5}$ at the LHC are compatible with the FONLL predictions within about 1σ in

pp collisions at $\sqrt{s} = 5.02\,\text{TeV}$ and about 1.4σ in pp collisions at $\sqrt{s} = 13\,\text{TeV}$. In the end, calculations based on a factorisation approach describe quantitatively the evolution of the $c\bar{c}$ cross section at midrapidity in pp collisions as a function of the centre-of-mass energy. The precise measurements from LHC data shown in figure 13 can provide useful constraints to reduce the uncertainties related either to the factorisation and renormalisation scales in pQCD calculations of the hard-scattering cross section, or to the PDFs.

6 Summary

In this article, the measurements of the production cross sections of prompt D^0, D^+, D_s^+, and D^{*+} mesons at midrapidity ($|y| < 0.5$) in pp collisions at $\sqrt{s} = 13\,\text{TeV}$ with the ALICE detector are reported. The D-meson production cross sections are described within uncertainties by perturbative QCD calculations based on a factorisation approach over the full p_T ranges of the measurements. The p_T-differential ratios of the measured charm-hadron cross sections are compared with the same quantities measured in pp collisions at $\sqrt{s} = 5.02\,\text{TeV}$ and $7\,\text{TeV}$. Within the experimental uncertainties, no significant energy dependence of the D-meson ratios in pp collisions at the LHC is observed. These results suggest common fragmentation functions of charm quarks to pseudoscalar and vector mesons and to mesons with and without strange quark content in pp collisions at different LHC energies.

The production cross sections of prompt Λ_c^+ and Ξ_c^+ baryons in pp collisions at $\sqrt{s} = 13\,\text{TeV}$ are measured down to $p_T = 0$ and $p_T = 3\,\text{GeV}/c$, respectively. Similarly to the meson-to-meson ratios at the LHC, the measured Λ_c^+/D^0 ratio in pp collisions at $\sqrt{s} = 5.02\,\text{TeV}$, $7\,\text{TeV}$, and $13\,\text{TeV}$, and the $\Xi_c^{0,+}/D^0$ ratios in pp collisions at $\sqrt{s} = 5.02\,\text{TeV}$ and $13\,\text{TeV}$ do not show a significant energy dependence. Within the current uncertainties, the measurements do not discriminate among the model calculations that describe charm hadronisation at the LHC employing new mechanisms. However, the extended measurements of the Λ_c^+ and Ξ_c^+ production confirm the baryon-to-meson enhancement at the LHC compared to e^+e^- results down to lower p_T. These results support the scenario of charm-quark hadronisation in pp collisions at the LHC via mechanisms other than those in e^+e^- collisions.

The p_T-differential cross sections of prompt D mesons measured at midrapidity ($|y| < 0.5$) are compared with those measured at forward rapidity by the LHCb collaboration in three intervals $2 < y < 2.5$, $3 < y < 3.5$, and $4 < y < 4.5$ at the same collision energy. The mid-over-forward rapidity ratios show an increasing trend with p_T when going to more forward rapidities and a common trend is shared by all the D-meson species. This behaviour can be explained as a softening of the p_T spectra at forward rapidity, which is described by pQCD-based calculations (FONLL). The measurement of the D^0-meson mid-to-forward rapidity ratios between pp collisions at $\sqrt{s} = 5.02\,\text{TeV}$ and $13\,\text{TeV}$ is provided and compared with FONLL predictions employing the CTEQ6.6 and NNPDF30 sets of PDFs. The perturbative QCD calculations reproduce the magnitude and the p_T dependence of the ratios. The measurements are precise enough to constrain the gluon PDFs employed in the NNPDF30 set at low p_T, given that the uncertainties related to the scale variations in the pQCD calculations are found to be subdominant. A similar

comparison would be interesting considering predictions from pQCD-based calculations employing more recent PDF sets.

The D-meson strangeness suppression factor $\gamma_{\rm s}$ in pp collisions at $\sqrt{s} = 13\,{\rm TeV}$ is compared with previous measurements from the ALICE, ATLAS, H1, and ZEUS collaborations. The results are compatible within uncertainties and they agree with the average of LEP measurements. These results indicate that the production of prompt strange D mesons relative to that of prompt non-strange D mesons in e^+e^-, ep and pp collisions does not show any significant dependence on the collision system and energy.

The measurement of charm-quark fragmentation fractions in pp collisions at $\sqrt{s} = 13\,{\rm TeV}$ is provided. In addition to the charm-quark fragmentation fractions into D^0, D^+, $D_{\rm s}^+$, D^{*+}, $\Lambda_{\rm c}^+$, and $\Xi_{\rm c}^0$ hadrons, also the results for the fragmentation into J/ψ mesons and $\Xi_{\rm c}^+$ and $\Sigma_{\rm c}^{0,+,++}$ baryons are reported. The results are compared with those in pp collisions at $\sqrt{s} = 5.02\,{\rm TeV}$ and no significant energy dependence is observed according to the current uncertainties. These results confirm that the baryon enhancement at the LHC with respect to e^+e^- collisions is caused by different hadronisation mechanisms at play in the parton-rich environment produced in pp collisions. Finally, the first measurement in pp collisions at $\sqrt{s} = 13\,{\rm TeV}$ of the $c\bar{c}$ production cross section at midrapidity ($|y| < 0.5$) based on the sum of the production cross sections at midrapidity of D^0, D^+, $D_{\rm s}^+$, J/ψ, $\Lambda_{\rm c}^+$, $\Xi_{\rm c}^0$, and $\Xi_{\rm c}^+$ hadrons is reported. This measurement, whose maximum relative uncertainty is about 13%, is found to be compatible with the upper edge of the FONLL and NNLO predictions within uncertainties. Thanks to their better precision, the measurements at the LHC can provide useful constraints to reduce the theoretical uncertainties on the calculations of $c\bar{c}$ production at midrapidity in pp collisions.

Acknowledgments

References

[1] J.C. Collins, D.E. Soper and G.F. Sterman, *Factorization of Hard Processes in QCD*, in *Perturbative QCD*, *Advanced Series on Directions in High Energy Physics* **5**, World Scientific (1989), pp. 1–91 [`DOI:10.1142/9789814503266_0001`] [`hep-ph/0409313`] [INSPIRE].

[2] S. Catani, M. Ciafaloni and F. Hautmann, *High-energy factorization and small x heavy flavor production*, *Nucl. Phys. B* **366** (1991) 135 [INSPIRE].

[3] M. Luszczak, R. Maciuła and A. Szczurek, *Nonphotonic electrons at RHIC within k_t-factorization approach and with experimental semileptonic decay functions*, *Phys. Rev. D* **79** (2009) 034009 [`arXiv:0807.5044`] [INSPIRE].

[4] R. Maciuła and A. Szczurek, *Open charm production at the LHC: k_t-factorization approach*, *Phys. Rev. D* **87** (2013) 094022 [`arXiv:1301.3033`] [INSPIRE].

[5] R. Maciuła and A. Szczurek, *Consistent treatment of charm production in higher-orders at tree-level within k_T-factorization approach*, *Phys. Rev. D* **100** (2019) 054001 [`arXiv:1905.06697`] [INSPIRE].

[6] Y.M. Shabelski, A.G. Shuvaev and I.V. Surnin, *Heavy quark production in k_t factorization approach at LHC energies*, *Int. J. Mod. Phys. A* **33** (2017) 1850003 [`arXiv:1709.02203`] [INSPIRE].

[7] M. Benzke, M.V. Garzelli, B. Kniehl, G. Kramer, S. Moch and G. Sigl, *Prompt neutrinos from atmospheric charm in the general-mass variable-flavor-number scheme*, *JHEP* **12** (2017) 021 [`arXiv:1705.10386`] [INSPIRE].

[8] G. Kramer and H. Spiesberger, *Study of heavy meson production in p-Pb collisions at $\sqrt{s} = 5.02$ TeV in the general-mass variable-flavour-number scheme*, *Nucl. Phys. B* **925** (2017) 415 [`arXiv:1703.04754`] [INSPIRE].

[9] B.A. Kniehl, G. Kramer, I. Schienbein and H. Spiesberger, *Inclusive $D^{*\pm}$ production in $p\bar{p}$ collisions with massive charm quarks*, *Phys. Rev. D* **71** (2005) 014018 [`hep-ph/0410289`] [INSPIRE].

[10] B.A. Kniehl, G. Kramer, I. Schienbein and H. Spiesberger, *Collinear subtractions in hadroproduction of heavy quarks*, *Eur. Phys. J. C* **41** (2005) 199 [`hep-ph/0502194`] [INSPIRE].

[11] B.A. Kniehl, G. Kramer, I. Schienbein and H. Spiesberger, *Inclusive Charmed-Meson Production at the CERN LHC*, *Eur. Phys. J. C* **72** (2012) 2082 [`arXiv:1202.0439`] [INSPIRE].

[12] I. Helenius and H. Paukkunen, *Revisiting the D-meson hadroproduction in general-mass variable flavour number scheme*, *JHEP* **05** (2018) 196 [`arXiv:1804.03557`] [INSPIRE].

[13] M. Cacciari, M. Greco and P. Nason, *The p_T spectrum in heavy-flavour hadroproduction*, *JHEP* **05** (1998) 007 [`hep-ph/9803400`] [INSPIRE].

[14] M. Cacciari, S. Frixione, N. Houdeau, M.L. Mangano, P. Nason and G. Ridolfi, *Theoretical predictions for charm and bottom production at the LHC*, *JHEP* **10** (2012) 137 [arXiv:1205.6344] [INSPIRE].

[15] B. Guiot and A. van Hameren, *D and B-meson production using k_t-factorization calculations in a variable-flavor-number scheme*, *Phys. Rev. D* **104** (2021) 094038 [arXiv:2108.06419] [INSPIRE].

[16] D. Boer and C. Pisano, *Polarized gluon studies with charmonium and bottomonium at LHCb and AFTER*, *Phys. Rev. D* **86** (2012) 094007 [arXiv:1208.3642] [INSPIRE].

[17] J.P. Ma, J.X. Wang and S. Zhao, *Transverse momentum dependent factorization for quarkonium production at low transverse momentum*, *Phys. Rev. D* **88** (2013) 014027 [arXiv:1211.7144] [INSPIRE].

[18] Y.-Q. Ma and R. Venugopalan, *Comprehensive Description of J/ψ Production in Proton-Proton Collisions at Collider Energies*, *Phys. Rev. Lett.* **113** (2014) 192301 [arXiv:1408.4075] [INSPIRE].

[19] ALICE collaboration, *Measurement of D^0, D^+, D^{*+} and D_s^+ production in pp collisions at $\sqrt{s} = 5.02$ TeV with ALICE*, *Eur. Phys. J. C* **79** (2019) 388 [arXiv:1901.07979] [INSPIRE].

[20] ALICE collaboration, *Measurement of charm production at central rapidity in proton-proton collisions at $\sqrt{s} = 2.76$ TeV*, *JHEP* **07** (2012) 191 [arXiv:1205.4007] [INSPIRE].

[21] ALICE collaboration, *D_s^+ meson production at central rapidity in proton-proton collisions at $\sqrt{s} = 7$ TeV*, *Phys. Lett. B* **718** (2012) 279 [arXiv:1208.1948] [INSPIRE].

[22] ALICE collaboration, *Measurement of D-meson production at mid-rapidity in pp collisions at $\sqrt{s} = 7$ TeV*, *Eur. Phys. J. C* **77** (2017) 550 [arXiv:1702.00766] [INSPIRE].

[23] ALICE collaboration, *Measurement of beauty and charm production in pp collisions at $\sqrt{s} = 5.02$ TeV via non-prompt and prompt D mesons*, *JHEP* **05** (2021) 220 [arXiv:2102.13601] [INSPIRE].

[24] ATLAS collaboration, *Measurement of $D^{*\pm}$, $D^{\pm}$ and $D_s^{\pm}$ meson production cross sections in pp collisions at $\sqrt{s} = 7$ TeV with the ATLAS detector*, *Nucl. Phys. B* **907** (2016) 717 [arXiv:1512.02913] [INSPIRE].

[25] CMS collaboration, *Nuclear modification factor of D^0 mesons in PbPb collisions at $\sqrt{s_{NN}} = 5.02$ TeV*, *Phys. Lett. B* **782** (2018) 474 [arXiv:1708.04962] [INSPIRE].

[26] LHCb collaboration, *Prompt charm production in pp collisions at $\sqrt{s} = 7$ TeV*, *Nucl. Phys. B* **871** (2013) 1 [arXiv:1302.2864] [INSPIRE].

[27] LHCb collaboration, *Measurements of prompt charm production cross-sections in pp collisions at $\sqrt{s} = 13$ TeV*, *JHEP* **03** (2016) 159 [*Erratum ibid.* **09** (2016) 013] [arXiv:1510.01707] [INSPIRE].

[28] LHCb collaboration, *Measurements of prompt charm production cross-sections in pp collisions at $\sqrt{s} = 5$ TeV*, *JHEP* **06** (2017) 147 [arXiv:1610.02230] [INSPIRE].

[29] CMS collaboration, *Measurement of prompt open-charm production cross sections in proton-proton collisions at $\sqrt{s} = 13$ TeV*, *JHEP* **11** (2021) 225 [arXiv:2107.01476] [INSPIRE].

[30] M. Cacciari, M.L. Mangano and P. Nason, *Gluon PDF constraints from the ratio of forward heavy-quark production at the LHC at $\sqrt{s} = 7$ and 13 TeV*, *Eur. Phys. J. C* **75** (2015) 610 [arXiv:1507.06197] [INSPIRE].

[31] ALICE collaboration, *The ALICE experiment — A journey through QCD*, arXiv:2211.04384 [INSPIRE].

[32] ALICE collaboration, *Λ_c^+ Production and Baryon-to-Meson Ratios in pp and p-Pb Collisions at $\sqrt{s_{\mathrm{NN}}} = 5.02$ TeV at the LHC*, *Phys. Rev. Lett.* **127** (2021) 202301 [arXiv:2011.06078] [INSPIRE].

[33] ALICE collaboration, *Λ_c^+ production in pp and in p-Pb collisions at $\sqrt{s_{\mathrm{NN}}} = 5.02$ TeV*, *Phys. Rev. C* **104** (2021) 054905 [arXiv:2011.06079] [INSPIRE].

[34] CMS collaboration, *Production of Λ_c^+ baryons in proton-proton and lead-lead collisions at $\sqrt{s_{\mathrm{NN}}} = 5.02$ TeV*, *Phys. Lett. B* **803** (2020) 135328 [arXiv:1906.03322] [INSPIRE].

[35] ALICE collaboration, *First measurement of Λ_c^+ production down to $p_T = 0$ in pp and p-Pb collisions at $\sqrt{s_{\mathrm{NN}}} = 5.02$ TeV*, *Phys. Rev. C* **107** (2023) 064901 [arXiv:2211.14032] [INSPIRE].

[36] OPAL collaboration, *A Study of charm hadron production in $^0 \to c\bar{c}$ and $Z^0 \to b\bar{b}$ decays at LEP*, *Z. Phys. C* **72** (1996) 1 [INSPIRE].

[37] S. Frixione, P. Nason and G. Ridolfi, *A Positive-weight next-to-leading-order Monte Carlo for heavy flavour hadroproduction*, *JHEP* **09** (2007) 126 [arXiv:0707.3088] [INSPIRE].

[38] T. Sjostrand, S. Mrenna and P.Z. Skands, *PYTHIA 6.4 Physics and Manual*, *JHEP* **05** (2006) 026 [hep-ph/0603175] [INSPIRE].

[39] T. Sjöstrand et al., *An introduction to PYTHIA 8.2*, *Comput. Phys. Commun.* **191** (2015) 159 [arXiv:1410.3012] [INSPIRE].

[40] P. Skands, S. Carrazza and J. Rojo, *Tuning PYTHIA 8.1: the Monash 2013 Tune*, *Eur. Phys. J. C* **74** (2014) 3024 [arXiv:1404.5630] [INSPIRE].

[41] J. Bellm et al., *Herwig 7.0/Herwig++ 3.0 release note*, *Eur. Phys. J. C* **76** (2016) 196 [arXiv:1512.01178] [INSPIRE].

[42] SHERPA collaboration, *Event Generation with Sherpa 2.2*, *SciPost Phys.* **7** (2019) 034 [arXiv:1905.09127] [INSPIRE].

[43] J.R. Christiansen and P.Z. Skands, *String Formation Beyond Leading Colour*, *JHEP* **08** (2015) 003 [arXiv:1505.01681] [INSPIRE].

[44] M. He and R. Rapp, *Charm-Baryon Production in Proton-Proton Collisions*, *Phys. Lett. B* **795** (2019) 117 [arXiv:1902.08889] [INSPIRE].

[45] D. Ebert, R.N. Faustov and V.O. Galkin, *Spectroscopy and Regge trajectories of heavy baryons in the relativistic quark-diquark picture*, *Phys. Rev. D* **84** (2011) 014025 [arXiv:1105.0583] [INSPIRE].

[46] P. Braun-Munzinger, K. Redlich and J. Stachel, *Particle production in heavy ion collisions*, in *Quark-Gluon Plasma* **4**, R.C. Hwa and X.-N. Wang eds., World Scientific, Singapore (2010) [nucl-th/0304013] [DOI:10.1142/9789812795533_0008] [INSPIRE].

[47] V. Minissale, S. Plumari and V. Greco, *Charm hadrons in pp collisions at LHC energy within a coalescence plus fragmentation approach*, *Phys. Lett. B* **821** (2021) 136622 [arXiv:2012.12001] [INSPIRE].

[48] J. Song, H.-h. Li and F.-l. Shao, *New feature of low p_T charm quark hadronization in pp collisions at $\sqrt{s} = 7$ TeV*, *Eur. Phys. J. C* **78** (2018) 344 [arXiv:1801.09402] [INSPIRE].

[49] ALICE collaboration, *Measurement of Prompt D^0, Λ_c^+, and $\Sigma_c^{0,++}(2455)$ Production in Proton-Proton Collisions at $\sqrt{s} = 13$ TeV*, *Phys. Rev. Lett.* **128** (2022) 012001 [arXiv:2106.08278] [INSPIRE].

[50] BELLE collaboration, *Production cross sections of hyperons and charmed baryons from e^+e^- annihilation near $\sqrt{s} = 10.52$ GeV*, *Phys. Rev. D* **97** (2018) 072005 [arXiv:1706.06791] [INSPIRE].

[51] ALICE collaboration, *Measurement of the production cross section of prompt Ξ_c^0 baryons at midrapidity in pp collisions at $\sqrt{s} = 5.02$ TeV*, *JHEP* **10** (2021) 159 [arXiv:2105.05616] [INSPIRE].

[52] ALICE collaboration, *Measurement of the Cross Sections of Ξ_c^0 and Ξ_c^+ Baryons and of the Branching-Fraction Ratio $BR(\Xi_c^0 \to \Xi^- e^+ \nu_e)/BR(\Xi_c^0 \to \Xi^- \pi^+)$ in pp collisions at $\sqrt{s} = 13$ TeV*, *Phys. Rev. Lett.* **127** (2021) 272001 [arXiv:2105.05187] [INSPIRE].

[53] ALICE collaboration, *First measurement of Ω_c^0 production in pp collisions at $\sqrt{s} = 13$ TeV*, *Phys. Lett. B* **846** (2023) 137625 [arXiv:2205.13993] [INSPIRE].

[54] ALICE collaboration, *Charm-quark fragmentation fractions and production cross section at midrapidity in pp collisions at the LHC*, *Phys. Rev. D* **105** (2022) L011103 [arXiv:2105.06335] [INSPIRE].

[55] M. Lisovyi, A. Verbytskyi and O. Zenaiev, *Combined analysis of charm-quark fragmentation-fraction measurements*, *Eur. Phys. J. C* **76** (2016) 397 [arXiv:1509.01061] [INSPIRE].

[56] P. Braun-Munzinger and J. Stachel, *(Non)thermal aspects of charmonium production and a new look at J/ψ suppression*, *Phys. Lett. B* **490** (2000) 196 [nucl-th/0007059] [INSPIRE].

[57] X. Zhao and R. Rapp, *Medium Modifications and Production of Charmonia at LHC*, *Nucl. Phys. A* **859** (2011) 114 [arXiv:1102.2194] [INSPIRE].

[58] Y.-p. Liu, Z. Qu, N. Xu and P.-f. Zhuang, *J/ψ Transverse Momentum Distribution in High Energy Nuclear Collisions at RHIC*, *Phys. Lett. B* **678** (2009) 72 [arXiv:0901.2757] [INSPIRE].

[59] ALICE collaboration, *Prompt D^0, D^+, and D^{*+} production in Pb-Pb collisions at $\sqrt{s_{\mathrm{NN}}} = 5.02$ TeV*, *JHEP* **01** (2022) 174 [arXiv:2110.09420] [INSPIRE].

[60] ALICE collaboration, *Observation of a multiplicity dependence in the p_T-differential charm baryon-to-meson ratios in proton-proton collisions at $\sqrt{s} = 13$ TeV*, *Phys. Lett. B* **829** (2022) 137065 [arXiv:2111.11948] [INSPIRE].

[61] ALICE collaboration, *The ALICE experiment at the CERN LHC*, 2008 *JINST* **3** S08002 [INSPIRE].

[62] ALICE collaboration, *Performance of the ALICE Experiment at the CERN LHC*, *Int. J. Mod. Phys. A* **29** (2014) 1430044 [arXiv:1402.4476] [INSPIRE].

[63] ALICE collaboration, *Alignment of the ALICE Inner Tracking System with cosmic-ray tracks*, 2010 *JINST* **5** P03003 [arXiv:1001.0502] [INSPIRE].

[64] ALICE collaboration, *ALICE 2016-2017-2018 luminosity determination for pp collisions at $\sqrt{s} = 13$ TeV*, ALICE-PUBLIC-2021-005 (2021).

[65] R. Brun et al., *GEANT: Detector Description and Simulation Tool*, in *CERN Program Library*, CERN-W-5013 (1993).

[66] PARTICLE DATA collaboration, *Review of Particle Physics*, *Prog. Theor. Exp. Phys.* **2022** (2022) 083C01 [INSPIRE].

[67] BELLE collaboration, *First measurements of absolute branching fractions of the Ξ_c^+ baryon at Belle*, *Phys. Rev. D* **100** (2019) 031101 [arXiv:1904.12093] [INSPIRE].

[68] ALICE collaboration, *The ALICE definition of primary particles*, ALICE-PUBLIC-2017-005 (2017).

[69] I. Kisel, I. Kulakov and M. Zyzak, *Standalone first level event selection package for the CBM experiment*, in the proceedings of the *18th Real-Time Conference (RT2012)*, Berkley, CA, U.S.A., 11–15 June 2012, pp. 1–6 [DOI:10.1109/RTC.2012.6418385] [INSPIRE].

[70] T. Chen and C. Guestrin, *XGBoost: A Scalable Tree Boosting System*, in the proceedings of the *22nd ACM SIGKDD International Conference on Knowledge Discovery and Data Mining (KDD 16)*, San Francisco, CA, U.S.A., 13–17 August 2016, pp. 785–794 [arXiv:1603.02754] [DOI:10.1145/2939672.2939785] [INSPIRE].

[71] L. Barioglio et al., *hipe4ml/hipe4ml*, Zenodo (2022) [DOI:10.5281/ZENODO.7014886].

[72] ALICE collaboration, *Particle identification in ALICE: a Bayesian approach*, *Eur. Phys. J. Plus* **131** (2016) 168 [arXiv:1602.01392] [INSPIRE].

[73] A. Hoecker et al., *TMVA — Toolkit for Multivariate Data Analysis*, physics/0703039 [INSPIRE].

[74] ALICE collaboration, Λ_c^+ *production in pp collisions at $\sqrt{s} = 7$ TeV and in p-Pb collisions at $\sqrt{s_{NN}} = 5.02$ TeV*, *JHEP* **04** (2018) 108 [arXiv:1712.09581] [INSPIRE].

[75] LHCb collaboration, *Measurement of b hadron fractions in 13 TeV pp collisions*, *Phys. Rev. D* **100** (2019) 031102 [arXiv:1902.06794] [INSPIRE].

[76] L. Gladilin, *Fragmentation fractions of c and b quarks into charmed hadrons at LEP*, *Eur. Phys. J. C* **75** (2015) 19 [arXiv:1404.3888] [INSPIRE].

[77] ALICE collaboration, *Data-driven precision determination of the material budget in ALICE*, 2023 *JINST* **18** P11032 [arXiv:2303.15317] [INSPIRE].

[78] LHCb collaboration, *Measurement of the mass and production rate of Ξ_b^- baryons*, *Phys. Rev. D* **99** (2019) 052006 [arXiv:1901.07075] [INSPIRE].

[79] J. Pumplin, D.R. Stump, J. Huston, H.L. Lai, P.M. Nadolsky and W.K. Tung, *New generation of parton distributions with uncertainties from global QCD analysis*, *JHEP* **07** (2002) 012 [hep-ph/0201195] [INSPIRE].

[80] A. Beraudo, A. De Pace, D. Pablos, F. Prino, M. Monteno and M. Nardi, *Heavy-flavor transport and hadronization in pp collisions*, arXiv:2306.02152 [INSPIRE].

[81] HOTQCD collaboration, *Heavy Quark Diffusion from $2 + 1$ Flavor Lattice QCD with 320 MeV Pion Mass*, *Phys. Rev. Lett.* **130** (2023) 231902 [arXiv:2302.08501] [INSPIRE].

[82] NNPDF collaboration, *Parton distributions for the LHC Run II*, *JHEP* **04** (2015) 040 [arXiv:1410.8849] [INSPIRE].

[83] ALICE collaboration, *Measurement of charm production at central rapidity in proton-proton collisions at $\sqrt{s} = 7$ TeV*, *JHEP* **01** (2012) 128 [arXiv:1111.1553] [INSPIRE].

[84] R. Averbeck, N. Bastid, Z.C. del Valle, P. Crochet, A. Dainese and X. Zhang, *Reference Heavy Flavour Cross Sections in pp Collisions at $\sqrt{s} = 2.76$ TeV, using a pQCD-Driven $\sqrt{s}$-Scaling of ALICE Measurements at $\sqrt{s} = 7$ TeV*, arXiv:1107.3243 [INSPIRE].

[85] ALEPH collaboration, *Study of charm production in Z decays*, *Eur. Phys. J. C* **16** (2000) 597 [hep-ex/9909032] [INSPIRE].

[86] E. Braaten, K.-M. Cheung, S. Fleming and T.C. Yuan, *Perturbative QCD fragmentation functions as a model for heavy quark fragmentation*, *Phys. Rev. D* **51** (1995) 4819 [hep-ph/9409316] [INSPIRE].

[87] ALICE collaboration, *Prompt and non-prompt J/ψ production cross sections at midrapidity in proton-proton collisions at $\sqrt{s} = 5.02$ and 13 TeV*, *JHEP* **03** (2022) 190 [arXiv:2108.02523] [INSPIRE].

[88] H1 collaboration, *Inclusive production of D^+, D^0, D_s^+ and D^{*+} mesons in deep inelastic scattering at HERA*, *Eur. Phys. J. C* **38** (2005) 447 [hep-ex/0408149] [INSPIRE].

[89] ZEUS collaboration, *Measurement of charm fragmentation fractions in photoproduction at HERA*, *JHEP* **09** (2013) 058 [arXiv:1306.4862] [INSPIRE].

[90] F. Becattini, M. Gazdzicki and J. Sollfrank, *On chemical equilibrium in nuclear collisions*, *Eur. Phys. J. C* **5** (1998) 143 [hep-ph/9710529] [INSPIRE].

[91] D. d'Enterria and A.M. Snigirev, *Triple parton scatterings in high-energy proton-proton collisions*, *Phys. Rev. Lett.* **118** (2017) 122001 [arXiv:1612.05582] [INSPIRE].

[92] D. d'Enterria and A.M. Snigirev, *Triple-parton scatterings in proton-nucleus collisions at high energies*, *Eur. Phys. J. C* **78** (2018) 359 [arXiv:1612.08112] [INSPIRE].

[93] M. Czakon, P. Fiedler and A. Mitov, *Total Top-Quark Pair-Production Cross Section at Hadron Colliders Through $O(\alpha_S^4)$*, *Phys. Rev. Lett.* **110** (2013) 252004 [arXiv:1303.6254] [INSPIRE].

[94] Y.-K. Hsiao, L. Yang, C.-C. Lih and S.-Y. Tsai, *Charmed Ω_c weak decays into Ω in the light-front quark model*, *Eur. Phys. J. C* **80** (2020) 1066 [arXiv:2009.12752] [INSPIRE].

[95] T. Gutsche, M.A. Ivanov, J.G. Körner and V.E. Lyubovitskij, *Nonleptonic two-body decays of single heavy baryons Λ_Q, Ξ_Q, and Ω_Q ($Q = b, c$) induced by W emission in the covariant confined quark model*, *Phys. Rev. D* **98** (2018) 074011 [arXiv:1806.11549] [INSPIRE].

[96] H.-Y. Cheng, *Nonleptonic weak decays of bottom baryons*, *Phys. Rev. D* **56** (1997) 2799 [*Erratum ibid.* **99** (2019) 079901] [hep-ph/9612223] [INSPIRE].

[97] S. Hu, G. Meng and F. Xu, *Hadronic weak decays of the charmed baryon Ω_c*, *Phys. Rev. D* **101** (2020) 094033 [arXiv:2003.04705] [INSPIRE].

[98] E. Solovieva et al., *Study of Ω_c^0 and Ω_c^{*0} Baryons at Belle*, *Phys. Lett. B* **672** (2009) 1 [arXiv:0808.3677] [INSPIRE].

[99] H.-L. Lai et al., *New parton distributions for collider physics*, *Phys. Rev. D* **82** (2010) 074024 [arXiv:1007.2241] [INSPIRE].

[100] S. Dulat, T.-J. Hou, J. Gao et al., *New parton distribution functions from a global analysis of quantum chromodynamics*, *Phys. Rev. D* **93** (2016) 033006 [arXiv:1506.07443] [INSPIRE].

[101] T.-J. Hou et al., *New CTEQ Global Analysis with High Precision Data from the LHC*, arXiv:1908.11238 [INSPIRE].

[102] P.M. Nadolsky, H.-L. Lai, Q.-H. Cao et al., *Implications of CTEQ global analysis for collider observables*, *Phys. Rev. D* **78** (2008) 013004 [`arXiv:0802.0007`] [ɪɴSPIRE].

[103] S. Forte and S. Carrazza, *Parton distribution functions*, `arXiv:2008.12305` [ɪɴSPIRE].

[104] ALICE collaboration, *Dielectron and heavy-quark production in inelastic and high-multiplicity proton-proton collisions at* $\sqrt{s_{\mathrm{NN}}} = 13$ *TeV*, *Phys. Lett. B* **788** (2019) 505 [`arXiv:1805.04407`] [ɪɴSPIRE].

[105] STAR collaboration, *Measurements of* D^0 *and* D^* *Production in* $p + p$ *Collisions at* $\sqrt{s} = 200$ *GeV*, *Phys. Rev. D* **86** (2012) 072013 [`arXiv:1204.4244`] [ɪɴSPIRE].

[106] PHENIX collaboration, *Heavy Quark Production in* $p + p$ *and Energy Loss and Flow of Heavy Quarks in Au+Au Collisions at* $\sqrt{s_{\mathrm{NN}}} = 200$ *GeV*, *Phys. Rev. C* **84** (2011) 044905 [`arXiv:1005.1627`] [ɪɴSPIRE].

The ALICE collaboration

S. Acharya [126], D. Adamová [86], G. Aglieri Rinella [33], M. Agnello [30], N. Agrawal [51],
Z. Ahammed [134], S. Ahmad [16], S.U. Ahn [71], I. Ahuja [38], A. Akindinov [142],
M. Al-Turany [97], D. Aleksandrov [142], B. Alessandro [56], H.M. Alfanda [6],
R. Alfaro Molina [67], B. Ali [16], A. Alici [26], N. Alizadehvandchali [115], A. Alkin [33],
J. Alme [21], G. Alocco [52], T. Alt [64], A.R. Altamura [50], I. Altsybeev [95], M.N. Anaam [6],
C. Andrei [46], N. Andreou [114], A. Andronic [137], V. Anguelov [94], F. Antinori [54],
P. Antonioli [51], N. Apadula [74], L. Aphecetche [103], H. Appelshäuser [64], C. Arata [73],
S. Arcelli [26], M. Aresti [23], R. Arnaldi [56], J.G.M.C.A. Arneiro [110], I.C. Arsene [20],
M. Arslandok [139], A. Augustinus [33], R. Averbeck [97], M.D. Azmi [16], H. Baba [123],
A. Badalà [53], J. Bae [104], Y.W. Baek [41], X. Bai [119], R. Bailhache [64], Y. Bailung [48],
R. Bala [91], A. Balbino [30], A. Baldisseri [129], B. Balis [2], D. Banerjee [4], Z. Banoo [91],
R. Barbera [27], F. Barile [32], L. Barioglio [95], M. Barlou [78], B. Barman [42], G.G. Barnaföldi [138],
L.S. Barnby [85], V. Barret [126], L. Barreto [110], C. Bartels [118], K. Barth [33], E. Bartsch [64],
N. Bastid [126], S. Basu [75], G. Batigne [103], D. Battistini [95], B. Batyunya [143], D. Bauri [47],
J.L. Bazo Alba [101], I.G. Bearden [83], C. Beattie [139], P. Becht [97], D. Behera [48],
I. Belikov [128], A.D.C. Bell Hechavarria [137], F. Bellini [26], R. Bellwied [115],
S. Belokurova [142], Y.A.V. Beltran [45], G. Bencedi [138], S. Beole [25], Y. Berdnikov [142],
A. Berdnikova [94], L. Bergmann [94], M.G. Besoiu [63], L. Betev [33], P.P. Bhaduri [134],
A. Bhasin [91], M.A. Bhat [4], B. Bhattacharjee [42], L. Bianchi [25], N. Bianchi [49],
J. Bielčík [36], J. Bielčíková [86], J. Biernat [107], A.P. Bigot [128], A. Bilandzic [95], G. Biro [138],
S. Biswas [4], N. Bize [103], J.T. Blair [108], D. Blau [142], M.B. Blidaru [97], N. Bluhme [39],
C. Blume [64], G. Boca [22,55], F. Bock [87], T. Bodova [21], A. Bogdanov [142], S. Boi [23],
J. Bok [58], L. Boldizsár [138], M. Bombara [38], P.M. Bond [33], G. Bonomi [133,55], H. Borel [129],
A. Borissov [142], A.G. Borquez Carcamo [94], H. Bossi [139], E. Botta [25], Y.E.M. Bouziani [64],
L. Bratrud [64], P. Braun-Munzinger [97], M. Bregant [110], M. Broz [36], G.E. Bruno [96,32],
M.D. Buckland [24], D. Budnikov [142], H. Buesching [64], S. Bufalino [30], P. Buhler [102],
N. Burmasov [142], Z. Buthelezi [68,122], A. Bylinkin [21], S.A. Bysiak [107], M. Cai [6],
H. Caines [139], A. Caliva [29], E. Calvo Villar [101], J.M.M. Camacho [109], P. Camerini [24],
F.D.M. Canedo [110], M. Carabas [125], A.A. Carballo [33], F. Carnesecchi [33], R. Caron [127],
L.A.D. Carvalho [110], J. Castillo Castellanos [129], F. Catalano [33,25], C. Ceballos Sanchez [143],
I. Chakaberia [74], P. Chakraborty [47], S. Chandra [134], S. Chapeland [33], M. Chartier [118],
S. Chattopadhyay [134], S. Chattopadhyay [99], T.G. Chavez [45], T. Cheng [97,6],
C. Cheshkov [127], B. Cheynis [127], V. Chibante Barroso [33], D.D. Chinellato [111],
E.S. Chizzali [I,95], J. Cho [58], S. Cho [58], P. Chochula [33], D. Choudhury [42],
P. Christakoglou [84], C.H. Christensen [83], P. Christiansen [75], T. Chujo [124], M. Ciacco [30],
C. Cicalo [52], F. Cindolo [51], M.R. Ciupek [97], G. Clai [II,51], F. Colamaria [50], J.S. Colburn [100],
D. Colella [96,32], M. Colocci [26], M. Concas [III,33], G. Conesa Balbastre [73],
Z. Conesa del Valle [130], G. Contin [24], J.G. Contreras [36], M.L. Coquet [129], P. Cortese [132,56],
M.R. Cosentino [112], F. Costa [33], S. Costanza [22,55], C. Cot [130], J. Crkovská [94],
P. Crochet [126], R. Cruz-Torres [74], P. Cui [6], A. Dainese [54], M.C. Danisch [94], A. Danu [63],
P. Das [80], P. Das [4], S. Das [4], A.R. Dash [137], S. Dash [47], R.M.H. David [45], A. De Caro [29],

G. de Cataldo [50], J. de Cuveland [39], A. De Falco [23], D. De Gruttola [29], N. De Marco [56],
C. De Martin [24], S. De Pasquale [29], R. Deb [133], R. Del Grande [95], L. Dello Stritto [29],
W. Deng [6], P. Dhankher [19], D. Di Bari [32], A. Di Mauro [33], B. Diab [129], R.A. Diaz [143,7],
T. Dietel [113], Y. Ding [6], J. Ditzel [64], R. Divià [33], D.U. Dixit [19], Ø. Djuvsland [21],
U. Dmitrieva [142], A. Dobrin [63], B. Dönigus [64], J.M. Dubinski [135], A. Dubla [97],
S. Dudi [90], P. Dupieux [126], M. Durkac [106], N. Dzalaiova [13], T.M. Eder [137], R.J. Ehlers [74],
F. Eisenhut [64], R. Ejima [92], D. Elia [50], B. Erazmus [103], F. Ercolessi [26], B. Espagnon [130],
G. Eulisse [33], D. Evans [100], S. Evdokimov [142], L. Fabbietti [95], M. Faggin [28], J. Faivre [73],
F. Fan [6], W. Fan [74], A. Fantoni [49], M. Fasel [87], P. Fecchio [30], A. Feliciello [56],
G. Feofilov [142], A. Fernández Téllez [45], L. Ferrandi [110], M.B. Ferrer [33], A. Ferrero [129],
C. Ferrero [56], A. Ferretti [25], V.J.G. Feuillard [94], V. Filova [36], D. Finogeev [142],
F.M. Fionda [52], F. Flor [115], A.N. Flores [108], S. Foertsch [68], I. Fokin [94], S. Fokin [142],
E. Fragiacomo [57], E. Frajna [138], U. Fuchs [33], N. Funicello [29], C. Furget [73], A. Furs [142],
T. Fusayasu [98], J.J. Gaardhøje [83], M. Gagliardi [25], A.M. Gago [101], T. Gahlaut [47],
C.D. Galvan [109], D.R. Gangadharan [115], P. Ganoti [78], C. Garabatos [97], A.T. Garcia [130],
J.R.A. Garcia [45], E. Garcia-Solis [9], C. Gargiulo [33], P. Gasik [97], A. Gautam [117],
M.B. Gay Ducati [66], M. Germain [103], A. Ghimouz [124], C. Ghosh [134], M. Giacalone [51],
G. Gioachin [30], P. Giubellino [97,56], P. Giubilato [28], A.M.C. Glaenzer [129], P. Glässel [94],
E. Glimos [121], D.J.Q. Goh [76], V. Gonzalez [136], M. Gorgon [2], K. Goswami [48], S. Gotovac [34],
V. Grabski [67], L.K. Graczykowski [135], E. Grecka [86], A. Grelli [59], C. Grigoras [33],
V. Grigoriev [142], S. Grigoryan [143,1], F. Grosa [33], J.F. Grosse-Oetringhaus [33], R. Grosso [97],
D. Grund [36], N.A. Grunwald [94], G.G. Guardiano [111], R. Guernane [73], M. Guilbaud [103],
K. Gulbrandsen [83], T. Gündem [64], T. Gunji [123], W. Guo [6], A. Gupta [91], R. Gupta [91],
R. Gupta [48], S.P. Guzman [45], K. Gwizdziel [135], L. Gyulai [138], C. Hadjidakis [130],
F.U. Haider [91], S. Haidlova [36], H. Hamagaki [76], A. Hamdi [74], Y. Han [140],
B.G. Hanley [136], R. Hannigan [108], J. Hansen [75], M.R. Haque [135], J.W. Harris [139],
A. Harton [9], H. Hassan [116], D. Hatzifotiadou [51], P. Hauer [43], L.B. Havener [139],
S.T. Heckel [95], E. Hellbär [97], H. Helstrup [35], M. Hemmer [64], T. Herman [36],
G. Herrera Corral [8], F. Herrmann [137], S. Herrmann [127], K.F. Hetland [35], B. Heybeck [64],
H. Hillemanns [33], B. Hippolyte [128], F.W. Hoffmann [70], B. Hofman [59], G.H. Hong [140],
M. Horst [95], A. Horzyk [2], Y. Hou [6], P. Hristov [33], C. Hughes [121], P. Huhn [64],
L.M. Huhta [116], T.J. Humanic [88], A. Hutson [115], D. Hutter [39], R. Ilkaev [142], H. Ilyas [14],
M. Inaba [124], G.M. Innocenti [33], M. Ippolitov [142], A. Isakov [84,86], T. Isidori [117],
M.S. Islam [99], M. Ivanov [97], M. Ivanov [13], V. Ivanov [142], K.E. Iversen [75], M. Jablonski [2],
B. Jacak [74], N. Jacazio [26], P.M. Jacobs [74], S. Jadlovska [106], J. Jadlovsky [106], S. Jaelani [82],
C. Jahnke [111], M.J. Jakubowska [135], M.A. Janik [135], T. Janson [70], S. Ji [17], S. Jia [10],
A.A.P. Jimenez [65], F. Jonas [87], D.M. Jones [118], J.M. Jowett [33,97], J. Jung [64],
M. Jung [64], A. Junique [33], A. Jusko [100], M.J. Kabus [33,135], J. Kaewjai [105], P. Kalinak [60],
A.S. Kalteyer [97], A. Kalweit [33], V. Kaplin [142], A. Karasu Uysal [72], D. Karatovic [89],
O. Karavichev [142], T. Karavicheva [142], P. Karczmarczyk [135], E. Karpechev [142],
U. Kebschull [70], R. Keidel [141], D.L.D. Keijdener [59], M. Keil [33], B. Ketzer [43], S.S. Khade [48],
A.M. Khan [119,6], S. Khan [16], A. Khanzadeev [142], Y. Kharlov [142], A. Khatun [117],
A. Khuntia [36], B. Kileng [35], B. Kim [104], C. Kim [17], D.J. Kim [116], E.J. Kim [69],

J. Kim [140], J.S. Kim [41], J. Kim [58], J. Kim [69], M. Kim [19], S. Kim [18], T. Kim [140],
K. Kimura [92], S. Kirsch [64], I. Kisel [39], S. Kiselev [142], A. Kisiel [135], J.P. Kitowski [2],
J.L. Klay [5], J. Klein [33], S. Klein [74], C. Klein-Bösing [137], M. Kleiner [64], T. Klemenz [95],
A. Kluge [33], A.G. Knospe [115], C. Kobdaj [105], T. Kollegger [97], A. Kondratyev [143],
N. Kondratyeva [142], E. Kondratyuk [142], J. Konig [64], S.A. Konigstorfer [95], P.J. Konopka [33],
G. Kornakov [135], S.D. Koryciak [2], A. Kotliarov [86], V. Kovalenko [142], M. Kowalski [107],
V. Kozhuharov [37], I. Králik [60], A. Kravčáková [38], L. Krcal [33,39], M. Krivda [100,60],
F. Krizek [86], K. Krizkova Gajdosova [33], M. Kroesen [94], M. Krüger [64], D.M. Krupova [36],
E. Kryshen [142], V. Kučera [58], C. Kuhn [128], P.G. Kuijer [84], T. Kumaoka [124], D. Kumar [134],
L. Kumar [90], N. Kumar [90], S. Kumar [32], S. Kundu [33], P. Kurashvili [79], A. Kurepin [142],
A.B. Kurepin [142], A. Kuryakin [142], S. Kushpil [86], M.J. Kweon [58], Y. Kwon [140],
S.L. La Pointe [39], P. La Rocca [27], A. Lakrathok [105], M. Lamanna [33], R. Langoy [120],
P. Larionov [33], E. Laudi [33], L. Lautner [33,95], R. Lavicka [102], R. Lea [133,55], H. Lee [104],
I. Legrand [46], G. Legras [137], J. Lehrbach [39], T.M. Lelek [2], R.C. Lemmon [85],
I. León Monzón [109], M.M. Lesch [95], E.D. Lesser [19], P. Lévai [138], X. Li [10], J. Lien [120],
R. Lietava [100], I. Likmeta [115], B. Lim [25], S.H. Lim [17], V. Lindenstruth [39], A. Lindner [46],
C. Lippmann [97], D.H. Liu [6], J. Liu [118], G.S.S. Liveraro [111], I.M. Lofnes [21],
C. Loizides [87], S. Lokos [107], J. Lomker [59], P. Loncar [34], X. Lopez [126], E. López Torres [7],
P. Lu [97,119], F.V. Lugo [67], J.R. Luhder [137], M. Lunardon [28], G. Luparello [57], Y.G. Ma [40],
M. Mager [33], A. Maire [128], M.V. Makariev [37], M. Malaev [142], G. Malfattore [26],
N.M. Malik [91], Q.W. Malik [20], S.K. Malik [91], L. Malinina [VI,143], D. Mallick [130,80],
N. Mallick [48], G. Mandaglio [31,53], S.K. Mandal [79], V. Manko [142], F. Manso [126],
V. Manzari [50], Y. Mao [6], R.W. Marcjan [2], G.V. Margagliotti [24], A. Margotti [51],
A. Marín [97], C. Markert [108], P. Martinengo [33], M.I. Martínez [45], G. Martínez García [103],
M.P.P. Martins [110], S. Masciocchi [97], M. Masera [25], A. Masoni [52], L. Massacrier [130],
O. Massen [59], A. Mastroserio [131,50], O. Matonoha [75], S. Mattiazzo [28], A. Matyja [107],
C. Mayer [107], A.L. Mazuecos [33], F. Mazzaschi [25], M. Mazzilli [33], J.E. Mdhluli [122],
Y. Melikyan [44], A. Menchaca-Rocha [67], J.E.M. Mendez [65], E. Meninno [102,29],
A.S. Menon [115], M. Meres [13], S. Mhlanga [113,68], Y. Miake [124], L. Micheletti [33],
D.L. Mihaylov [95], K. Mikhaylov [143,142], A.N. Mishra [138], D. Miśkowiec [97], A. Modak [4],
B. Mohanty [80], M. Mohisin Khan [IV,16], M.A. Molander [44], S. Monira [135], C. Mordasini [116],
D.A. Moreira De Godoy [137], I. Morozov [142], A. Morsch [33], T. Mrnjavac [33],
V. Muccifora [49], S. Muhuri [134], J.D. Mulligan [74], A. Mulliri [23], M.G. Munhoz [110],
R.H. Munzer [64], H. Murakami [123], S. Murray [113], L. Musa [33], J. Musinsky [60],
J.W. Myrcha [135], B. Naik [122], A.I. Nambrath [19], B.K. Nandi [47], R. Nania [51],
E. Nappi [50], A.F. Nassirpour [18], A. Nath [94], C. Nattrass [121], M.N. Naydenov [37],
A. Neagu [20], A. Negru [125], L. Nellen [65], R. Nepeivoda [75], S. Nese [20], G. Neskovic [39],
N. Nicassio [50], B.S. Nielsen [83], E.G. Nielsen [83], S. Nikolaev [142], S. Nikulin [142],
V. Nikulin [142], F. Noferini [51], S. Noh [12], P. Nomokonov [143], J. Norman [118],
N. Novitzky [87], P. Nowakowski [135], A. Nyanin [142], J. Nystrand [21], M. Ogino [76], S. Oh [18],
A. Ohlson [75], V.A. Okorokov [142], J. Oleniacz [135], A.C. Oliveira Da Silva [121],
A. Onnerstad [116], C. Oppedisano [56], A. Ortiz Velasquez [65], J. Otwinowski [107], M. Oya [92],
K. Oyama [76], Y. Pachmayer [94], S. Padhan [47], D. Pagano [133,55], G. Paić [65],

A. Palasciano [50], S. Panebianco [129], H. Park [124], H. Park [104], J. Park [58],
J.E. Parkkila [33], Y. Patley [47], R.N. Patra [91], B. Paul [23], H. Pei [6], T. Peitzmann [59],
X. Peng [11], M. Pennisi [25], S. Perciballi [25], D. Peresunko [142], G.M. Perez [7], Y. Pestov [142],
V. Petrov [142], M. Petrovici [46], R.P. Pezzi [103,66], S. Piano [57], M. Pikna [13], P. Pillot [103],
O. Pinazza [51,33], L. Pinsky [115], C. Pinto [95], S. Pisano [49], M. Płoskoń [74], M. Planinic [89],
F. Pliquett [64], M.G. Poghosyan [87], B. Polichtchouk [142], S. Politano [30], N. Poljak [89],
A. Pop [46], S. Porteboeuf-Houssais [126], V. Pozdniakov [143], I.Y. Pozos [45], K.K. Pradhan [48],
S.K. Prasad [4], S. Prasad [48], R. Preghenella [51], F. Prino [56], C.A. Pruneau [136],
I. Pshenichnov [142], M. Puccio [33], S. Pucillo [25], Z. Pugelova [106], S. Qiu [84], L. Quaglia [25],
S. Ragoni [15], A. Rai [139], A. Rakotozafindrabe [129], L. Ramello [132,56], F. Rami [128],
S.A.R. Ramirez [45], T.A. Rancien [73], M. Rasa [27], S.S. Räsänen [44], R. Rath [51],
M.P. Rauch [21], I. Ravasenga [84], K.F. Read [87,121], C. Reckziegel [112], A.R. Redelbach [39],
K. Redlich [V,79], C.A. Reetz [97], A. Rehman [21], F. Reidt [33], H.A. Reme-Ness [35],
Z. Rescakova [38], K. Reygers [94], A. Riabov [142], V. Riabov [142], R. Ricci [29], M. Richter [20],
A.A. Riedel [95], W. Riegler [33], A.G. Riffero [25], C. Ristea [63], M.V. Rodriguez [33],
M. Rodríguez Cahuantzi [45], K. Røed [20], R. Rogalev [142], E. Rogochaya [143],
T.S. Rogoschinski [64], D. Rohr [33], D. Röhrich [21], P.F. Rojas [45], S. Rojas Torres [36],
P.S. Rokita [135], G. Romanenko [26], F. Ronchetti [49], A. Rosano [31,53], E.D. Rosas [65],
K. Roslon [135], A. Rossi [54], A. Roy [48], S. Roy [47], N. Rubini [26], D. Ruggiano [135],
R. Rui [24], P.G. Russek [2], R. Russo [84], A. Rustamov [81], E. Ryabinkin [142], Y. Ryabov [142],
A. Rybicki [107], H. Rytkonen [116], J. Ryu [17], W. Rzesa [135], O.A.M. Saarimaki [44],
S. Sadhu [32], S. Sadovsky [142], J. Saetre [21], K. Šafařík [36], P. Saha [42], S.K. Saha [4],
S. Saha [80], B. Sahoo [47], B. Sahoo [48], R. Sahoo [48], S. Sahoo [61], D. Sahu [48], P.K. Sahu [61],
J. Saini [134], K. Sajdakova [38], S. Sakai [124], M.P. Salvan [97], S. Sambyal [91], D. Samitz [102],
I. Sanna [33,95], T.B. Saramela [110], P. Sarma [42], V. Sarritzu [23], V.M. Sarti [95], M.H.P. Sas [139],
S. Sawan [80], J. Schambach [87], H.S. Scheid [64], C. Schiaua [46], R. Schicker [94], A. Schmah [97],
C. Schmidt [97], H.R. Schmidt [93], M.O. Schmidt [33], M. Schmidt [93], N.V. Schmidt [87],
A.R. Schmier [121], R. Schotter [128], A. Schröter [39], J. Schukraft [33], K. Schweda [97],
G. Scioli [26], E. Scomparin [56], J.E. Seger [15], Y. Sekiguchi [123], D. Sekihata [123], M. Selina [84],
I. Selyuzhenkov [97], S. Senyukov [128], J.J. Seo [94,58], D. Serebryakov [142], L. Šerkšnytė [95],
A. Sevcenco [63], T.J. Shaba [68], A. Shabetai [103], R. Shahoyan [33], A. Shangaraev [142],
A. Sharma [90], B. Sharma [91], D. Sharma [47], H. Sharma [54,107], M. Sharma [91], S. Sharma [76],
S. Sharma [91], U. Sharma [91], A. Shatat [130], O. Sheibani [115], K. Shigaki [92], M. Shimomura [77],
J. Shin [12], S. Shirinkin [142], Q. Shou [40], Y. Sibiriak [142], S. Siddhanta [52], T. Siemiarczuk [79],
T.F. Silva [110], D. Silvermyr [75], T. Simantathammakul [105], R. Simeonov [37], B. Singh [91],
B. Singh [95], K. Singh [48], R. Singh [80], R. Singh [91], R. Singh [48], S. Singh [16],
V.K. Singh [134], V. Singhal [134], T. Sinha [99], B. Sitar [13], M. Sitta [132,56], T.B. Skaali [20],
G. Skorodumovs [94], M. Slupecki [44], N. Smirnov [139], R.J.M. Snellings [59], E.H. Solheim [20],
J. Song [17], C. Sonnabend [33,97], F. Soramel [28], A.B. Soto-hernandez [88], R. Spijkers [84],
I. Sputowska [107], J. Staa [75], J. Stachel [94], I. Stan [63], P.J. Steffanic [121],
S.F. Stiefelmaier [94], D. Stocco [103], I. Storehaug [20], P. Stratmann [137], S. Strazzi [26],
A. Sturniolo [31,53], C.P. Stylianidis [84], A.A.P. Suaide [110], C. Suire [130], M. Sukhanov [142],
M. Suljic [33], R. Sultanov [142], V. Sumberia [91], S. Sumowidagdo [82], S. Swain [61], I. Szarka [13],

M. Szymkowski [135], S.F. Taghavi [95], G. Taillepied [97], J. Takahashi [111], G.J. Tambave [80], S. Tang [6], Z. Tang [119], J.D. Tapia Takaki [117], N. Tapus [125], L.A. Tarasovicova [137], M.G. Tarzila [46], G.F. Tassielli [32], A. Tauro [33], G. Tejeda Muñoz [45], A. Telesca [33], L. Terlizzi [25], C. Terrevoli [115], S. Thakur [4], D. Thomas [108], A. Tikhonov [142], A.R. Timmins [115], M. Tkacik [106], T. Tkacik [106], A. Toia [64], R. Tokumoto [92], K. Tomohiro [92], N. Topilskaya [142], M. Toppi [49], T. Tork [130], V.V. Torres [103], A.G. Torres Ramos [32], A. Trifiró [31,53], A.S. Triolo [33,31,53], S. Tripathy [51], T. Tripathy [47], S. Trogolo [33], V. Trubnikov [3], W.H. Trzaska [116], T.P. Trzcinski [135], A. Tumkin [142], R. Turrisi [54], T.S. Tveter [20], K. Ullaland [21], B. Ulukutlu [95], A. Uras [127], G.L. Usai [23], M. Vala [38], N. Valle [22], L.V.R. van Doremalen [59], M. van Leeuwen [84], C.A. van Veen [94], R.J.G. van Weelden [84], P. Vande Vyvre [33], D. Varga [138], Z. Varga [138], M. Vasileiou [78], A. Vasiliev [142], O. Vázquez Doce [49], O. Vazquez Rueda [115], V. Vechernin [142], E. Vercellin [25], S. Vergara Limón [45], R. Verma [47], L. Vermunt [97], R. Vértesi [138], M. Verweij [59], L. Vickovic [34], Z. Vilakazi [122], O. Villalobos Baillie [100], A. Villani [24], A. Vinogradov [142], T. Virgili [29], M.M.O. Virta [116], V. Vislavicius [75], A. Vodopyanov [143], B. Volkel [33], M.A. Völkl [94], K. Voloshin [142], S.A. Voloshin [136], G. Volpe [32], B. von Haller [33], I. Vorobyev [95], N. Vozniuk [142], J. Vrláková [38], J. Wan [40], C. Wang [40], D. Wang [40], Y. Wang [40], Y. Wang [6], A. Wegrzynek [33], F.T. Weiglhofer [39], S.C. Wenzel [33], J.P. Wessels [137], S.L. Weyhmiller [139], J. Wiechula [64], J. Wikne [20], G. Wilk [79], J. Wilkinson [97], G.A. Willems [137], B. Windelband [94], M. Winn [129], J.R. Wright [108], W. Wu [40], Y. Wu [119], R. Xu [6], A. Yadav [43], A.K. Yadav [134], S. Yalcin [72], Y. Yamaguchi [92], S. Yang [21], S. Yano [92], Z. Yin [6], I.-K. Yoo [17], J.H. Yoon [58], H. Yu [12], S. Yuan [21], A. Yuncu [94], V. Zaccolo [24], C. Zampolli [33], F. Zanone [94], N. Zardoshti [33], A. Zarochentsev [142], P. Závada [62], N. Zaviyalov [142], M. Zhalov [142], B. Zhang [6], C. Zhang [129], L. Zhang [40], S. Zhang [40], X. Zhang [6], Y. Zhang [119], Z. Zhang [6], M. Zhao [10], V. Zherebchevskii [142], Y. Zhi [10], D. Zhou [6], Y. Zhou [83], J. Zhu [97,6], Y. Zhu [6], S.C. Zugravel [56]

1 *A.I. Alikhanyan National Science Laboratory (Yerevan Physics Institute) Foundation, Yerevan, Armenia*
2 *AGH University of Krakow, Cracow, Poland*
3 *Bogolyubov Institute for Theoretical Physics, National Academy of Sciences of Ukraine, Kiev, Ukraine*
4 *Bose Institute, Department of Physics and Centre for Astroparticle Physics and Space Science (CAPSS), Kolkata, India*
5 *California Polytechnic State University, San Luis Obispo, California, United States*
6 *Central China Normal University, Wuhan, China*
7 *Centro de Aplicaciones Tecnológicas y Desarrollo Nuclear (CEADEN), Havana, Cuba*
8 *Centro de Investigación y de Estudios Avanzados (CINVESTAV), Mexico City and Mérida, Mexico*
9 *Chicago State University, Chicago, Illinois, United States*
10 *China Institute of Atomic Energy, Beijing, China*
11 *China University of Geosciences, Wuhan, China*
12 *Chungbuk National University, Cheongju, Republic of Korea*
13 *Comenius University Bratislava, Faculty of Mathematics, Physics and Informatics, Bratislava, Slovak Republic*
14 *COMSATS University Islamabad, Islamabad, Pakistan*
15 *Creighton University, Omaha, Nebraska, United States*
16 *Department of Physics, Aligarh Muslim University, Aligarh, India*

[17] *Department of Physics, Pusan National University, Pusan, Republic of Korea*

[18] *Department of Physics, Sejong University, Seoul, Republic of Korea*

[19] *Department of Physics, University of California, Berkeley, California, United States*

[20] *Department of Physics, University of Oslo, Oslo, Norway*

[21] *Department of Physics and Technology, University of Bergen, Bergen, Norway*

[22] *Dipartimento di Fisica, Università di Pavia, Pavia, Italy*

[23] *Dipartimento di Fisica dell'Università and Sezione INFN, Cagliari, Italy*

[24] *Dipartimento di Fisica dell'Università and Sezione INFN, Trieste, Italy*

[25] *Dipartimento di Fisica dell'Università and Sezione INFN, Turin, Italy*

[26] *Dipartimento di Fisica e Astronomia dell'Università and Sezione INFN, Bologna, Italy*

[27] *Dipartimento di Fisica e Astronomia dell'Università and Sezione INFN, Catania, Italy*

[28] *Dipartimento di Fisica e Astronomia dell'Università and Sezione INFN, Padova, Italy*

[29] *Dipartimento di Fisica 'E.R. Caianiello' dell'Università and Gruppo Collegato INFN, Salerno, Italy*

[30] *Dipartimento DISAT del Politecnico and Sezione INFN, Turin, Italy*

[31] *Dipartimento di Scienze MIFT, Università di Messina, Messina, Italy*

[32] *Dipartimento Interateneo di Fisica 'M. Merlin' and Sezione INFN, Bari, Italy*

[33] *European Organization for Nuclear Research (CERN), Geneva, Switzerland*

[34] *Faculty of Electrical Engineering, Mechanical Engineering and Naval Architecture, University of Split, Split, Croatia*

[35] *Faculty of Engineering and Science, Western Norway University of Applied Sciences, Bergen, Norway*

[36] *Faculty of Nuclear Sciences and Physical Engineering, Czech Technical University in Prague, Prague, Czech Republic*

[37] *Faculty of Physics, Sofia University, Sofia, Bulgaria*

[38] *Faculty of Science, P.J. Šafárik University, Košice, Slovak Republic*

[39] *Frankfurt Institute for Advanced Studies, Johann Wolfgang Goethe-Universität Frankfurt, Frankfurt, Germany*

[40] *Fudan University, Shanghai, China*

[41] *Gangneung-Wonju National University, Gangneung, Republic of Korea*

[42] *Gauhati University, Department of Physics, Guwahati, India*

[43] *Helmholtz-Institut für Strahlen- und Kernphysik, Rheinische Friedrich-Wilhelms-Universität Bonn, Bonn, Germany*

[44] *Helsinki Institute of Physics (HIP), Helsinki, Finland*

[45] *High Energy Physics Group, Universidad Autónoma de Puebla, Puebla, Mexico*

[46] *Horia Hulubei National Institute of Physics and Nuclear Engineering, Bucharest, Romania*

[47] *Indian Institute of Technology Bombay (IIT), Mumbai, India*

[48] *Indian Institute of Technology Indore, Indore, India*

[49] *INFN, Laboratori Nazionali di Frascati, Frascati, Italy*

[50] *INFN, Sezione di Bari, Bari, Italy*

[51] *INFN, Sezione di Bologna, Bologna, Italy*

[52] *INFN, Sezione di Cagliari, Cagliari, Italy*

[53] *INFN, Sezione di Catania, Catania, Italy*

[54] *INFN, Sezione di Padova, Padova, Italy*

[55] *INFN, Sezione di Pavia, Pavia, Italy*

[56] *INFN, Sezione di Torino, Turin, Italy*

[57] *INFN, Sezione di Trieste, Trieste, Italy*

[58] *Inha University, Incheon, Republic of Korea*

[59] *Institute for Gravitational and Subatomic Physics (GRASP), Utrecht University/Nikhef, Utrecht, The Netherlands*

[60] *Institute of Experimental Physics, Slovak Academy of Sciences, Košice, Slovak Republic*

[61] *Institute of Physics, Homi Bhabha National Institute, Bhubaneswar, India*

[62] *Institute of Physics of the Czech Academy of Sciences, Prague, Czech Republic*

[63] *Institute of Space Science (ISS), Bucharest, Romania*

[64] *Institut für Kernphysik, Johann Wolfgang Goethe-Universität Frankfurt, Frankfurt, Germany*

[65] *Instituto de Ciencias Nucleares, Universidad Nacional Autónoma de México, Mexico City, Mexico*

[66] *Instituto de Física, Universidade Federal do Rio Grande do Sul (UFRGS), Porto Alegre, Brazil*

[67] *Instituto de Física, Universidad Nacional Autónoma de México, Mexico City, Mexico*

[68] *iThemba LABS, National Research Foundation, Somerset West, South Africa*

[69] *Jeonbuk National University, Jeonju, Republic of Korea*

[70] *Johann-Wolfgang-Goethe Universität Frankfurt Institut für Informatik, Fachbereich Informatik und Mathematik, Frankfurt, Germany*

[71] *Korea Institute of Science and Technology Information, Daejeon, Republic of Korea*

[72] *KTO Karatay University, Konya, Turkey*

[73] *Laboratoire de Physique Subatomique et de Cosmologie, Université Grenoble-Alpes, CNRS-IN2P3, Grenoble, France*

[74] *Lawrence Berkeley National Laboratory, Berkeley, California, United States*

[75] *Lund University Department of Physics, Division of Particle Physics, Lund, Sweden*

[76] *Nagasaki Institute of Applied Science, Nagasaki, Japan*

[77] *Nara Women's University (NWU), Nara, Japan*

[78] *National and Kapodistrian University of Athens, School of Science, Department of Physics, Athens, Greece*

[79] *National Centre for Nuclear Research, Warsaw, Poland*

[80] *National Institute of Science Education and Research, Homi Bhabha National Institute, Jatni, India*

[81] *National Nuclear Research Center, Baku, Azerbaijan*

[82] *National Research and Innovation Agency - BRIN, Jakarta, Indonesia*

[83] *Niels Bohr Institute, University of Copenhagen, Copenhagen, Denmark*

[84] *Nikhef, National institute for subatomic physics, Amsterdam, The Netherlands*

[85] *Nuclear Physics Group, STFC Daresbury Laboratory, Daresbury, United Kingdom*

[86] *Nuclear Physics Institute of the Czech Academy of Sciences, Husinec-Řež, Czech Republic*

[87] *Oak Ridge National Laboratory, Oak Ridge, Tennessee, United States*

[88] *Ohio State University, Columbus, Ohio, United States*

[89] *Physics department, Faculty of science, University of Zagreb, Zagreb, Croatia*

[90] *Physics Department, Panjab University, Chandigarh, India*

[91] *Physics Department, University of Jammu, Jammu, India*

[92] *Physics Program and International Institute for Sustainability with Knotted Chiral Meta Matter (SKCM2), Hiroshima University, Hiroshima, Japan*

[93] *Physikalisches Institut, Eberhard-Karls-Universität Tübingen, Tübingen, Germany*

[94] *Physikalisches Institut, Ruprecht-Karls-Universität Heidelberg, Heidelberg, Germany*

[95] *Physik Department, Technische Universität München, Munich, Germany*

[96] *Politecnico di Bari and Sezione INFN, Bari, Italy*

[97] *Research Division and ExtreMe Matter Institute EMMI, GSI Helmholtzzentrum für Schwerionenforschung GmbH, Darmstadt, Germany*

[98] *Saga University, Saga, Japan*

[99] *Saha Institute of Nuclear Physics, Homi Bhabha National Institute, Kolkata, India*

[100] *School of Physics and Astronomy, University of Birmingham, Birmingham, United Kingdom*

[101] *Sección Física, Departamento de Ciencias, Pontificia Universidad Católica del Perú, Lima, Peru*

[102] *Stefan Meyer Institut für Subatomare Physik (SMI), Vienna, Austria*

[103] *SUBATECH, IMT Atlantique, Nantes Université, CNRS-IN2P3, Nantes, France*

[104] *Sungkyunkwan University, Suwon City, Republic of Korea*

[105] *Suranaree University of Technology, Nakhon Ratchasima, Thailand*

[106] *Technical University of Košice, Košice, Slovak Republic*

[107] *The Henryk Niewodniczanski Institute of Nuclear Physics, Polish Academy of Sciences, Cracow, Poland*

[108] *The University of Texas at Austin, Austin, Texas, United States*

[109] *Universidad Autónoma de Sinaloa, Culiacán, Mexico*

[110] *Universidade de São Paulo (USP), São Paulo, Brazil*

[111] *Universidade Estadual de Campinas (UNICAMP), Campinas, Brazil*

[112] *Universidade Federal do ABC, Santo Andre, Brazil*

[113] *University of Cape Town, Cape Town, South Africa*

[114] *University of Derby, Derby, United Kingdom*

[115] *University of Houston, Houston, Texas, United States*

[116] *University of Jyväskylä, Jyväskylä, Finland*

[117] *University of Kansas, Lawrence, Kansas, United States*

[118] *University of Liverpool, Liverpool, United Kingdom*

[119] *University of Science and Technology of China, Hefei, China*

[120] *University of South-Eastern Norway, Kongsberg, Norway*

[121] *University of Tennessee, Knoxville, Tennessee, United States*

[122] *University of the Witwatersrand, Johannesburg, South Africa*

[123] *University of Tokyo, Tokyo, Japan*

[124] *University of Tsukuba, Tsukuba, Japan*

[125] *University Politehnica of Bucharest, Bucharest, Romania*

[126] *Université Clermont Auvergne, CNRS/IN2P3, LPC, Clermont-Ferrand, France*

[127] *Université de Lyon, CNRS/IN2P3, Institut de Physique des 2 Infinis de Lyon, Lyon, France*

[128] *Université de Strasbourg, CNRS, IPHC UMR 7178, F-67000 Strasbourg, France*

[129] *Université Paris-Saclay, Centre d'Etudes de Saclay (CEA), IRFU, Départment de Physique Nucléaire (DPhN), Saclay, France*

[130] *Université Paris-Saclay, CNRS/IN2P3, IJCLab, Orsay, France*

[131] *Università degli Studi di Foggia, Foggia, Italy*

[132] *Università del Piemonte Orientale, Vercelli, Italy*

[133] *Università di Brescia, Brescia, Italy*

[134] *Variable Energy Cyclotron Centre, Homi Bhabha National Institute, Kolkata, India*

[135] *Warsaw University of Technology, Warsaw, Poland*

[136] *Wayne State University, Detroit, Michigan, United States*

[137] *Westfälische Wilhelms-Universität Münster, Institut für Kernphysik, Münster, Germany*

[138] *Wigner Research Centre for Physics, Budapest, Hungary*

[139] *Yale University, New Haven, Connecticut, United States*

[140] *Yonsei University, Seoul, Republic of Korea*

[141] *Zentrum für Technologie und Transfer (ZTT), Worms, Germany*

[142] *Affiliated with an institute covered by a cooperation agreement with CERN*

[143] *Affiliated with an international laboratory covered by a cooperation agreement with CERN.*

[I] *Also at: Max-Planck-Institut für Physik, Munich, Germany*

[II] *Also at: Italian National Agency for New Technologies, Energy and Sustainable Economic Development (ENEA), Bologna, Italy*

[III] *Also at: Dipartimento DET del Politecnico di Torino, Turin, Italy*

[IV] *Also at: Department of Applied Physics, Aligarh Muslim University, Aligarh, India*

[V] *Also at: Institute of Theoretical Physics, University of Wroclaw, Poland*

[VI] *Also at: An institution covered by a cooperation agreement with CERN*